University of Alberta

Advanced load shedding scheme for voltage collapse prevention

by

Yunfei Wang

A thesis submitted to the Faculty of Graduate Studies and Research
in partial fulfillment of the requirements for the degree of

Doctor of Philosophy
in
Power Engineering and Power Electronics

Department of Electrical and Computer Engineering

Fall 2011
Edmonton, Alberta

Abstract

Present-day economic and environmental constraints push power systems to be operated closer to their limits. A common limiting factor for power transmission is the risk of voltage instability in recent years. As the ultimate countermeasure to voltage collapse, load shedding is normally considered the last resort, when there are no other alternatives to stop an approaching voltage collapse. The requirements of a practical load shedding scheme are to prevent a power system from voltage collapse and to maximize its reliability. In order to design such a scheme, the following tasks are equally important:

1. Recognizing the approaching voltage collapse.
2. Determining the best load shedding locations.
3. Minimizing the amount of load shedding.

This thesis firstly investigates the widely used undervoltage load shedding schemes (UVLS) and the single-port impedance match (SPIM) based schemes. The findings explain the difficulties faced by them. An original load shedding oriented voltage stability monitoring scheme, which involves developing a new multi-port network equivalent, is then developed. With the help of the multi-port network equivalent, the monitoring scheme can not only recognize the approaching voltage collapse in time, but also can easily rank the load buses

based on their weakness. The results of ranking are consistent with those obtained from modal analysis method.

This thesis then proposes a practical event-driven load shedding scheme based on the experiences learned from the schemes implemented by various utilities. The scheme involves developing a multistage method, which is to optimize the amount of load shedding. A general design procedure for the scheme is presented in the thesis. Using a real 2038 bus system as an example, the design methodology is described in detail. The methodology is expected to help power system engineers develop their own load shedding schemes.

A practical emergency demand response scheme is also developed and presented in the appendix. It is aimed at choosing the proper demand response participants and minimizing the total cost while achieving a certain level of operation reserves.

Acknowledgements

I should like to express my sincere appreciation to my supervisor Dr. Wilsun Xu. Without his endless help, this dissertation would never have been written. His extensive knowledge and sharp critiques have always guided me to think, to analyze, and to become a mature researcher.

I am grateful to Dr. Tongwen Chen, for his discussions and suggestions throughout the whole research.

Thanks to Dr. Weixing Li and Dr. Jin Hao, for assisting me with the simulations and verifications. We worked together extensively to implement the proposed algorithm in both PSS/E and MATLAB.

I thank all the fellow students in the power lab, including Alexandre Nassif, Enrique Nino, Janak Acharya, Iraj Rahimi Pordanjani, Khaled Alawasa, Ali Arefifar, Joey Gallant, Xun Long, Hui Wang, and Hooman Erfanian Mazin, for their friendships and rewarding discussions. I also want to extend my thanks to Ms. Patricia Barnes for helping me navigate the administrative challenges during my graduate studies.

My family has always been supportive and encouraging. I give a hearty thanks to all my family members.

Contents

List of Tables

List of Figures

Chapter 1

Introduction

Power system stability has long been a concern in system operations. As the power system evolved, different forms of power system instability have emerged as important during different periods [1]. The methods of analysis, evaluations, and countermeasures to the instability problems have evolved continuously over the last century.

Due to economic and environmental constraints, power systems are being operated closer to their transmission limits nowadays. A common limiting factor for power system operations is the risk of voltage instability. A number of major power-grid blackouts in recent years have manifested voltage instability problems [2]. In this introductory chapter, a general description of power system voltage stability phenomena and the countermeasures to voltage instability are presented. This chapter also defines the scope of the thesis and outlines its main contents.

1.1 Power system voltage stability

Power system stability is normally defined as the ability of an electric power system, for a given initial operating condition, to regain a state of operating equilibrium after being subjected to a physical disturbance, with most system variables bounded so that practically the entire system remains intact [3]. The

instability of a power system may be manifested in many different ways depending on the system configuration and operating mode. Examples are generator instability, shaft torsion oscillation, and voltage collapse. The classification of the different types of power system stability can be found in [1-3].

Increased utility competition, environmental considerations, opening up of the electricity market, and rapidly increased load consumptions are making power systems more and more stressed. Under these stressed conditions a power system experiences a kind of stability problem, which manifests as slow or sudden voltage drops at some buses. These kinds of stability problems are usually referred to as voltage stability problems.

1.1.1 Voltage stability and its phenomena

Although slow or sudden and continuous voltage drops can be spotted as a sign of voltage instability, voltage stability is often defined as:

The ability of a power system to maintain steady voltages at all buses in the system after being subjected to a disturbance from a given initial operating condition [3].

As long as the voltage and power of the system are controllable at all times, the voltage stability is maintained. Otherwise, the system becomes voltage unstable

(also called voltage collapse). Depending on the evolution of the voltage profiles at all buses, the phenomena of voltage instability can be classified as:

Short-term voltage instability: voltage collapse occurs in the order of fractions of a second to a few seconds. This kind of voltage collapse is usually associated with the fast response of voltage controllers, such as generators' automatic voltage regulator (AVRs). Proper tuning of the system voltage controllers can normally avoid short-term voltage instability problems.

Long-term voltage stability: voltage collapses occurs in a few minutes to hours. Long-term voltage stability problems are frequently caused by the slow dynamic interactions inside the distribution network, such as the voltage control actions arising from transformers' on load tap changing (OLTC) and automatically load recovery. Special countermeasures have to be designed to prevent the system from voltage collapse.

In general, short-term voltage instability and long-term voltage instability are all caused by the inability of the system to supply the required load demand.

1.1.2 Mechanisms leading to voltage instability

There are generally four factors that play a very important role in voltage instability problems. The four factors are

a) Transmission network capability

b) Generator's reactive power output limit

c) Load characteristics

d) Network response in the system

Other factors can normally be considered when analyzing these four factors. To get a better understanding of the factors involved in voltage stability problems, a simple generator-load model depicted in Figure 1.1 is used to explain the mechanisms that may ultimately lead to voltage collapse.

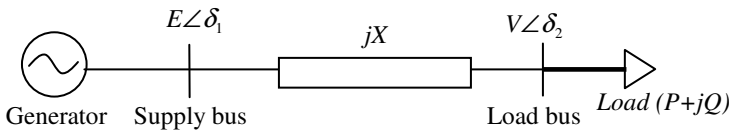

Figure 1.1 A simple one generator and one load system

1.1.2.1 Transmission network capability

Generally there will be some limits on the power that can be transmitted to the load and this limit (also refers to transmission network capability) can be used to determine how stable the power system is. To easily obtain this transmission network capability, the load will be represented by its static voltage characteristics. The power flow model of the sample system can then be described by the following equations:

$$P = \frac{EV}{X}\sin(\delta_2 - \delta_1)$$
$$Q = \frac{EV}{X}\cos(\delta_2 - \delta_1) - \frac{V^2}{X} \tag{1.1}$$

Eliminating the phase angle δ_1 and δ_2 by using the fact $\cos^2(\delta_2 - \delta_1) + \sin^2(\delta_2 - \delta_1) = 1$, equation (1.1) can be rewritten as,

$$E^2 = \left(\frac{PX}{V}\right)^2 + \left(V + \frac{QX}{V}\right)^2 \tag{1.2}$$

The above relationship is shown in the phasor diagram of the sample power system (Figure 1.2). It can be seen that the term *QX* somewhat represents the voltage drop on the line caused by the reactive power demand and *PX* is related to the voltage drop caused by the active power demand. The phasor diagram clearly shows that there is a maximum power that can be transferred to the load and the maximum power can be calculated by the following equations.

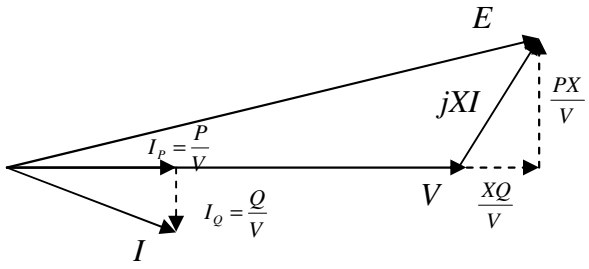

Figure 1.2 Phasor diagram of the sample power system

$$\left(\frac{EV}{X}\right)^2 = P^2 + \left(Q + \frac{V^2}{X}\right)^2 \tag{1.3}$$

The static relationship between the active power P and the reactive power Q is normally defined with the constant power factor, which means

$$Q = P\tan(\theta) \tag{1.4}$$

Substituting equation (1.4) into equation (1.3) gives

$$P^2 + P^2\tan^2(\theta) + 2P\frac{V^2}{X} = \left(\frac{EV}{X}\right)^2 - \frac{V^4}{X^2} \tag{1.5}$$

Solving equation (1.5), we get

$$P = -\frac{E^2}{X}\left(\frac{V}{E}\right)^2 \sin(\theta)\cos(\theta) \pm \frac{E^2}{X}\left(\frac{V}{E}\right)\cos(\theta)\sqrt{1-\left(\frac{V}{E}\right)^2\cos^2(\theta)} \tag{1.6}$$

Equation (1.6) determines there is maximum power P for any given power factor angle θ. For example, equation (1.7) can be obtained when $\theta = 0$.

$$P = \frac{E^2}{X}\left(\frac{V}{E}\right)\sqrt{1-\left(\frac{V}{E}\right)^2} = C \times ab \tag{1.7}$$

where the constant C is equal to $\frac{E^2}{X}$, the variable a and b are equals to $\frac{V}{E}$ and $\sqrt{1-\left(\frac{V}{E}\right)^2}$, respectively.

Based on the Cauchy Inequality equation $a^2 + b^2 \geq 2ab$, the maximum power $P_{\max}$ obtained from equation (1.7) is

$$P_{\max} = \frac{E^2}{2X}, \text{ when } V = \frac{E}{\sqrt{2}} \tag{1.8}$$

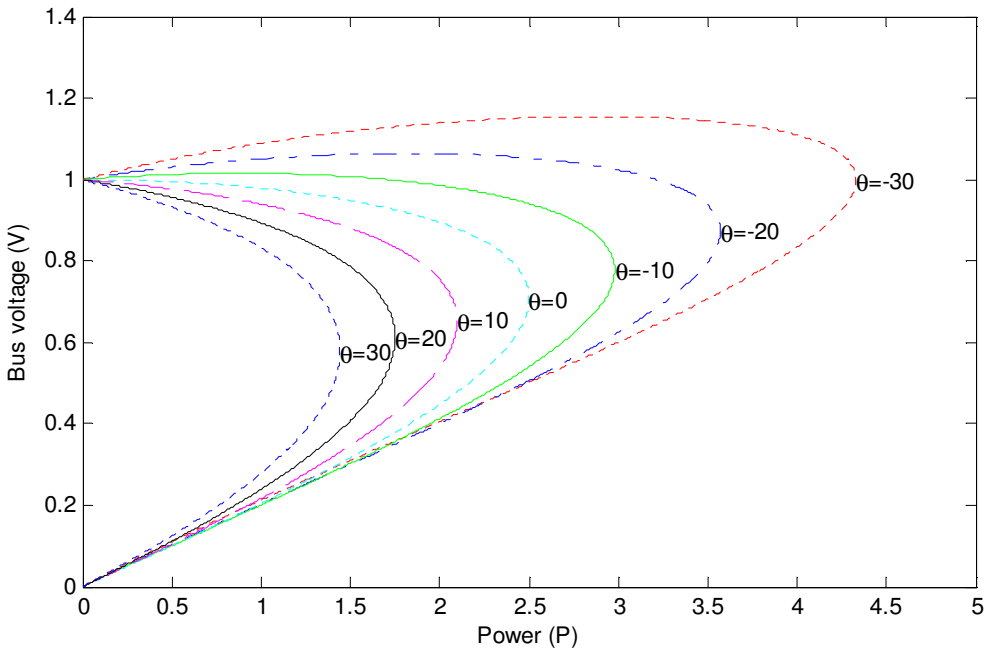

Figure 1.3 PV curves with θ as a parameter

Furthermore, a family of curves with the power factor angle θ as a parameter can be obtained from (1.7) and is plotted in Figure 1.3. Since these curves describe the

relationship between the power P and the bus voltage V, they are normally called *PV curves*. Due to their characteristic shape, they are also referred to as *nose curves.*

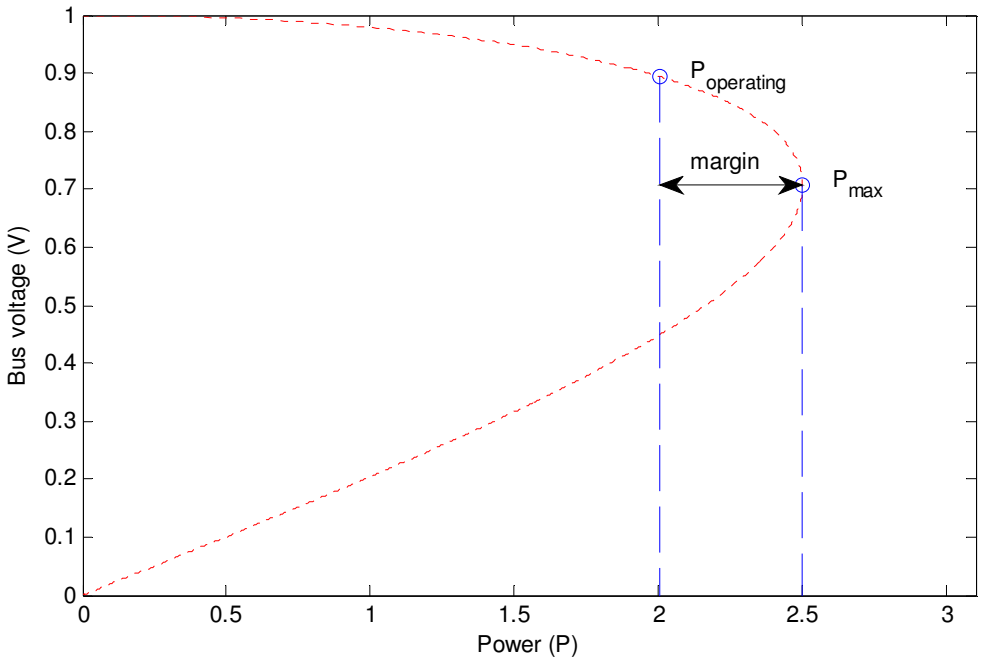

Figure 1.4 Definition of the voltage stability margin

These PV curves define the transmission network capability, which is the power at the *nose point*. If the system load is less than the transmission network capability, power flow solutions exist. If some contingencies reduce the transmission network capability to less than the steady-state load demand, there are no feasible solutions to the power flow equations and voltage collapse may occur in the system. The stability of the system is determined by the voltage stability margin of the operating point, which is the difference between the maximum power that can be delivered by the system and the actual power

demand, as depicted by Figure 1.4. The margin is normally defined as a percentage value of the actual demand, as described by equation (1.9). As for the margin, a 3% to 10% value is a commonly accepted threshold for voltage stability.

$$\text{Margin} = \frac{P_{\max} - P_{operating}}{P_{operating}} \times 100\% \tag{1.9}$$

1.1.2.2 The generator's reactive power output limit

As mentioned at the beginning of section 1.1.2, the reactive power limit also plays an important role in the voltage stability problems and can be considered when evaluating the transmission network capability. In the system depicted by Figure 1.1, the generator is modeled by a constant voltage source E without considering the generator's internal impedance. When the reactive power of the generator reaches its limit or the generator's AVR is not operative, the internal impedance has to be explicitly considered in the circuit. The generator now is modeled by its synchronous electromotive force (EMF) E_f acting behind its synchronous impedance Z_g, as shown by Figure 1.5.

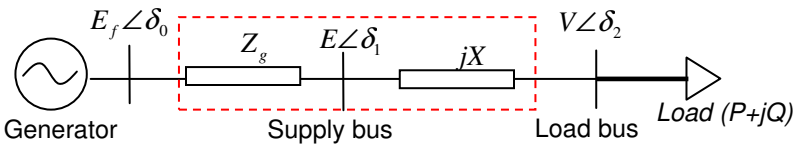

Figure 1.5 The example with consideration of generator reactive power output limit

Clearly, in the above case, if the generator's impedance is combined with the transmission impedance as shown in the red-dashed rectangle, the same PV curves method can be applied to evaluate the stability of the power system. Figure 1.6 shows the PV curves with and without considering the reactive power limit of the generator. As the transmission network capability is drastically reduced when the generator reaches its limit, so too is the system voltage stability.

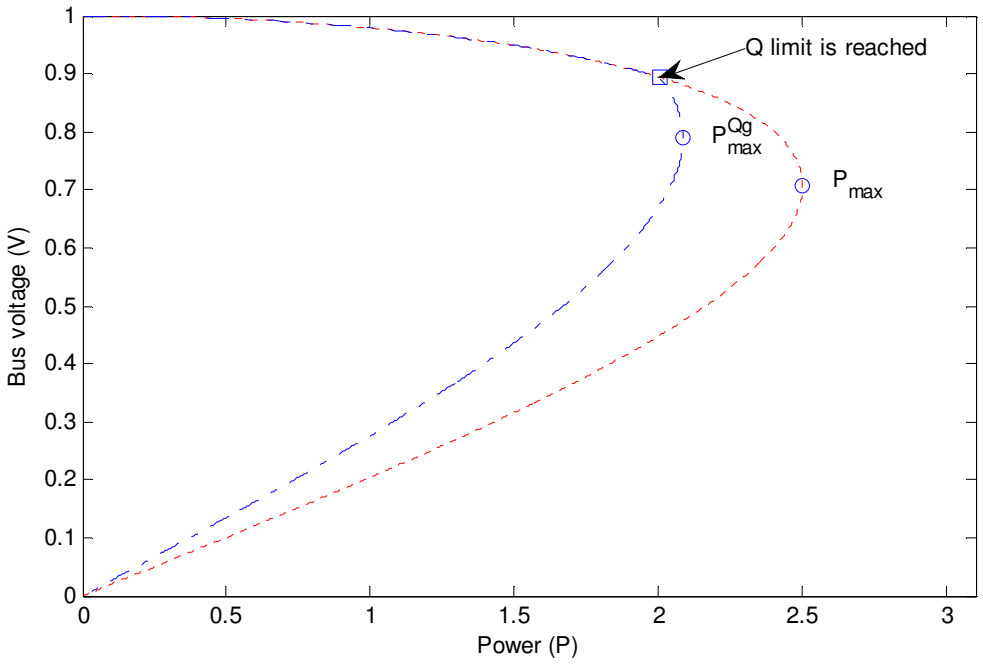

Figure 1.6 The PV curves with consideration of the reactive power limit of the generators

1.1.2.3 Load characteristics

As discussed in the previous section, the main factor contributing to voltage instability is usually the voltage drop that occurs when active and/or reactive

power flows through inductive reactance associated with the transmission network, which limits the capability of the transmission network for power transfer. The transmission capability is further limited when some of the generators hit their reactive power output limits. However, the main driving force for voltage instability is the load [1][4]. The reason will be explained in this subsection. Although the load characteristics are assumed to be independent of the supply voltage—i.e., they are constant characteristics—when the transmission network capability is calculated as in the previous section, the loads are actually voltage dependent in real life [5].

A power system load is usually comprised of a large variety of individual equipment. For each equipment, the steady-state load characteristic can be constant power, constant current, or constant impedance depending on its inherent distinction. Due to the large numbers of individual loads, it is not practical or realistic to model the network load by the modeling of the individual equipment. Therefore, an aggregate load model approach is widely used. The steady-state characteristics of the aggregate load are typically represented by equation (1.10), which is a composition of constant power, constant current, and constant impedance load [6]. The reactive power can also be represented by a similar expression.

$$P = P_0\left(d_2V^2 + d_1V + d_0\right) \tag{1.10}$$

where P_0 is the rated power, d_0, d_1, and d_2 are constants determined by the field tests.

With the load characteristics described by equation (1.10), the power system may not be voltage unstable even if the transmission network capability is less than the present operating loads, as shown in Figure 1.7. Since the load is dependent on the voltage, the post-disturbance transmission network can still supply power to all the equipment although the total power consumed by the equipment is decreased.

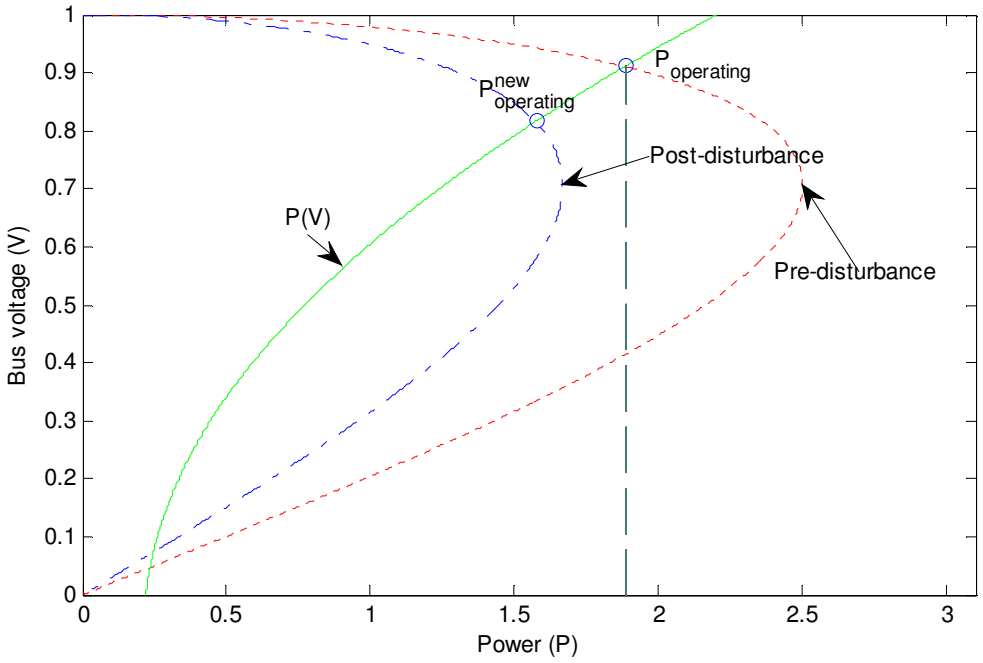

Figure 1.7 Voltage stability considering the load characteristics

Besides the steady-state load characteristics, the load dynamics characteristic also plays an important role in voltage instability problems. Field test results from [6]

and [7] indicate that the usual response of an aggregate load to step voltage changes is of the form shown in Figure 1.8. Depending on the load composition, the transient time ranges from a few seconds to several minutes. The responses for real and reactive power are qualitatively similar.

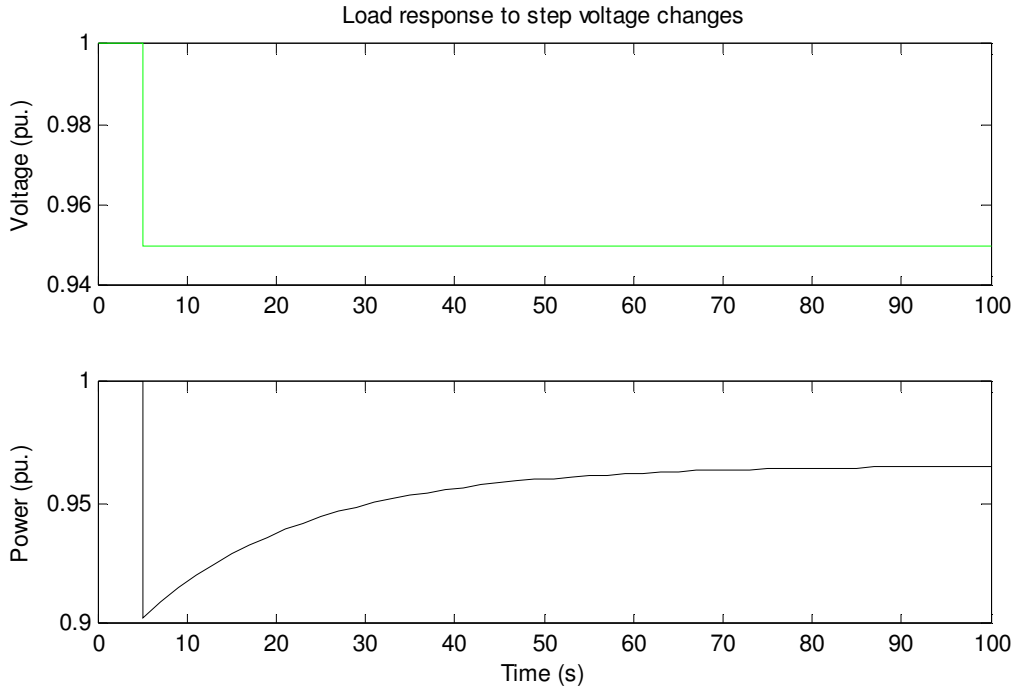

Figure 1.8 Typical response of an aggregate load to step voltage changes

A generic dynamic load model (see equation (1.11)) is presented in [6-7] to describe the load response to voltage changes in the time-domain. The dynamics of the reactive power is described by a qualitatively similar formula.

$$\begin{aligned} T_p \frac{dx}{dt} &= P_s(V) - P \\ P &= xP_t(V)) \end{aligned} \tag{1.11}$$

where T_p is the time-constant, x is the state variable of this model, $P_s(V)$ is the steady-state load response as described by equation (1.10). $P_t(V)$ is the transient characteristic of the load, which is defined as the instantaneous power demand change associated with the sudden voltage changes.

Combining the dynamic load responses and the transmission network capability analysis, the voltage at the load bus after a disturbance can be depicted by Figure 1.9. In Figure 1.9, the voltage dynamics in the transmission network are assumed much faster than the dynamics of the load. Therefore, the transmission network is modeled by three different PV curves: pre-disturbance, post-disturbance, and post-disturbance with some kind of remediation. The power system initially operates at the intersection of the curve $P_s(V)$ and the pre-disturbance PV curve, i.e. point a. The transmission network capability is significantly reduced after a disturbance happens in the system, as shown by the post-disturbance PV curve. The load responds with its transient characteristic $P_t(V)$ and the system operating point jumps to point b.

From equation (1.11), the power difference is positive $dx/dt > 0$, which means that the state variable x is going to increase and the load will try to draw more power $P = xP_t(V)$. This forces the operating point to lower voltage along the post-disturbance PV curve, as shown by the curve bc or bc'. If the remediation is applied when the system is operating at point c, then the operating point jumps back to point d based on the load's transient characteristic. At this point,

$$T_p \frac{dx}{dt} = P_s(V) - P < 0,$$

the state variable x is going to decrease and the load will draw less power. The operating point moves along the PV curve and is stabilized at point e.

On the other hand, if the remediation is applied so late that the operating point reaches the point c', the operating point can only recover to point d'. However, at this point, the load demand and the network supply imbalance is still in deficit, and the system voltage will continuously decrease. Eventually, voltage collapse happens in the system.

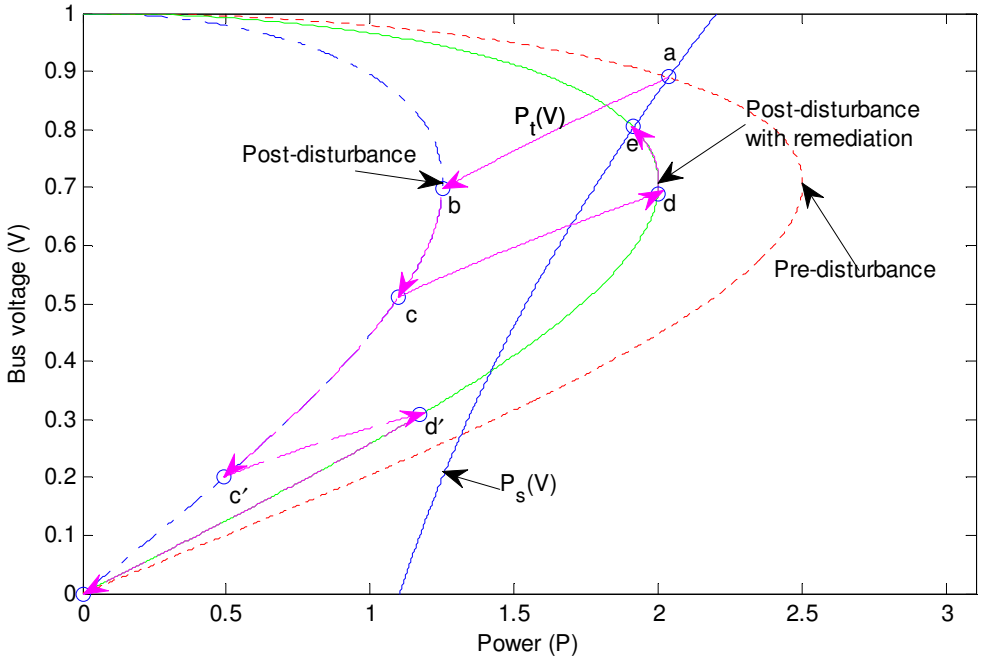

Figure 1.9 Voltage stability analysis considering load dynamics

1.1.2.4 Network response in the system

Besides the inherent load characteristics, network responses to system disturbance or changes are also important in the analysis of voltage instability problems. Network response is highly influenced by the slow-acting voltage control devices, such as transformer on-load tap changers (OLTCs), under-voltage load shedding relays (UVLSs), and switched shunt compensations. Among all these devices, the OLTCs generally need more attention since they are the main cause of voltage instability in some power systems [8-9]. One of the key important features of OLTCs is the voltage regulation performed automatically, which leads to load restorations in power systems. Figure 1.10 shows a typical configuration of OLTCs in power system applications using the same sample power system.

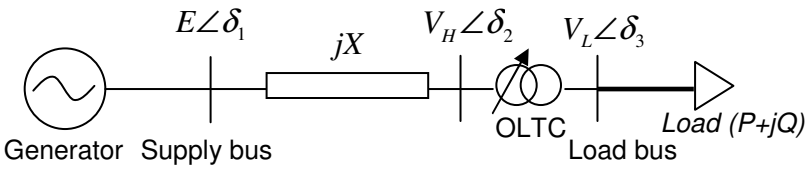

Figure 1.10 A sample power system with OLTCs

The tap changer controls the voltage of the load side V by changing the transformer ratio r. In most cases the variable tap is on the high voltage side. The reasons for that are 1) the current is lower, which makes the commutation easier; and 2) more turns are available at the high voltage side, which makes the voltage

control more precise. The OLTC changes the tap by one step at a time, if the voltage error between the set voltage and the operating voltage remains outside a deadband longer than a specified time delay. The minimum time required for the tap changer to complete one tap is usually close to 5 seconds (mechanical time delay requirement). Some kind of intentional time delays are always added to avoid frequent or unnecessary tap movement, which are the main cause of wear to equipment.

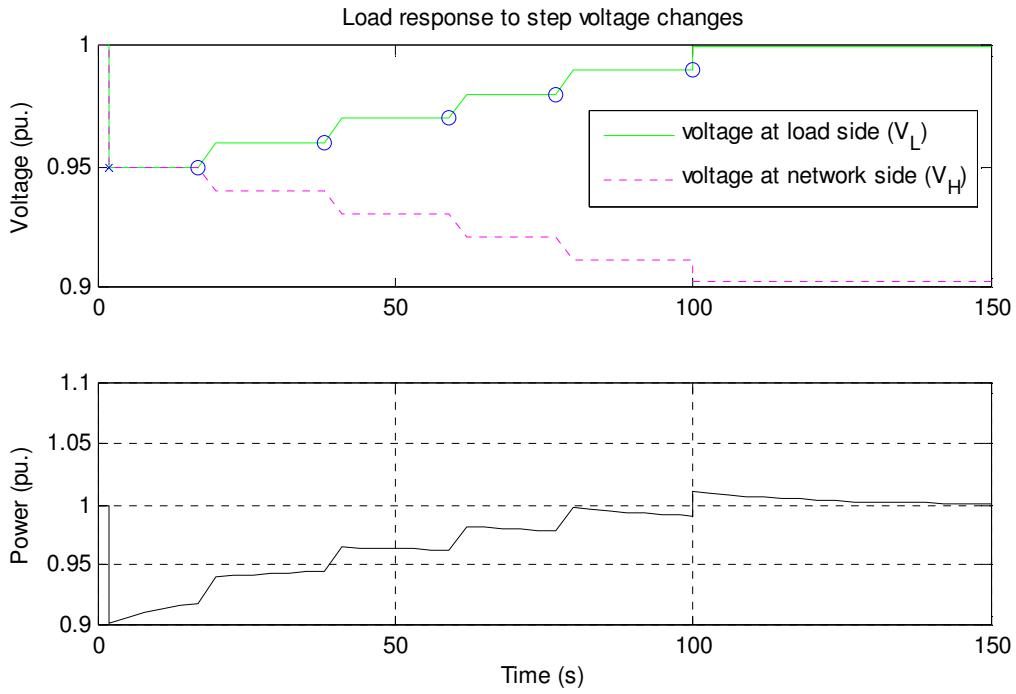

Figure 1.11 Load restorations due to OLTC movements

Equipped with OLTCs on the power delivery transformer, the load eventually becomes the constant power type, although it is inherently voltage dependent. Figure 1.11 shows the load bus voltage profile and load demand profile with

respect to the tap changer movements. Compared to Figure 1.8, the load is restored to the nominal value in the system with OLTCs. The load side voltage is restored to the reference value. However, due to the increasing load demand, the voltage (V_H) at the transmission network side is gradually decreasing. The points 'o' denote the instant when the OLTCs begin to change the transformer ratios.

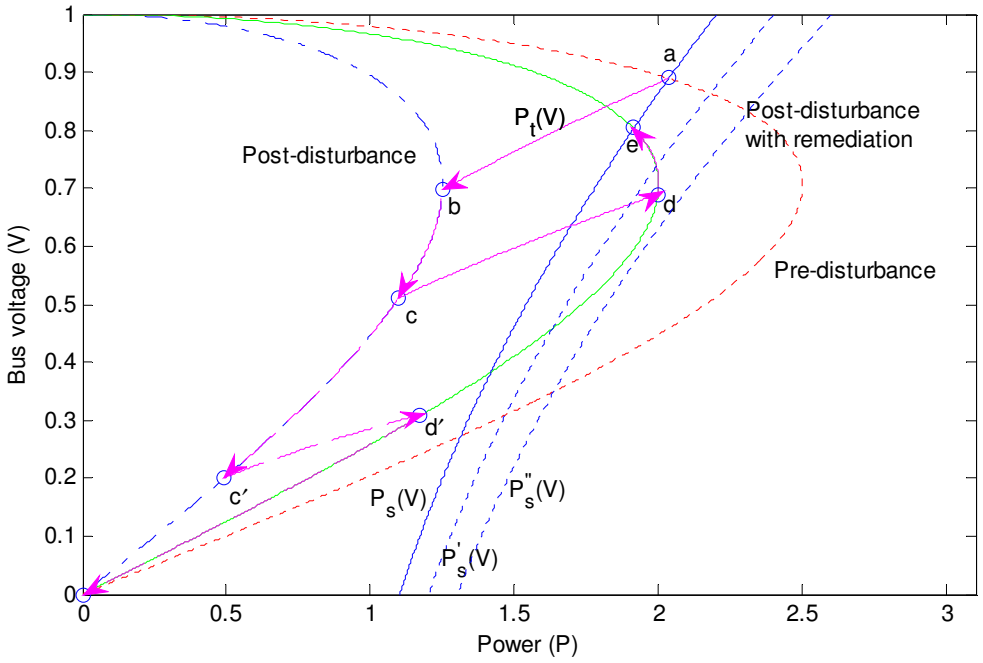

Figure 1.12 Voltage collapse procedure due to OLTC movements

Furthermore, when the OLTCs succeed in restoring the bus voltage to its reference value step by step, the load demand of the system is also moving towards its pre-disturbance value. If the post-disturbance network cannot support the pre-disturbance load demand, voltage collapse will happen. For instance, the system described in Figure 1.9, without OLTCs, is stable as long as the

remediation is applied on time. However, when the OLTCs are present, voltage collapse cannot be prevented even with the same remediation, as shown by $P_S^{''}(V)$ in Figure 1.12.

1.2 Countermeasures to power system voltage instability

The mechanisms behind voltage collapse determine that voltage instability is typically associated with relatively slow variations in network and load characteristics. There are two defense lines to prevent voltage instability of power systems [10]:

a) Preventive actions: by analyzing the system security margins with respect to credible contingencies, i.e. occurrences with a reasonable probability, preventive actions are taken in a pre-contingency situation in order to increase the security margin.

b) Corrective actions: through the special protection schemes (SPS), corrective actions are taken in a given post-disturbance configuration in order to restore system stability.

The following methods are usually used to mitigate voltage instability problems in practice. Most of them can be classified either as corrective actions or as preventive actions depending on how they are to be used.

1) Must-Run Generator (MRG)

MRGs are generally uneconomic generators. They only operate to change power flow patterns in order to increase the security margin or to provide additional voltage support during emergencies. They normally act as a preventive action and are operated in a pre-contingency condition.

2) Series compensation

Since the network transmission capability is decidedly limited by the line reactance, series capacitors can be added to the long transmission line for the purpose of decreasing the net reactive loss. Thus, the network transmission capability is improved and voltage stability is enhanced.

3) Shunt compensation

In general, reactive power should be supplied locally, with the generators supplying active power in order to limit the power loss on the transmission network. The function of shunt compensation is to provide such reactive power support to the local load demand. Although the use of shunt compensations, including shunt capacitors (SVCs) and static compensators (STATCOMs), can considerably improve voltage stability margin their definite limitations must be

recognized. Numbers of voltage collapse incidents indicate that voltage collapse mostly happens in systems heavily dependent on shunt compensations. When a disturbance drives the shunt compensations to hit their ceilings, their performance on voltage support will dramatically downgrade.

4) OLTCs blocking

As mentioned earlier, the movement of OLTCs could considerably degrade voltage stability margin. OLTC blocking can be used for slowing down the system degradation by stopping the load restoration process, which in turn can maintain voltage stability in the system.

5) Load shedding

Since voltage collapse is principally caused by the inability of the system to supply the required load demand, load reduction or load shedding can provide a considerable relief to the highly stressed system. Sometimes a small load shedding can make the difference between collapse and survival.

There are generally two types of load shedding schemes: event-driven based load shedding and response-based load shedding. The event-driven based load shedding schemes are installed to guard against specific contingencies. These contingencies have severe consequences for power systems and are usually

selected based on experience. On the other hand, the response-based load shedding schemes use the real measurement, such as bus voltage, to identify the risk of voltage collapse, then the pre-designed or online computed load shedding will be implemented.

From the viewpoint of customer voltage quality, load shedding is definitely not preferred. However, enacted as a safety net to power systems, load shedding is the only effective way to prevent voltage collapse in some severe conditions. According to the final report on the Northeast USA-Canada blackout of August 14, 2003, the blackout could have been averted if manual or automatic load shedding of 1,500 MW had occurred within the Cleveland-Akron area before the outage of the Sammis-Star 345 kV line, which is the critical event that led to widespread cascading in Ohio and beyond [11]. Although many types of load shedding schemes have been developed in recent years, there are still big challenges faced by the engineers in the area of recognizing the approaching voltage collapse in time and developing a general procedure to design and to optimize the load shedding schemes for their specific power systems.

1.3 Thesis scope and outline

The scope of this thesis is to design a technically sound and practically useful load shedding scheme for voltage collapse prevention. With the help of modern computer hardware and software technology, power systems have been more

observable (using the synchronized phasor measurement units PMUs) and controllable (using fast acting breakers with remote controllability). This thesis aims to develop an advanced load shedding scheme for modern power systems by utilizing advanced information technology and infrastructures.

Load shedding schemes have long been implemented in power systems for preventing frequency instability. Undervoltage load shedding schemes are widely used in power systems for preventing voltage collapse, even though they are not as effective as underfrequency load shedding schemes. Reasons for the lack of effectiveness are twofold. First, the increasing complexity of modern power systems makes it hard to find the suitable load shedding locations. Second, the heavy use of reactive power support flats the voltage profile. Therefore, much effort has been spent on developing new types of load shedding schemes. Due to its simplicity and powerful theory basis, the impedance matching based load shedding scheme has attracted the attention of many researchers and engineers in recent years [12-14]. However, the difficulties in obtaining the Thevenin equivalent parameters limit its application in power systems. Chapter 2 analyzes the above issue in detail.

Following the analysis of the principle behind the difficulties faced by the single-port impedance match based load shedding scheme, Chapter 3 presents a new type of power system equivalent. The proposed network equivalent reveals that there are coupling effects between each individual load. By explicitly considering

these coupling effects, a promising direction of overcoming the difficulties in estimating the Thevenin equivalent parameters is revealed. Three different models are proposed to model the coupling effects. The three models represent the three basic elements in electric circuits: voltage source, impedance, and load. The characteristics of each model have been analyzed and compared. The results indicate the most suitable model is impedance.

In Chapter 4, modeling the coupling effects as impedance, the network equivalent is used to estimate voltage stability margin. The impedance matching theory is used here to give an initial estimate of the voltage stability. Subsequently an iteration procedure is applied to find the steady-state voltage stability margin with consideration of the reactive power limit and the movement of slow acting devices, such as OLTCs and the switched shunts.

Based on the impedance ratio obtained from the network equivalent, Chapter 4 also ranks the load buses. The results of bus ranking show that they are consistent with the ones calculated by the modal analysis method. The weakest load bus can be used to determine the best locations for load shedding. Upon finding the load shedding locations, a practical strategy for minimization of load shedding amount is presented in Chapter 4 as well. The strategy is called multistage method as it solves this optimization problem stage by stage. At each stage, the most effective location is selected and a fixed amount of load is shed. At the last stage, the

voltage stability margin is recovered to the required value and the load shedding rules (location and amount) are obtained.

Chapter 5 presents the proposed event-driven load shedding scheme. An extensive investigation of the load shedding schemes implemented at various utility companies is discussed. By studying these practical industry experiences, Chapter 5 details the implementation procedure and the functions of each component of the new scheme. Chapter 5 gives power system engineers a clear idea of the advantages of the proposed event driven load shedding scheme. In order to facilitate practical applications, a design methodology for the event driven load shedding scheme is explained in Chapter 6. The chapter provides a comprehensive guideline, which can be used by power system engineers to design an event driven load shedding scheme for their specific power systems. As an implementation example, a sample event-driven load shedding scheme designed for a real 2038-bus power system is presented.

The main conclusions from this work and suggestions for future studies and improvement are presented in Chapter 7. Last but not least, the event driven concept and the proposed multi-port network equivalent can also be used to design a practical emergency demand response scheme. The demand response application has been tested on several power systems, and the results demonstrate the advantages of the proposed event driven demand response scheme in terms of reducing cost.

Chapter 2

The difficulties of conventional load shedding schemes

Since voltage stability monitoring methods are essential to design a proper load shedding scheme, the research on voltage stability index has long been paid a great deal of attention. This chapter reviews the voltage stability indices proposed in the literature. Although many indices presented in publications can be used to design load shedding schemes, the most widely used load shedding schemes still fall into the two categories of undervoltage load shedding schemes and single-port impedance match based load shedding schemes. The rest of this chapter investigates the difficulties faced by these two conventional schemes.

2.1 Introduction

One basic requirement of a proper load shedding scheme is that it should be able to recognize the approaching risk of voltage collapse. The task of load shedding is activated once it senses a forthcoming voltage collapse. To fulfill this requirement, load shedding schemes always involve developing a voltage stability monitoring platform. The voltage stability monitoring platform should be able to obtain an accurate knowledge of how close the operation point of the system is to its voltage stability limit within a proper time delay.

Moreover, from the viewpoint of power quality and reliability, the number of locations and the amount of load shedding should be as little as possible. Hence, the voltage stability monitoring method should not only be aware of the approaching voltage collapse, but also should be capable of identifying the weakest location(s) and thus helping determine the minimum amount of load shedding. To be practically useful, the voltage stability monitoring method should be as simple as possible. This is the reason why the impedance matching based method proposed in [12] attracts considerable interest.

In order to seek an effective voltage stability monitoring scheme to satisfy the above requirements, a thorough literature review was conducted. The review revealed that the prevailing load shedding schemes fell into two categories: undervoltage load shedding schemes and the single-port impedance match based load shedding schemes. However, although these two types of schemes are very popular in real applications, many researchers and engineers have doubted their performance in recent years [15-18]. An extensive investigation of these widely used schemes was performed to reveal the difficulties they face and to explain why their performances are unsatisfactory.

2.2 Power system voltage stability indices

Many voltage stability indices have been proposed in relation to the evolution of voltage instability problems. The indices intended for on-line applications are categorized and summarized in Figure 2.1.

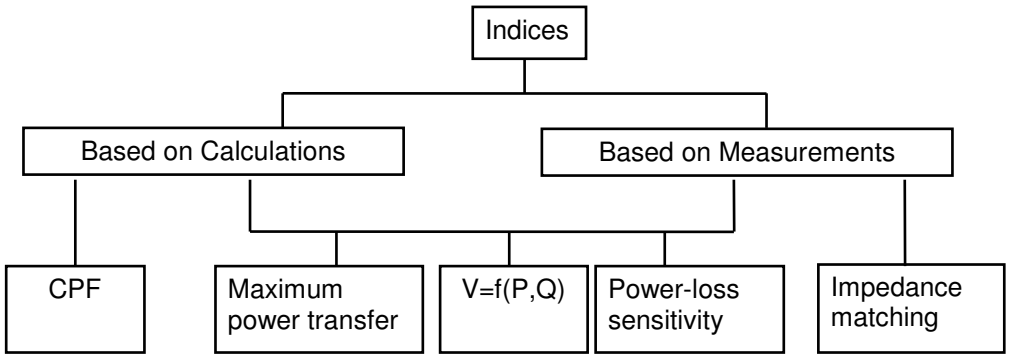

Figure 2.1 Voltage stability indices proposed in recent years

Although all these indices are based on different principles, all of them can reach a max/min value as the power system approaches voltage instability. When the indices reach or run close to their respect thresholds, voltage collapse occurs.

2.2.1 Indices based on calculations

With the support of modern computing capability, many attempts have been made to use the traditional off-line continuation power flow (CPF) method for on-line applications [19-21]. The advantage of CPF is that it can rank the load buses and find the proper corrective control actions (such as load shedding or enhancements on reactive power support). The disadvantage is that it can be used only for checking the presence of a stable equilibrium on the post-disturbance PV curves. CFP is unable to determine how fast the remediation should be applied due to lack of timing information for the power flow method. Moreover, due to a large number of contingencies that need to be studied for a large-scale power system, excessive computing time is still an issue for on-line applications.

2.2.2 Indices based on measurements

Among all the real-time voltage collapse protection schemes, those based on the impedance (or voltage) matching schemes are the most attractive, since they use only the local measurements [12-14, 22-24].

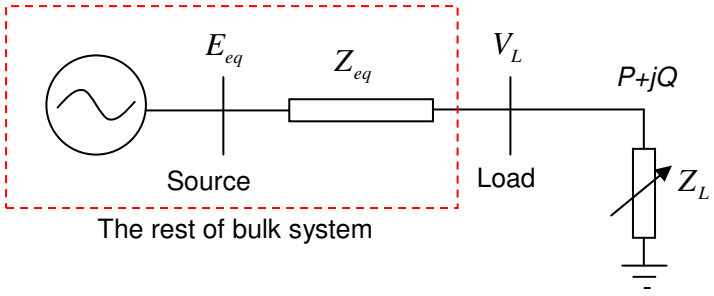

Figure 2.2 The Thevenin equivalent of a bulk transmission system

Separating the load bus and representing the rest of the system as a Thevenin equivalent is shown in Figure 2.2. The impedance matching theory can be adopted to monitor how close the operating point is to the network transmission limit. The impedance matching theory shows that the maximum power that can be delivered is reached when the impedance ratio (r_Z) is equal to 1, where r_Z is defined as (2.1).

$$r_Z = \frac{|Z_L|}{|Z_{eq}|} \tag{2.1}$$

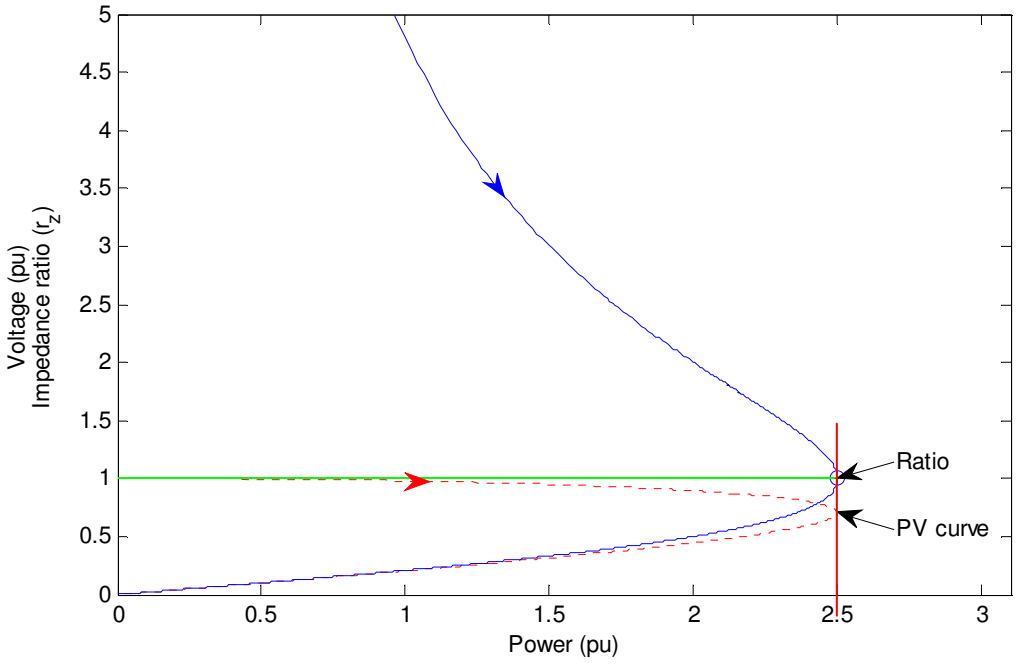

Figure 2.3 Relationship between transmission capability and impedance ratio r_z

Figure 2.3 shows the relationship between the network transmission capability and the impedance ratio for the same sample power system in Figure 1.1. It indicates that the network transmission reaches its limit when the impedance ratio is equal to 1.

Although the impedance match based method attracts a great deal of attention, it is not free of difficulties. The primary difficulty of this method lies in estimating the Thevenin equivalent parameters. Due to the difficulties in obtaining accurate Thevenin equivalent parameters, it becomes very difficult to obtain satisfying performance in terms of voltage stability monitoring [15-17]. More detailed discussions on the impedance match based method are presented in section 2.4.

2.2.3 Indices based on the combination of calculations and measurements

Many voltage instability indices utilizing the advantages of both calculation and measurements based methods have been proposed recently. Reference [25] presented a voltage collapse prediction index (VCPI) for every load bus in the system based on a function of the system's maximum power transfer. The value of VCPI varies from 0 to 1. Voltage collapse happens when VCPI becomes 1. However, finding a proper threshold for VCPI is not an easy task. Additionally, the job of deciding what kind of remediation actions should be initiated is also a challenge, because it is difficult to analyze the sensitivities of controllable variables (such as loads and generator active power output) with respect to the voltage collapse prediction index VCPI.

Based on the power flow equation, which is similar to equation (1.6), a voltage stability index (L_{mn}) is proposed in [26]. The index L_{mn} is used to monitor the current loading of the transmission line. As long as L_{mn} remains less than 1, the power system is within the transmission capability and voltage stability exists. References [27-30] further developed this idea to make their proposed voltage stability indices calculation much faster and more accurate. However, the problem with these indices is that the equivalent voltage sources take account of all the influence from all the other loads except the one under study. Therefore, when the other loads change the equivalent voltage sources could not remain constant, which in turn affects the accuracy of their proposed voltage stability indices.

The power-loss-sensitivity method [31] is based on the fact that the power loss on the transmission network starts to grow rapidly in the vicinity of voltage collapse. The sensitivity of power loss with respect to the demand increase will go to infinity at voltage collapse point, which is also known as the nose point of the PV curves. However, because voltage collapse may not happen at the nose point owing to the characteristics of power systems, this index may fail to identify some potential voltage instability risks. For example, the event of the generator hitting its reactive power limit may trigger voltage collapse even if the operation point is far away from the nose point.

In summary, all the above described indices can determine whether or not the operating condition is stable. The main drawback is that they are nonlinear with respect to load changes. Thus it is difficult to quantify how stable the present condition is. Furthermore, it is not easy to use them to design remediation actions, such as load shedding schemes, since the sensitivities of the indices with respect to the parameters (locations, amount, etc.) of shedding schemes are not easy to analyze.

Although the literature review shows that several voltage stability indices have been proposed recently, the prevailing load shedding schemes still fall into the two categories of undervoltage load shedding schemes and single-port impedance match based load shedding schemes. A comprehensive investigation of these schemes is performed in the next two sections.

2.3 The undervoltage load shedding scheme

Power system voltage stability or security is assessed by off-line operation planning studies, which would perform the off-line power flow on the power system under the selected forecasted contingencies. The results from these studies are loaded into lookup tables to assess the on-line security of the operating conditions and to trigger the pre-designed prevention control actions, such as undervoltage load shedding (UVLS). The above procedure can be described by using a simple double-circuit two-bus power system, as shown in Figure 2.4.

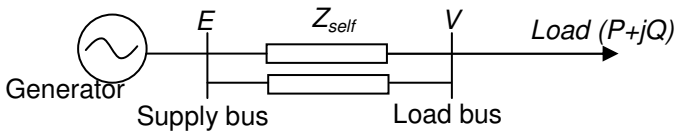

Figure 2.4 A simple double-circuit two-bus power system

In Figure 2.4, E stands for output voltage of the generator, Z_{self} is for the equivalent line impedance, and V is the voltage at the load end ($P + jQ$).

In the past, power systems were lightly stressed and normally operated in a well-structured manner. For this lightly stressed and well-structured two-bus power system, the supply bus can be treated as infinite generation bus (slack bus), so that E remains constant for all operating points. The disturbance to be studied here is

the contingencies of the transmission lines (one line is in outage), which can be described by the changes in line impedance. Power flow calculations can be made on these contingency cases. The results are then plotted as PV curves, as shown in Figure 2.5. Based on the obtained PV curves, the stability level is examined and UVLS are designed.

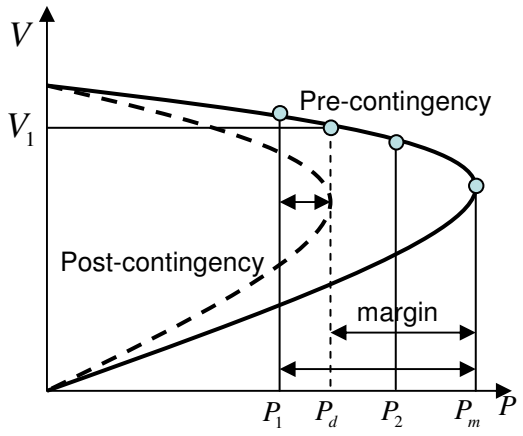

Figure 2.5 Off-line PV curves on contingencies studies and UVLS setting

Figure 2.5 shows a set of PV curves for the base case and line contingency case of the power system in Figure 2.4. Because the load level P_2 is greater than the transfer limit P_d of the post-contingency case, voltage collapse will most likely happen if the line contingency occurs when the system is operating at the P_2 load level.

To prevent voltage collapse, on-line UVLS schemes are designed. Based on Figure 2.5, the UVLS should be triggered when the normal operating bus voltage

is less than V_1, which indicates the transmission limit of the post-contingency operation scenario. This procedure describes the basic principle of the off-line voltage stability monitoring and control. However, some other criteria should also be considered to design the load shedding.

The above description would suggest that it is easy to design a UVLS for a simple power system such as is depicted in Figure 2.4. However, modern power systems are heavily stressed and have numerous combinations of operating conditions. The number of disturbances that need to be investigated has increased enormously. Unlike the number of contingencies in the system shown in Figure 2.4, the number of contingencies for a real power system can be very large, if not infinite, especially for a large-scale interconnected power system. Furthermore, the supply-bus cannot be treated as slack bus any more due to the capacity limitation on the generators and the long-distance transmission caused by opening of the electricity market.

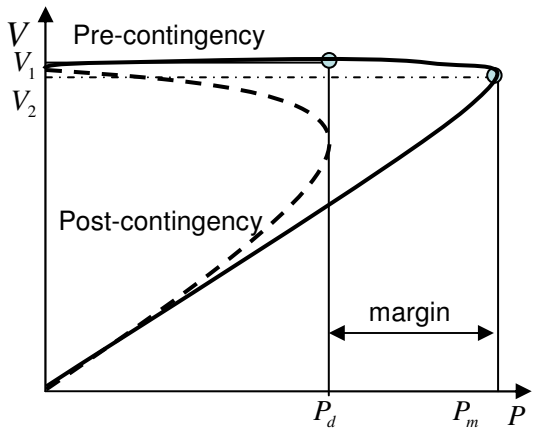

Figure 2.6 Flattened PV curves due to heavy use of reactive power supports

Moreover, the shunt compensations, which are used to improve the capability of the transmission network, and other various reactive power supports are heavily used in power systems. The excessive use of these devices brings the voltage at the nose point close to the voltage at the nominal operation point (i.e. the voltage is flattened). As shown in Figure 2.6, the bus voltage V_1 is very close to the normal value. However, it is the voltage below which the undervoltage load shedding should be in action. The closeness between V_1 and the normal bus voltage makes it very difficult to deal with the voltage threshold settings of UVLS, which have to ensure security and reliability simultaneously. Neither voltage level alone nor off-line studies are a good way to assess the security of the operating point. More details on the limitations of UVLS can be found in [18].

2.4 The single-port impedance match based load shedding scheme

In order to overcome the difficulties associated with the UVLS and to prevent modern power systems from voltage collapse, the load shedding schemes based on the voltage stability index mentioned in section 2.2.2 attracted the attention of many researchers. The author of this work is one of them. This section is presented there to fully explain the difficulties faced by this Thevenin equivalent based method. For simplicity, the term "single-port network equivalent" is adopted to describe the various schemes derived from the impedance matching theorem in this thesis.

A general load shedding scheme using the single-port network equivalent is described as follows:

1) One of the load buses (the monitored bus) is separated from the system and the rest of the system is treated as a Thevenin equivalent circuit, as shown in Figure 2.2.
2) The impedance matching theory is applied to predict the voltage stability margin at the studied bus.
3) Load shedding is triggered if the estimated voltage stability margin is below a certain threshold.

The last two steps are straightforward. However, in the first step, the circuit parameters (E_{eq} , Z_{eq}) are really hard to obtain. Based on the Thevenin theorem, these two parameters can be obtained by (2.2) and (2.3).

$$Z_{eq} = \frac{V_k - V_k^{'}}{I_k^{'} - I_k} \tag{2.2}$$

$$E_{eq} = Z_{eq} I_k + V_k \tag{2.3}$$

where V_k and I_k are the load voltage and load current phasors measured at time t , while $V_k^{'}$ and $I_k^{'}$ are measured at time $t^{'}$, and $t = t^{'} + \Delta t$

The above equations seem simple and faultless. However, they require one assumption. The assumption is that the Thevenin equivalent parameters do not

change during the movement of the power system from t to t' [31]. Such a requirement can hardly be satisfied as power systems always change, especially during the process of voltage collapse. When voltage collapse is approaching, the power system would experience continuous and consecutive changes such as line tripping, shunt capacitor switching, and reaching generators' reactive power output limits, etc. To make the above assumption valid, the time interval ($t - t'$) between the two consecutive measurements at local buses should also be small enough. However, if the two measurements are too close to each other, it may result in a large calculation error since the estimation process may experience an extremely small value of the denominator in (2.2).

A sample power system shown in Figure 2.7 will be used to investigate the problem of the single-port impedance match based method. The system parameters are Vs = 1.0; X_1 = 0.2; X_2 = 0.3; P_{1max} = 2.5, where P_{1max} is the maximum active power transferred to load 1 when P_2 = 0. The investigation was approached in three steps with an increased accuracy in modeling practical situations:

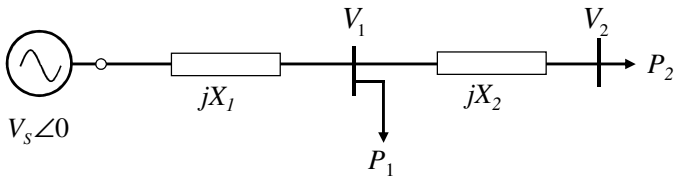

Figure 2.7 Sample power system diagram

- Case 1: P_1 remains constant while P_2 is changed (i.e., increased). The P_2 change is needed to create two states for Thevenin impedance estimation. This case is closest to the assumptions on which the impendence match (*Z*-match) theorem is based. The only difference between this case and the *Z*-match condition is that P_1 is a constant power load in the case, not a constant impedance as required by the Z-match condition. Thus, this case examines the effect of approximating a constant power load as impedance on the margin estimation.
- Case 2: P_1 is increased in proportion to P_2. This case is more representative in terms of voltage stability assessment and is used in the well-established PV-curve-based voltage stability criteria. For example, the voltage stability criteria recommended by WECC/WSCC [32] require scaling up all loads in the study area when the system margin is determined with the PV-curve method. The purpose of this case is, therefore, to examine how well the measurements taken only on bus 2 can handle a realistic margin estimation requirement.
- Case 3: P_1 is increased in proportion to P_2 so that the PV-curve-based criteria are followed. However, the transient load characteristic of P_1 is assumed to be a constant impedance type[1] (The steady-state load characteristic of P_1 remains the constant power type). The reason for considering the transient load characteristic for P_1 is that all impedance estimation algorithms are based on

[1] The transient load characteristic is generally more voltage-dependent than the constant impedance type [33]. For simplicity, this study uses the constant impedance type.

the transient responses of the network seen from the measurement point. Thus, the loads included in the network also respond to its transient characteristics. This more realistic consideration will affect the estimation of Z_{eq}.

The results for the above cases are listed below.

(a) Case 1 result

The results corresponding to case 1 are shown in this section. Figure 2.8 compares the real system margin (which is obtained by using the continuation power flow method in MATLAB) (solid line) with the estimated margin (dashed line) obtained with the *Z*-match method. The figures show a family of curves, each curve representing a different P_1 level. Since P_1 does not change when P_2 increases, a different level of P_1, labeled as P_{10}, is used. Here, the subscript *0* stands for the base case.

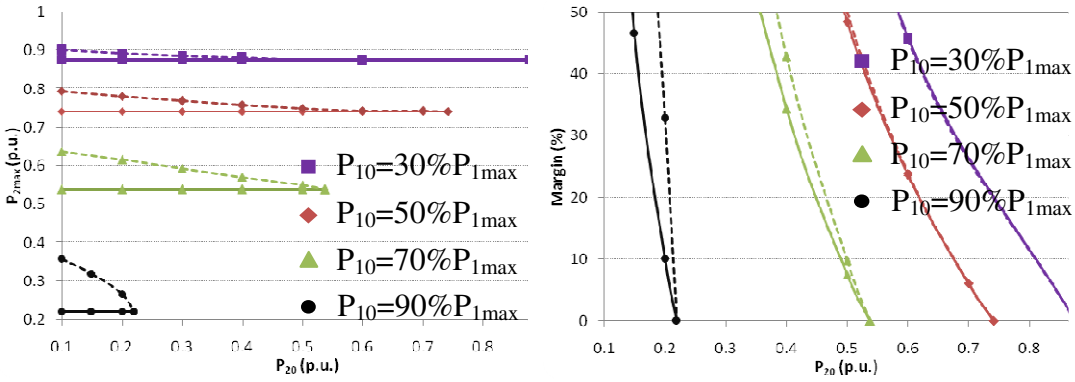

(a) Maximum power can be transferred (b) Power transfer margin at P_2

Figure 2.8 Comparison of maximum power for different base cases (case 1)

Figure 2.8(a) shows the maximum power that can be transferred to bus 2 (P_{2max}) as a function of the base case loading level at bus 2 (P_{20}). According to this figure, the estimated P_{2max} (dashed line) is higher than the actual P_{2max} (solid line). As expected, the difference (i.e., error) changes with the load level at bus 1. Figure 2.8(b) is based on the same data but is plotted in the form of the power margin versus the base load level at bus 2. This figure shows that the estimated margin is higher than the true margin, especially when the load at bus 1 is high.

(b) Case 2 results

In this case, both P_1 and P_2 are increased proportionally from their respective base levels. Again, the solid line represents actual results and the dashed line represents the estimated results. Figure 2.9(a) and Figure 2.9(b) reveal that the estimated P_{2max} becomes less than the true P_{2max}. An underestimation of the load margin occurs, leading to premature load shedding.

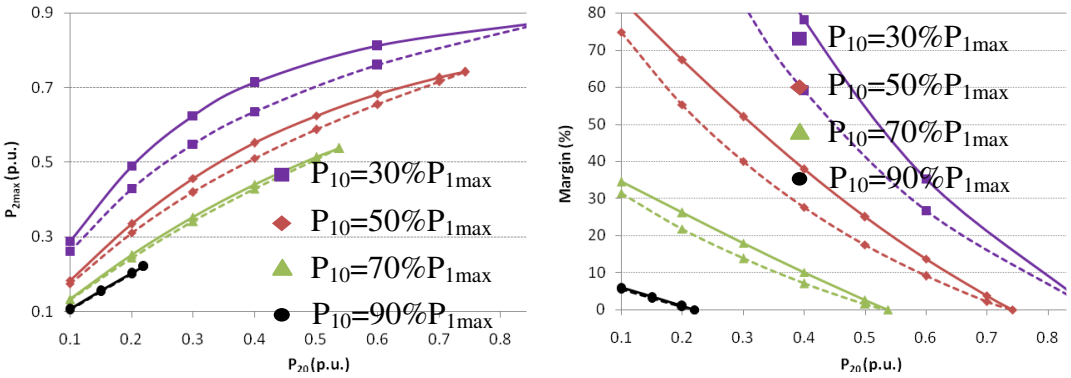

(a) Maximum power can be transferred (b) Power transfer margin at P_2

Figure 2.9 Comparison of the maximum power for different base cases (case 2)

(c) Case 3 results

This case is similar to Case 2. The only difference is that the estimated Z_{eq} is different because any change-based impedance measurement method can measure only the impedance produced by the transient load characteristics. Figure 2.10(a) and Figure 2.10(b) show that the estimated P_{2max} is significantly higher than the actual P_{2max}. This result will create a false sense of security, and the loads will not be shed sufficiently, especially when load P_1 is large.

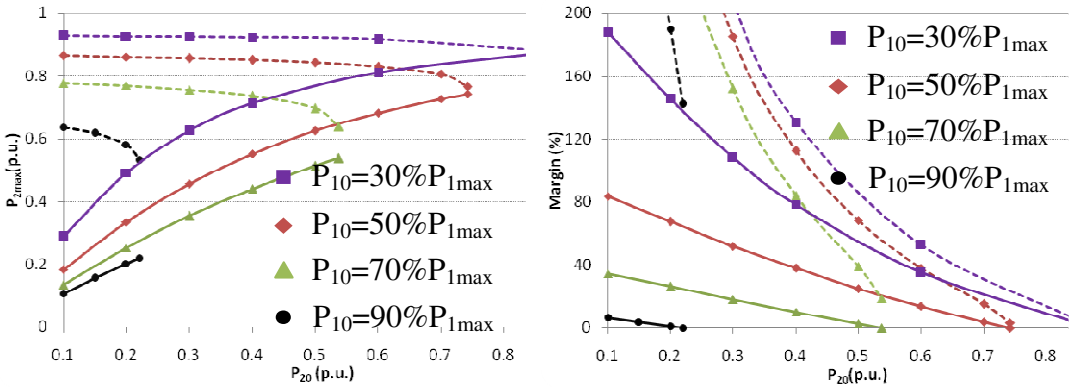

(a) Maximum power can be transferred (b) Power transfer margin at P_2

Figure 2.10 Comparison of maximum power for different base cases (case 3)

The case studies have shown that significant errors of margin estimation occurred in all cases. More simulations have been done on several IEEE test systems. The results can be found in [34]. All these results show similar phenomena as observed in the sample power system. We can, therefore, conclude that the

single-port impedance match based method does not work properly for power systems, which are generally multi-loaded.

Most researchers have tried to resolve the above problem by using various advanced numerical algorithms. For instance, reference [13] uses Tellegen's theorem to simplify the procedure of determining the Thevenin parameters. A real-time adaptive identification method is presented in [35]. However, the performance of those recently proposed methods is not commonly accepted [15-17]. Research is still needed to bring a satisfactory solution.

2.5 Summary and conclusions

A comprehensive study of the voltage stability indices was conducted in this chapter. The difficulties associated with the traditional undervoltage load shedding schemes are discussed in detail. Many advanced voltage indices have been proposed in recent years. The schemes involving impedance matching theory are very promising in terms of simplicity and practicality.

The most important feature of single-port network equivalent lies in using only the measurements at local buses. This feature makes its application possible with independent relays to monitor the approaching voltage collapse at interested buses.

Unfortunately, this important feature is also one of the main drawbacks of this single-port network equivalent. In the process of converting a power system to a

single-port network equivalent, an assumption is required. The assumption is that the power system remains unchanged during two or more consecutive measurements taken at the bus being studied. Such an assumption can hardly be justified during the process of voltage collapse as the power system would experience continuous changes. The two consecutive measurements have to be taken within a very short time interval in order to make the assumption valid. However, the risk of *0/0* error may fail the calculation if the interval is too short.

Many attempts have been made to resolve the aforementioned difficulty, utilizing advanced numerical techniques. Despite their performance, these advanced numerical techniques make the single-port network equivalent lose its simplicity. Instead of exploring these numerical techniques, this thesis is more focused on the topology level to overcome the difficulties faced by the single-port network equivalent. A new topology called multi-port network equivalent is proposed in the next chapter.

Chapter 3

The proposed multi-port network equivalent

The difficulties associated with the prevailing load shedding schemes motivated the author to explore a new voltage stability monitoring method. The new method should be based on the impedance matching theory in order to adopt the advantages of the single-port impedance match based method. However, it should also be able to overcome the difficulties encountered by that method.

With the help of modern measurement technologies (such as PMUs and SCADA), a multi-port network equivalent is proposed. It can effectively overcome the difficulties related to determining the Thevenin equivalent parameters. Since it is a new topology to represent power systems, there are no available approaches to be used for monitoring voltage collapse. This chapter investigates the characteristics of the multi-port network equivalent and proves its capabilities of accurate voltage stability monitoring.

3.1 Introduction

Due to its simplicity and practicality, the impedance match based method has more advantages than other types of algorithms. Many advanced numerical algorithms have been attempted to resolve the difficulties related to estimation of the Thevenin equivalent parameters, but their performance is not well accepted.

These advanced numerical techniques result in the single-port network equivalent losing its main advantage, which is simplicity. Instead of exploring the advanced numerical techniques, this chapter focuses on the topology level to overcome the difficulties faced by single-port network equivalent. After analyzing the characteristics of power system components in terms of linearity, a new topology called the multi-port network equivalent is proposed.

Thanks to modern measurement technologies (such as PMUs and SCADA), the proposed multi-port network equivalent can easily be obtained. By considering the system-wide information, the multi-port network equivalent can straightforwardly determine the Thevenin equivalent for each load bus. Compared to the single-port network equivalent, it only needs one snapshot measurement. Thus, it does not have the numerical problem inherently associated with the single-port network equivalent based methods.

Since it is a new topology, there are no available approaches to be used for voltage stability monitoring. Moreover, even how to use it to properly model the power systems remains to be discovered. This chapter introduces the concept of multi-port network equivalent. Then, the characteristics of the multi-port network equivalent are investigated at length. The results indicate that the multi-port network equivalent can be compared to polyphase power systems with regard to the coupling effects between each individual load. A concept called “coupled single-port network equivalent” results.

The characteristics of the coupled single-port equivalent are further studied to facilitate design of a voltage stability monitoring scheme. The concept of coupling voltages is then presented and its characteristics are investigated by using three different models: virtual voltage source, virtual impedance, and virtual load. The virtual impedance model is chosen in this work and that choice is theoretically explained and verified by using several test power systems.

3.2 The multi-port network equivalent

Theoretically, the impedance matching-based voltage stability monitoring method is faultless and should be highly recommended. However, in reality it is very difficult to obtain the required Thevenin equivalent parameters. This thesis focuses on improving the performance of impedance matching based method by changing the topology of the single-port network equivalent. The topology of the single-port network equivalent is depicted in Figure 3.1. In the equivalent, all the loads except the studied load are included in the system equivalence.

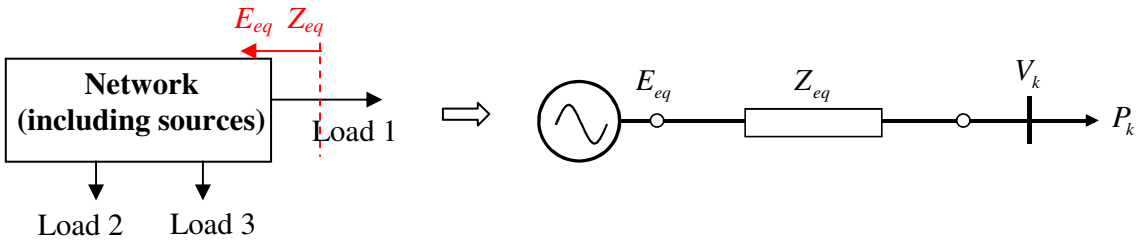

Figure 3.1 The topology of the single-port network equivalent

The definition of the Thevenin theorem is that,

> *A network consisting of **linear elements** with a pair of accessible terminals can be represented by an equivalent circuit with a voltage source and a series resistance (impedance).*

According to the load characteristics discussed in Chapter 1, the loads are inherently nonlinear in terms of the relationship between the supplied voltage and current, even at the steady-state operating condition. Figure 3.2 clearly shows the nonlinear characteristics of the loads.

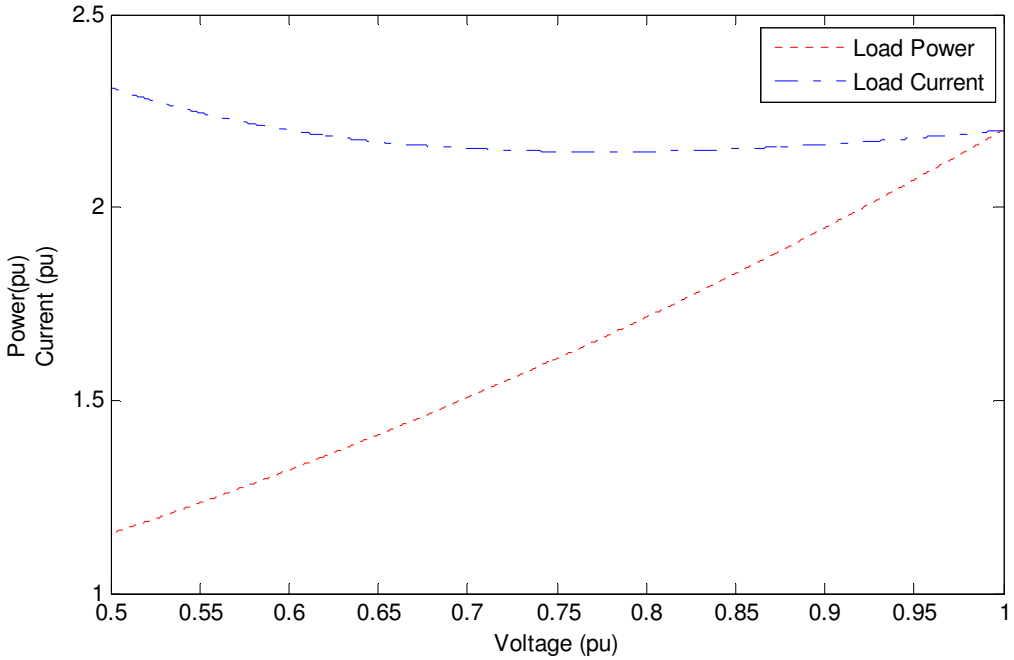

Figure 3.2 Nonlinear relationships between voltage and current of the load at steady-state

The conflict between the Thevenin theorem and the nonlinear characteristics of the power system components indicates that it is thorny to use the topology of single-port network equivalent. It is not surprising to see that voltage stability margin can be easily over- or under- estimated based on the impedance matching condition. This fact also confirms the findings described in the previous chapter. It would be more suitable to apply the impedance matching theory to a new topology explicitly considering the nonlinear components in power systems.

Technically speaking, all the components in power systems are nonlinear.[1] However, based on their behavior during operations, they can be classified as follows:

1) Loads: typically nonlinear as discussed.

2) Reactive power supports, such as switched shunts and SVCs.

Due to the slow action of the switched shunts, the single-port network equivalent can easily deal with them by using fast sampling and proper numerical algorithms. However, the power electronics-based reactive power supports, such as SVCs and STATCOM, act too fast to be handled by the single-port network equivalent without inducing problems. They can be modeled as generators with zero active power output because they are designed to control the bus voltage constant.

[1] The linearity mentioned here refers to the relationship between the terminal voltage and current of the devices.

3) OLTCs

The OLTCs are generally slow response devices. They are easily modeled by using piece-wise linear method or can be merged into the loads since they are usually connected close to the load centre.

4) Generators

The generators could be considered a constant voltage source, as long as they do not reach their reactive power output limit. Even when a generator reaches its reactive limit, it can be modeled as a constant voltage source behind constant internal impedance.

5) The transmission lines: typically linear.

6) Protection devices

These devices normally operate at ON/OFF states. They are monitored by the Supervisory Control and Data Acquisition system (SCADA). The information about their status can be used to notify the network topology changes. However, the devices themselves do not need to be modeled during the process of system equivalent.

In summary, among all the components of a power system, only the loads and generators manifest evidently nonlinear characteristics. The other devices are

either linear or can be linearised with the help of SCADA. For example, the switched shunt is normally a capacitor bank. If there is no switching action, the capacitance will be a constant value. If there are any switching actions (which can be notified by SCADA), the capacitance will be changed to another constant value. Thus, as long as the new network equivalent could take these changes into account, it should be able to model power systems more accurately.

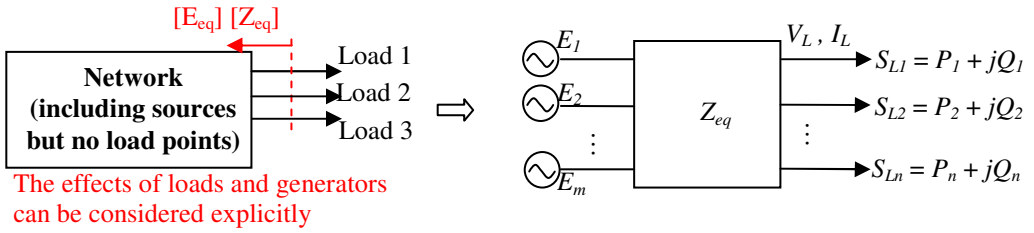

Figure 3.3 The topology of a multi-port network equivalent

In this study, a new network equivalent topology called "multi-port network equivalent" is proposed to triumph over the conflict faced by the single-port network equivalent method. The topology of the new multi-port network equivalent is shown in Figure 3.3. All the generators and loads (including power electronics based devices, such as SVCs) are separated from the transmission network. The transmission network, including the switched shunts and the protection devices, is modeled as an impedance matrix. The impedance matrix describes the topology and the status of transmission lines, the switched shunts, and other linear devices. The information on the topology and the status can be obtained from SCADA, which is generally available for modern power systems.

With the multiport network equivalent, the power system can be described by (3.1).

$$[V_L] = K[E] - [Z_{eq}][I_L] \tag{3.1}$$

where $[E] = [E_1 \quad E_2 \quad \cdots \quad E_m]^T$ is a vector with all voltage phasors at the generator buses, $[V_L] = [V_{L1} \quad V_{L2} \quad \cdots \quad V_{Ln}]^T$ and $[I_L] = [I_{L1} \quad I_{L2} \quad \cdots \quad I_{Ln}]^T$ are vectors of voltage and current phasors at the load bus, respectively. K and $[Z_{eq}]$ are obtained from power system admittance matrix (Y).

Equation (3.1) can be derived based on Kirchhoff's law for the node of generators and loads. The following equations show how (3.1) is obtained from generator voltage E and the system admittance matrix Y.

$$\begin{bmatrix} I_G \\ -I_L \end{bmatrix} = [Y] \begin{bmatrix} E \\ V_L \end{bmatrix} = \begin{bmatrix} Y_{GG} & Y_{GL} \\ Y_{LG} & Y_{LL} \end{bmatrix} \begin{bmatrix} E \\ V_L \end{bmatrix} \tag{3.2}$$

From equation (3.2), we get:

$$V_L = -Y_{LL}^{-1} I_L - Y_{LL}^{-1} Y_{LG} E \tag{3.3}$$

Let

$$Z_{eq} = Y_{LL}^{-1}, \qquad K = -Y_{LL}^{-1} Y_{LG}$$

Thus, the following can be obtained:

$$V_L = -Z_{eq} I_L + KE = -Z_{eq} I_L + E_{eq} \tag{3.4}$$

Since the system admittance matrix Y can be obtained from SCADA, the matrix Z_{eq} and $[K]$ can be easily obtained. The other parameter $\lfloor E_{eq} \rfloor$ of the multi-port equivalent network can be calculated by either of the following equations.

$$\lfloor E_{eq} \rfloor = K[E] \tag{3.5}$$

$$\lfloor E_{eq} \rfloor = [V_L] + \lfloor Z_{eq} \rfloor [I_L] \tag{3.6}$$

Equation (3.5) is used if the voltages at all the generators can be obtained from PMUs. Otherwise, equation (3.6) should be used if the measurements at the load buses can be easily taken.

The above equations indicate the following useful features of the proposed multi-port network equivalent:

a) It only needs one snapshot of the measurements. Therefore, it does not need any assumptions to get an accurate multi-port network equivalent model of power systems.

b) It eliminates the need for estimating the Thevenin equivalent impedances, which is the main difficulty associated with the single-port network equivalent based methods.

c) The multi-port network model takes advantage of modern information technology. It utilizes the global network information (network *Y* matrix from SCADA) and wide-area measurements. The voltage stability monitoring scheme based on this multi-port network model would be more informative.

Table 3.1 shows the comparison features between the single-port network equivalent and the proposed multi-port network equivalent.

The multi-port network equivalent clearly shows the advantages in terms of estimating the circuit parameters, i.e. the voltage source and the impedance matrix. Instead of using two or more consecutive measurements and assuming that power systems do not change during these measurements, the multi-port network equivalent needs only one snapshot of measurement. Then the circuit parameters can easily be calculated without bothering with complicated numerical algorithms.

Table 3.1 Features of single-port and multi-port network equivalent

Features	**Single-port equivalent**	**Multi-port equivalent**
Assumptions	The network is unchanged between two consecutive measurements	No assumption is needed
Number of measurement snapshots	At least two	One
Effort to calculate circuit parameters	Advanced numerical algorithms are needed	Simple matrix calculation theory is enough
Measurements	Local phasors	Phasor measurements at generator stations and interested load stations
Voltage collapse detection ability	Localized index	Globalized index

Despite the fact that the equivalent can be straightforwardly obtained, there are difficulties in terms of how to use this equivalent to fulfill the task of voltage stability monitoring. For the single-port network equivalent, the impedance matching theory is perfectly fit to estimate the maximum load power, which in turn can be used as a voltage stability index. However, there are no available theorems to deal with the multi-port network equivalent.

The impedance matching theorem, also known as the maximum power theorem, states that, to obtain the maximum external power from a source with a finite

internal resistance, the resistance of the load must be the same as that of the source [36]. When it comes to power systems (where the power factor of the load normally remains constant), the maximum power is transferred when the magnitude of the load impedance is equal to the magnitude of the system side impedance [37]. The single-port network equivalent can simply adopt the theorem to identify whether the current operating condition is approaching voltage collapse or not.

$$\left|Z_{Load}\right| = \left|Z_{system}\right| \tag{3.7}$$

where Z_{load} and Z_{system} are the impedance of the load and the impedance of the power system, respectively.

The multi-port impedance match theorem could be a perfect theoretical basis of voltage stability monitoring schemes. However, an extensive literature survey reveals that:

1) The multi-port impedance match was investigated extensively in the early 1970's [38-44].

2) The research on multi-port impedance match was focused on the best network configuration under which the maximum power transfer can be obtained.

3) The theories developed can not be applied to the case of power systems, in which the transmission networks already exist and can not be easily reconfigured.

Therefore, the multi-port impedance matching theorem developed in those references is only suitable for the electric circuit design or may be useful for power system planning. The multi-port impedance matching theorem is similar to the one used in single-port network equivalent, except that it requires that the load impedance matrix is equal to the transpose conjugate of the impedance matrix of power systems [44].

$$[Z_{load}] = [Z_{system}]^{*} \tag{3.8}$$

where $[Z_{load}]$ and $[Z_{system}]$ are the impedance matrix of the load and the impedance matrix of the power system, respectively. The superscript * stands for the method of conjugation.

These findings make it necessary to develop an alternative approach to solve the multi-port network equivalent. The alternative approach should be able to make use of the impedance matching theory. Moreover, it should be simple enough to be suitable for practical applications.

3.3 Characteristics of the coupling effects

In order to develop an algorithm to solve the multi-port network equivalent, a better understanding of the characteristics of the equivalent in the field of a power system is required. Thus, the objective of this section is to investigate its unique characteristics. The investigation reveals that the multi-port network equivalent can be compared to the polyphase power systems with regard to the coupling effects between each individual load. A concept called "coupled single-port network equivalent" is presented.

Based on (3.1), a multi-port network equivalent shown in Figure 3.4 is described by (3.9).

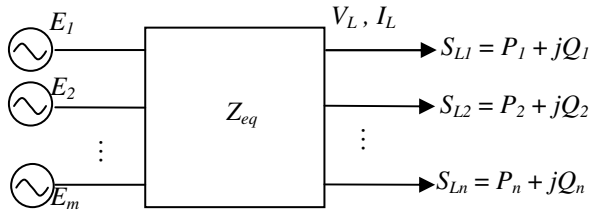

Figure 3.4 A multi-port network equivalent model

$$V_L = KE - Z_{eq} I_L \tag{3.9}$$

For any one of the load buses (without loss of generality, load bus j is chosen), equation (3.10) can be obtained.

$$V_{Lj} = [KE]_j - Z_{eq,jj} I_{Lj} - \sum_{i=1, i \neq j}^{n} Z_{eq,ji} I_{Li} \tag{3.10}$$

where $Z_{eq,jj}$ and $Z_{eq,ji}$ are the $(j,j)^{th}$ element and the $(j,i)^{th}$ element of impedance matrix Z_{eq}, respectively.

Equation (3.10) indicates that there are mutual couplings between each individual load. The multi-port network equivalent is depicted in Figure 3.5.

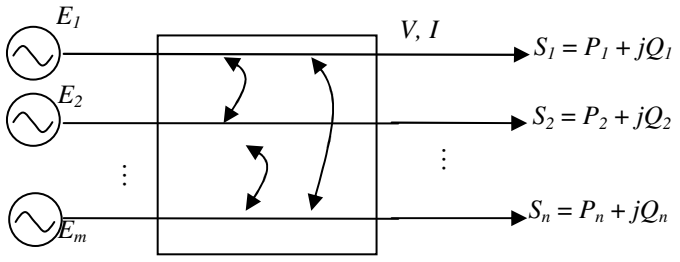

Figure 3.5 A multi-port network model with mutual couplings

Furthermore, equation (3.10) can be rewritten as equation (3.11).

$$V_{Lj} = E_{eq,j} - Z_{eq,jj} I_{Lj} - E_{coupled-j} \tag{3.11}$$

where $E_{coupled-j} = \sum_{i=1,i\neq j}^{n} Z_{eq,ji} I_{Li}$ denotes the coupling effects imported by the other loads on the load bus j.

Thus, based on (3.11), an equivalent circuit for load bus j can be constructed as shown in Figure 3.6.

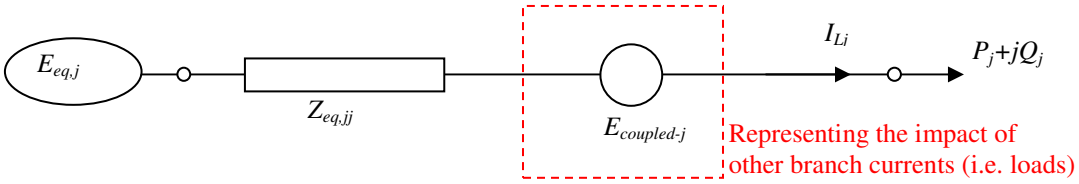

Figure 3.6 An equivalent circuit for load bus j

Compared to the single-port network equivalent, the new equivalent circuit lies mainly on the new term $E_{coupled-j}$ to represent the impact of other loads. It is worth mentioning that the new term is the only unknown variable in Figure 3.6. Using the coupling term $E_{coupled-j}$, the multi-port network equivalent can be broken down into a set of single-port networks. These new single-port networks have the impact (coupling effects) of other loads explicitly included (see Figure 3.7). Since there is a coupling term in each single-port network, the new single-port network equivalent is called a "coupled single-port network equivalent" in this study.

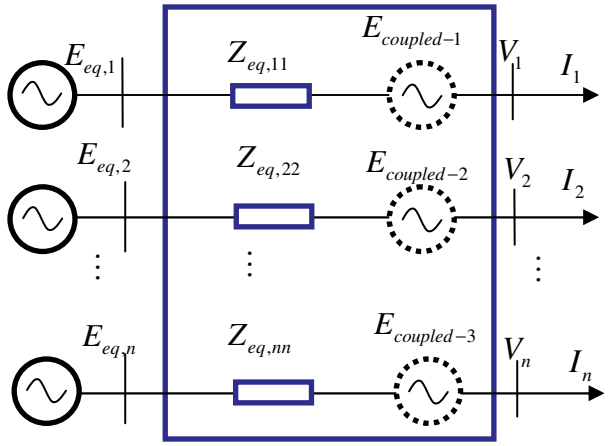

Figure 3.7 The multi-port network equivalent with coupling effects

In order to develop a voltage stability index for this coupled single-port network equivalent, the characteristics of the equivalent voltage source $E_{eq,j}$ and the coupling effect $E_{coupled-j}$ should first be understood. The impedance $Z_{eq,jj}$ can be computed from the network *Y* matrix and does not change with power systems' power flow patterns; therefore there is no need to investigate its characteristics.

The equivalent voltage source $E_{eq,j}$ is calculated based on the voltage phasors at all the *PV* buses of the power system, as described by equation (3.12).

$$E_{eq,j} = [KE]_j \tag{3.12}$$

The matrix K is computed from the network admittance matrix *Y* and as a result does not change with power systems' power flow patterns. Meanwhile, the voltages at the *PV* buses are controlled by generators' AVRs or other voltage

controllers. They maintain constant magnitude as long as the reactive power output of the generators is within the limit.

However, the coupling effect $E_{coupled-j}$ highly depends on the system's power flow patterns, as indicated by (3.13).

$$E_{coupled-j} = \sum_{i=1, i\neq j}^{n} Z_{eq,ji} I_{Li} \tag{3.13}$$

In equation (3.13), although the impedance $Z_{eq,ji}$ does not change, the load current I_{Li} could change a lot during the power system operation, especially when the loads of some specific areas are in the recovery mode.

The IEEE 30 bus system [45] is used to investigate the characteristics of both the equivalent voltage source and the coupling effects for each load bus. The following conditions are considered during the investigation:

a) All the loads are increased proportionally from their respective base loading levels with the same scaling factor λ following the standard *PV* curve approach. This uniformly increasing load pattern is widely used in the power industry [46].

b) The equivalent voltage source $E_{eq,j}$ and the coupling effect $E_{coupled-j}$ are computed corresponding to each λ. Thus, the evolution of these two parameters can be observed.

The results are illustrated in Figure 3.8 and Figure 3.9. Each curve in these two figures illustrates the equivalent voltage source or the coupling effects associated with one individual load bus.

It can be seen in Figure 3.8 that all equivalent voltage sources remain relatively constant from the base loading level $(\lambda = \lambda_0 = 1)$ to the maximum loading level $(\lambda = \lambda_{\max} = 2.95)$, which denotes the nose point of the *PV* curve. These results verify the conclusions obtained from equation (3.12). Consequently, it is reasonable to assume that the equivalent voltage source remains constant as long as there is no generator running over limit. The closer the operating point is to the maximum loading, the more accurate the approximation is.

The coupling effects, on the other hand, change dramatically with increasing the loading level, as shown in Figure 3.9. The implication is that the main factor causing voltage collapse is the reduction of the total voltage $(E_{eq,j} - E_{coupled-j})$ seen by the load bus due to rapid increase of the coupling effect. These findings confirm the suspicions in section 3.2, namely that the impact of other loads on the studied load bus must be considered.

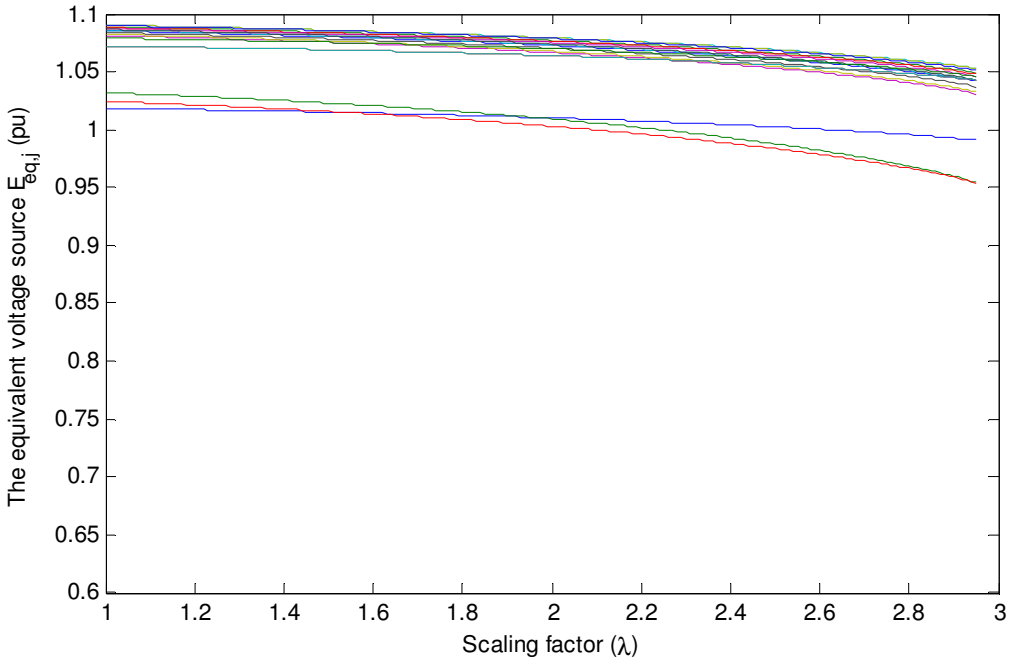

Figure 3.8 The characteristics of equivalent voltage source $E_{eq,j}$

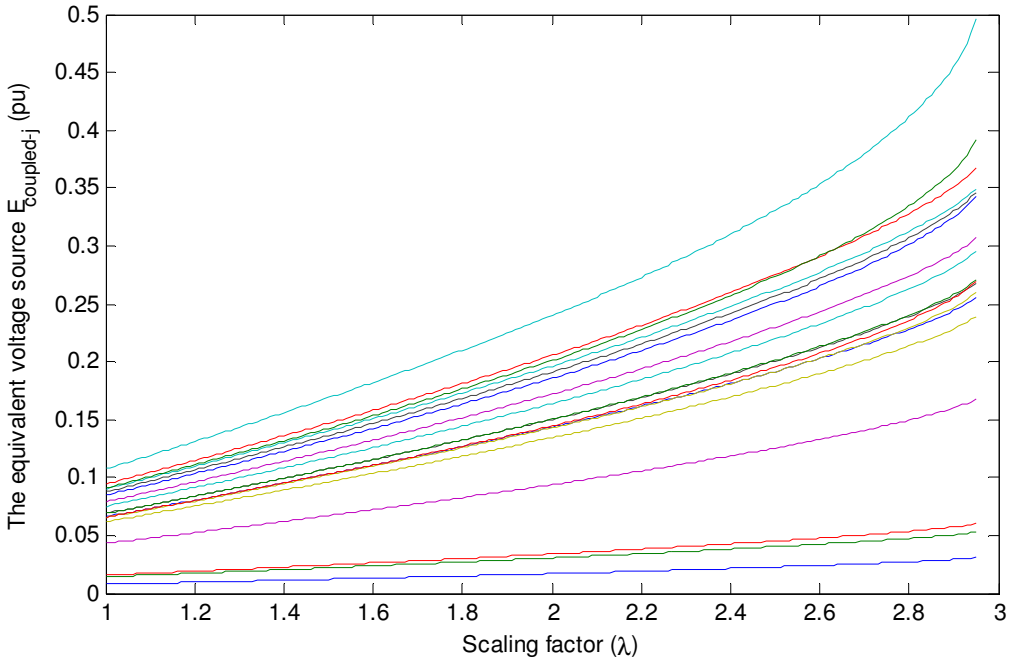

Figure 3.9 The characteristics of coupling effects $E_{coupled-j}$

To fully understand the voltage reduction impact, the projection of $E_{coupled-j}$ on its corresponding $E_{eq,j}$ is also studied and shown in Figure 3.10. The results in Figure 3.10(a) show that the projection of $E_{coupled-j}$ in the direction of the equivalent voltage source $E_{eq,j}$ increases dramatically when the power system approaches its voltage stability limit. Since this projection is in the direction of the voltage source, it acts as a negative voltage source. It significantly decreases the voltage level seen from the load buses. As a result, the network transmission capability is drastically decreased.

On the other hand, the perpendicular projection of the coupling effects $E_{coupled-j}$ on the equivalent voltage source also increases with increasing the loading level. Considering that the power factor of the load is usually close to 1 and the phase angle difference between the receiving-end bus voltage (load bus) and the sending-end bus voltage (generator bus) is relatively small under the normal operation condition, this part of the coupling effects acts like a reactive power sink, which would further downgrade the transmission capability.

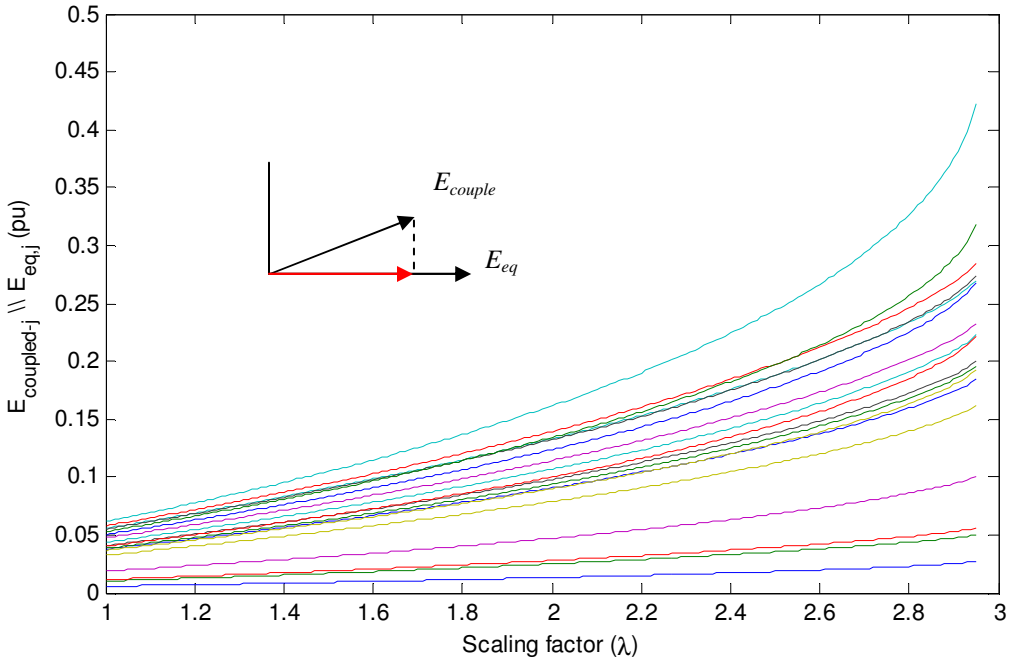

(a) Projection of the coupling effects in the direction of the equivalent source

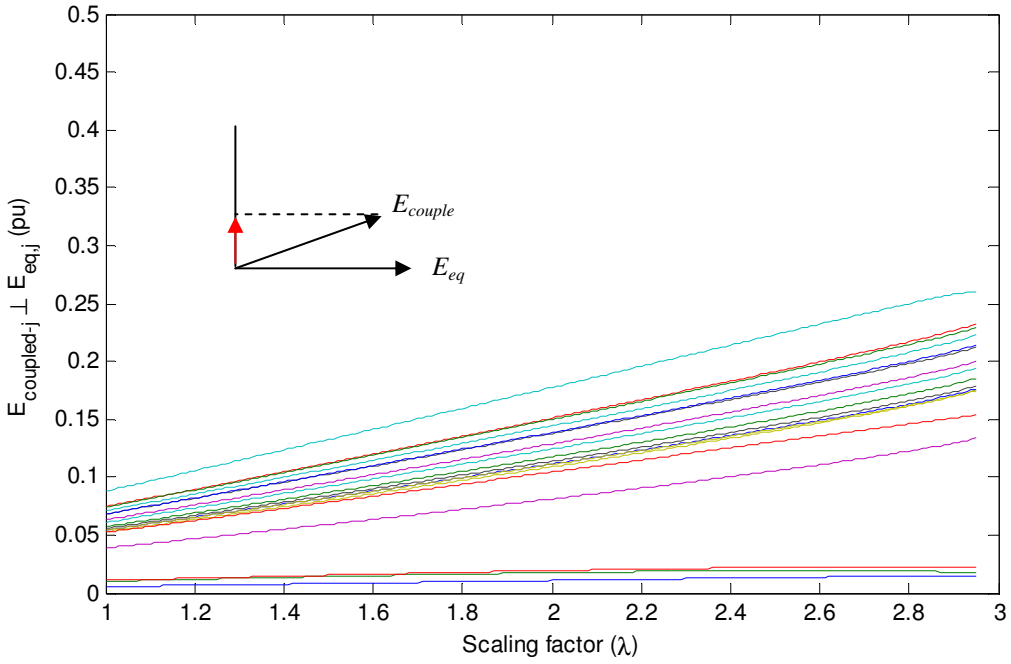

(b) Perpendicular projection of the coupling effects on the equivalent source

Figure 3.10 The projection of the coupling effects on the equivalent source

In summary, the concept of the coupled single-port network equivalent has helped to reveal the interactions between various loads in power systems and how such interactions affect the voltage stability. The results have shown that it is essential to model the coupling effects for accurately monitoring voltage stability in power systems.

3.4 Three different models for the coupling effects

The analysis in section 3.3 indicates that the coupling effects play an important role in the task of voltage stability monitoring. The main objective of voltage stability monitoring is to determine how close the current operating point is to the maximum loading level. Since the known information about power systems is for the current operating point, the voltage stability monitoring method would have to use the current circuit equivalent to anticipate the upcoming behaviour of the system. Thus, there is a fundamental requirement for the voltage stability monitoring method: the parameters of the circuit equivalent should remain nearly constant when increasing the loading levels of power systems.

Now, let us go back to the circuit of the coupled single-port network equivalent, as shown in Figure 3.11. Based on the analysis in section 3.3, the coupling effects are the only changing variables when increasing the loading level for a given power system. Therefore, how to model the coupling effects becomes vital.

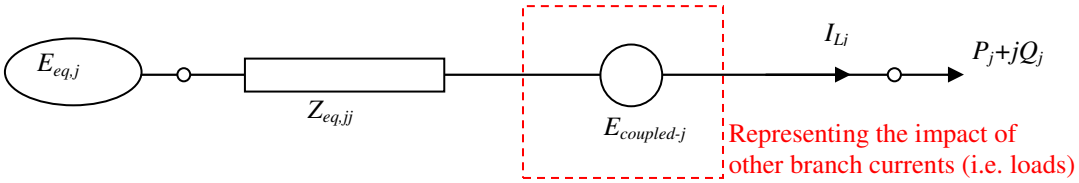

Figure 3.11 Circuit diagram of the coupled single-port network equivalent

For a general electrical circuit diagram, such as the one shown in Figure 3.11, there are three different electrical elements: voltage source, impedance, and load. Three different models are presented in this section to represent the coupling effects.

3.4.1 The virtual voltage source model

This approach is to approximate the coupling effects as an extra voltage source as depicted in Figure 3.12.

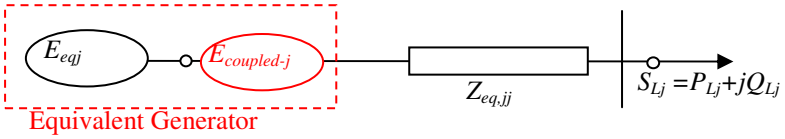

Figure 3.12 Modeling the coupling effects as a virtual voltage source

The virtual voltage source is equal to the coupling effects. Therefore, the voltage E_j at the equivalent generator is described by equation (3.14).

$$E_j = E_{eq,j} - E_{coupled-j} \tag{3.14}$$

The characteristic of the magnitude of voltage E_j is investigated on the same IEEE 30 bus system. The investigation results are shown in Figure 3.13. The large deviation on the voltage E_j with increasing loading level indicates that this model is not acceptable for voltage stability monitoring.

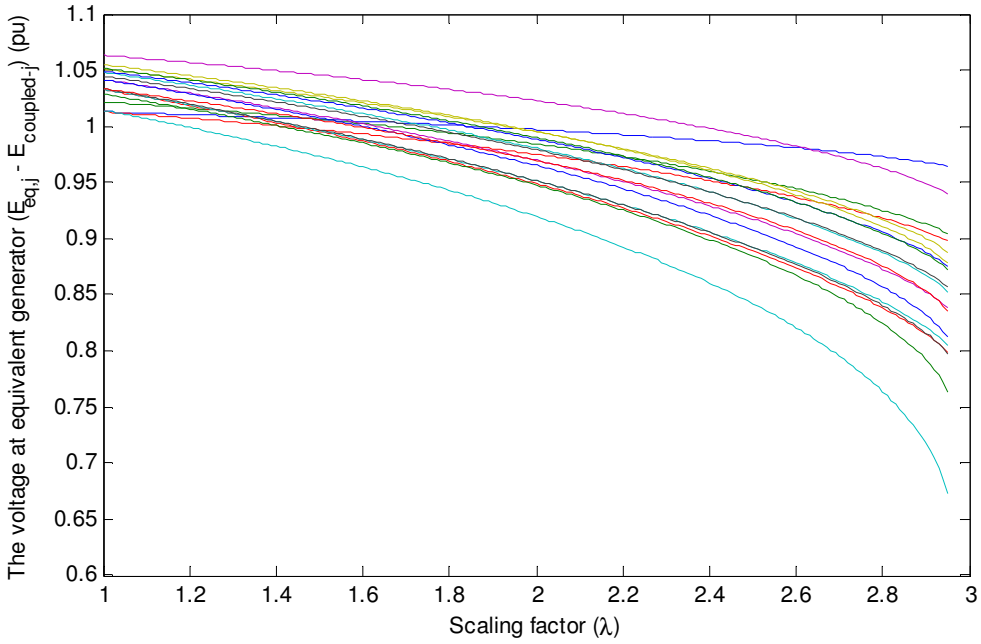

Figure 3.13 The characteristic of the voltage at the equivalent generator

3.4.2 The virtual load model

The virtual load model is to represent the coupling effects by an extra power demand at the load bus. Combining with the real load, an equivalent load is obtained by equation (3.15). The circuit diagram for this equivalent is shown in Figure 3.14. The equivalent load is highlighted by the red dash rectangular.

$$S_{cj} = P_{cj} + jQ_{cj} = E_{coupled-j} I_{Lj}^{*} \tag{3.15}$$

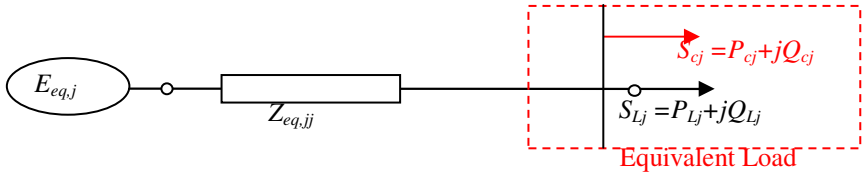

Figure 3.14 Modeling the coupling effects as a virtual load

In the above circuit, the source voltage $E_{eq,j}$ remains relatively constant and the system impedance $Z_{eq,jj}$ stays unchanged as long as there are no network topology changes in power systems. If the virtual load can remain constant or have a linear relationship with respect to increasing the loading level, then this representation should be suitable for voltage stability monitoring. It is worth mentioning here that using virtual load model to estimate the voltage stability margin is similar to the idea presented in [28]. Although these two ideas are moving toward the same objective using totally different approaches, they are

following the same principle, i.e., using a virtual load to represent the effects from other loads.

Figure 3.15 shows the profile of the virtual load when the loading level is increasing. The virtual load increases significantly when the voltage collapse point is approaching. This feature is easy to understand from the perspective of power loss in the transmission network. Many papers [31][47] have proved that the power loss in a transmission system becomes unreasonably high when power systems are operating close to voltage collapse.

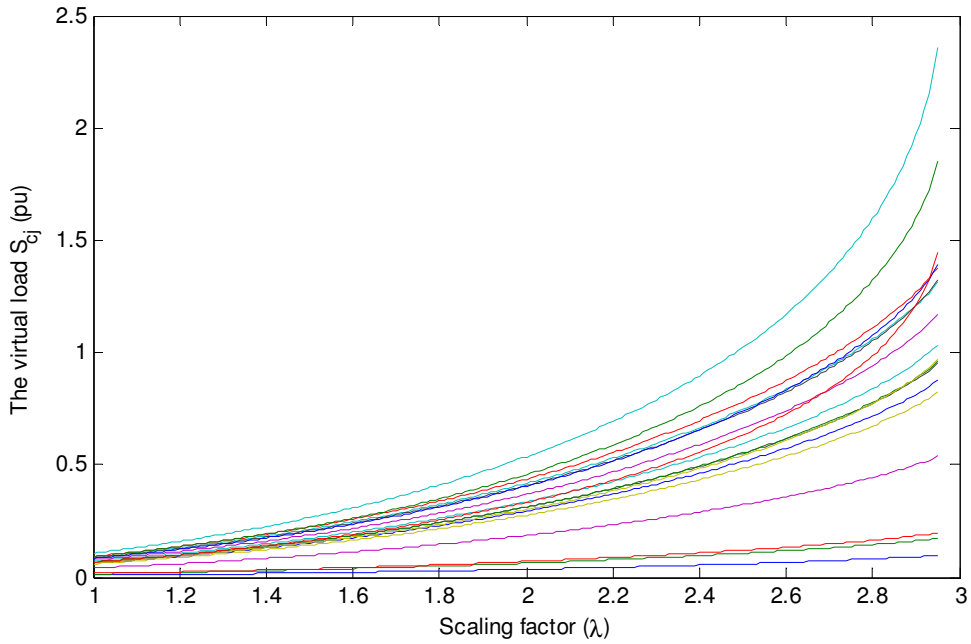

Figure 3.15 The characteristic of the virtual load model

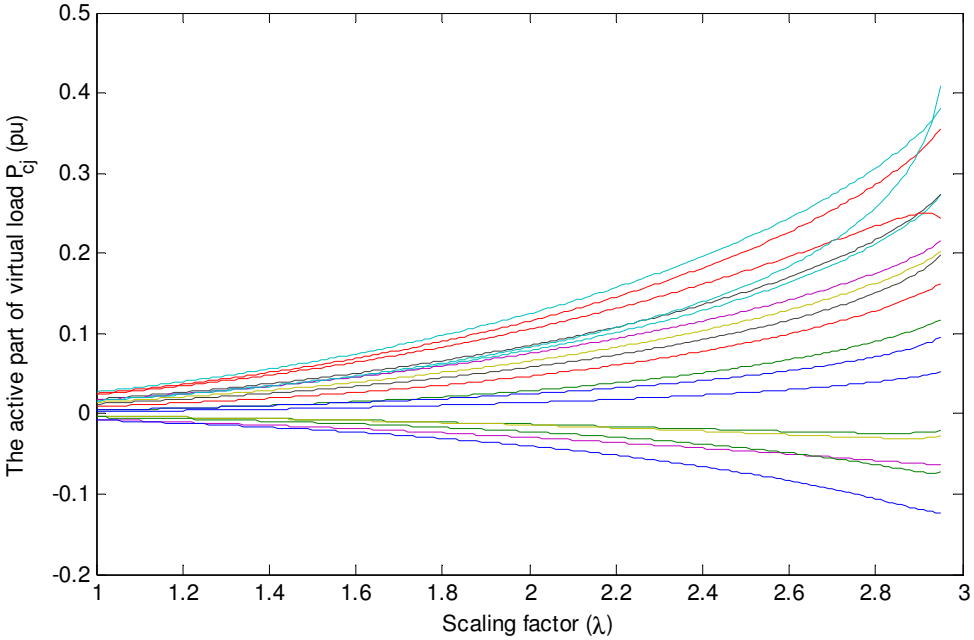

(a) Active power part of the virtual load

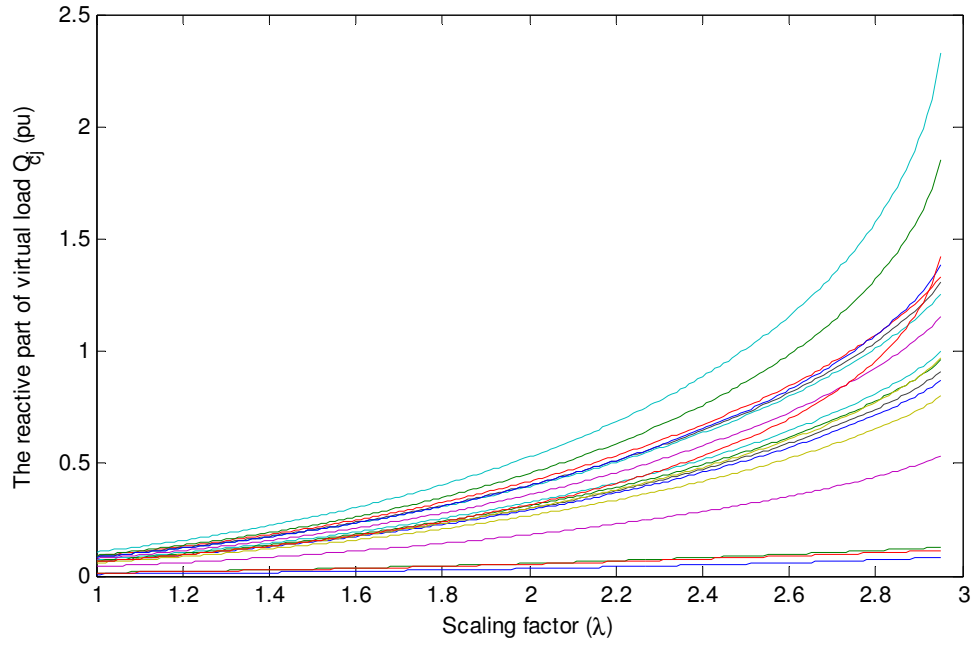

(b) Reactive power part of the virtual load

Figure 3.16 Active and reactive power part of the virtual load

The results of the active and reactive part of the virtual load are also plotted and shown in Figure 3.16. It is interesting to point out that the reactive power changes much faster than the active part. The variation of the reactive power is also much higher than the variation of the active power. This phenomenon verifies the importance of reactive power support. It can also be used as another explanation for the fact that the local reactive power support can significantly improve power system voltage stability.

In summary, the virtual load does not maintain constant during the increase of the loading level. This virtual load model is not suitable for the proposed coupled single-port network equivalent in terms of estimating the voltage stability margin.

3.4.3 The virtual impedance model

Based on (3.16), the coupling effects can be modeled as an extra impedance in the coupled single-port network equivalent. The circuit diagram containing this impedance is depicted in Figure 3.17. Adding the original system impedance and the virtual impedance together, the system equivalent impedance becomes Z_{eq-j} and can be calculated by (3.17).

$$Z_{cj} = \frac{E_{coupled-j}}{I_{Lj}} \tag{3.16}$$

$$Z_{eq-j} = Z_{cj} + Z_{eq,jj} \tag{3.17}$$

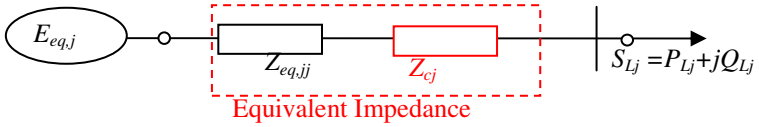

Figure 3.17 Modeling the coupling effects as a virtual impedance

From (3.13) and (3.16), the virtual impedance can be calculated by using the load currents as expressed by (3.18).

$$Z_{cj} = \frac{E_{coupled-j}}{I_{Lj}} = \sum_{i=1, i\neq j}^{n} Z_{eq,ji}\left(\frac{I_{Li}}{I_{Lj}}\right) \tag{3.18}$$

Equation (3.18) indicates that the virtual impedance is the summation of the weighted current ratio, which is division of the current at the other loads with respect to the current at the studied load. The weighting factor $Z_{eq,ji}$ is the mutual impedance between the two loads. The above explanation shows the following two features.

a) The weighting factor (mutual impedance $Z_{eq,ji}$) is highly dependent on how electrically close the two load buses are in power systems.

b) The current ratio can be calculated by (3.19). If the two load buses are electrically close (large weighting factor), then the voltage at the two load

buses should be changing with a similar proportion. Therefore, the current ratio will generally remain constant based on (3.19).

$$\frac{I_{Li}}{I_{Lj}} = \left(\frac{S_{Li}}{S_{Lj}} \times \frac{V_{Lj}}{V_{Li}} \right)^* = a \times \left(\frac{V_{Lj}}{V_{Li}} \right)^* \tag{3.19}$$

where $a = \left(\frac{S_{Li}}{S_{Lj}} \right)^*$ is constant when the loads are increasing with the same scaling factor, which is the widely used power flow pattern in the power industry for operation planning studies [46]. This power flow pattern also describes most of the load recovery processes during and/or after a disturbance in power systems.

Based on the above two features, the virtual impedance should be expected to be relatively constant. To verify the observation, an investigation on the variation of the virtual impedance is conducted by using the IEEE 30 bus system. The results are shown in Figure 3.18, which validates the above theoretical analysis.

Both the theoretical analysis and the simulation results clearly prove that the virtual impedance remains relatively constant when stressing the system. By using this virtual impedance model to represent the coupling effects, the circuit parameters (source voltage $E_{eq,j}$ and system impedance Z_{eq-j}) remain approximately constant. This feature makes it very promising in terms of voltage

stability monitoring. Thus, the impedance matching theorem could be applied to the coupled single-port network equivalents.

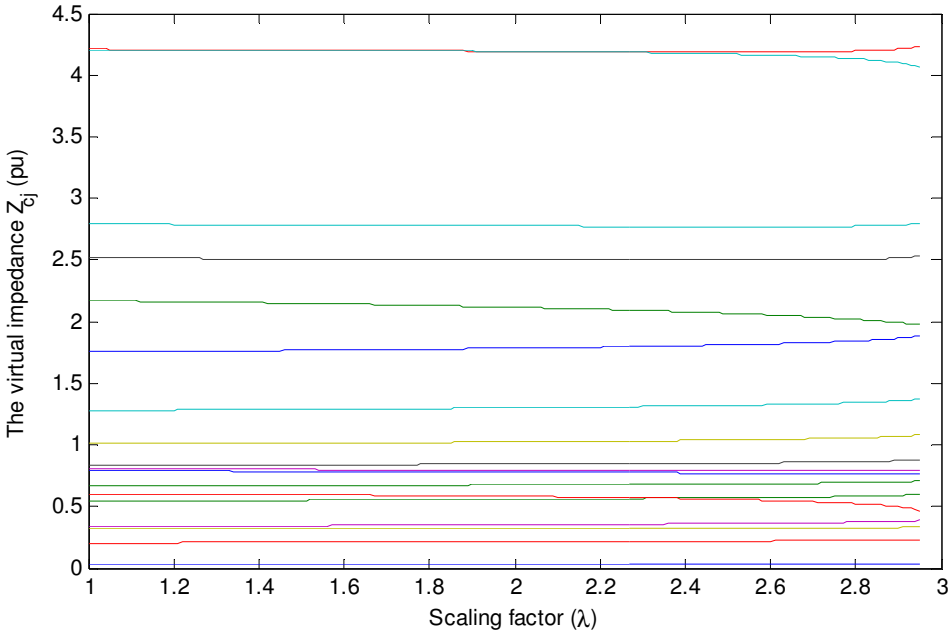

Figure 3.18 The characteristic of the virtual impedance

3.5 Summary and conclusions

With the help of modern measurement technology (PMUs and SCADA), the multi-port network equivalent can effectively overcome the difficulties faced by the single-port network equivalent. However, since it is a new topology, there are no available approaches for monitoring of the voltage collapse. A comprehensive literature review shows that a new algorithm needs to be proposed since there are no available theorems on multi-port impedance matching. In order to develop a

novel voltage stability monitoring technique, the characteristics of the multi-port network equivalent have been investigated in this chapter.

The mathematical description of the multi-port network model suggests that there is mutual coupling between each load in power systems. The coupling effect on a load is the summation of the weighted current from other loads. Thus, the coupling effects increase dramatically when the loads are increased in power systems. During and/or after the disturbances, the loads are trying to recover to their pre-disturbance value through OLTCs or embedded motors. The currents at the load buses become larger and larger during the above process, as do the coupling effects.

By explicitly separating the coupling effects from the voltage drop on the transmission network, a concept called the coupled single-port network equivalent is proposed. The coupled single-port network equivalent is composed of one voltage source, one system side impedance, the coupling effect, and the load. The multi-port network equivalent is broke down into a set of coupled single-port network equivalents.

Since the objective of voltage stability monitoring is to anticipate how close the current operating condition is to the power systems' limits, it is vital to know how the electrical elements change with stressing the power systems. Due to the action of AVRs, the voltages at the generator buses are kept approximately constant as

long as the generator is not hitting its output limit. As a result, the voltage source in the coupled single-port network equivalent is independent of the load patterns. The system side impedance is calculated based on the admittance matrix, which only depends on the network topology. Thus, it remains constant as well (it would be updated once there are network topology changes recognized by SCADA).

On the other hand, the coupling effects experience radical changes during increasing the loading level. Three different models are presented to model the coupling effects. Both the theoretical analysis and the simulation results have proved that the virtual impedance model is the best one in terms of voltage stability monitoring. Using the virtual impedance model, all the equivalent circuit parameters of the proposed model are approximately constant despite the load increasing. Thus, the impedance matching theorem can be applied. The application of the impedance matching theorem to the coupled single-port network equivalent is studied in the next chapters.

Chapter 4

Application of the multi-port network equivalent

The previous chapter studied the characteristics associated with the multiport network equivalent. A coupled single-port network equivalent was also proposed and properly modeled for the purpose of voltage stability margin estimation. The applications of the multi-port network equivalent are developed in this study. Three main applications including load shedding oriented voltage stability monitoring, the weak bus identification, and a novel algorithm to minimize the amount of load shedding, are described in this chapter.

The impedance matching theorem is applied to each coupled single-port network equivalent. Consequently, the maximum power that can be transferred to each load bus is obtained. The scaling factor (the ratio between the maximum power and the power at the base case) of that load bus is then calculated.

To consider the actions of switched shunts and the effect of generator over excitation limiters (OEL), a continuation power flow (CPF) method with a new predictor/corrector is also presented. The predictor is the estimated scaling factor obtained from the impedance matching theorem. The advantage of the presented CPF method is that it searches for the maximum scaling factor with little computation effort.

4.1 Introduction

One of the main tasks of voltage stability monitoring is to evaluate how close the current operating point is to the point of voltage collapse. The point of voltage collapse is also known as the point that the loads reach the maximum power in power systems. To describe the distance between the current operating point and the point of voltage collapse, the voltage stability margin is often defined, as expressed by (4.1). A 3% to 10% margin value is commonly accepted as a safe margin in power systems [48-49].

$$\text{margin} = \frac{S_{\max} - S_0}{S_0} \times 100\% \tag{4.1}$$

where $S_{\max}$ is the power at the point of voltage collapse, and S_0 is the power at the current operating point.

As mentioned in Chapter 1, the standard PV curves are normally adopted by the power industry to calculate voltage stability margins. Since this is a very time consuming procedure, the standard PV curves are generally used for power system planning studies. Many efforts have been made to improve the computation speed and to make this method suitable for real-time applications. Using parallel computing is one example of these efforts [50-51]. Based on the

fact that the diagonal elements of Jacobian matrix are dominant for most of the operation conditions, fast decoupled power flow is generally used for PV curve calculation [52-57]. Other methods using prediction and/or correction to speed up the calculation, such as the method in [21], are also used.

Continuation power flow (CPF) is a powerful tool to simulate power system steady-state behaviours in terms of finding the voltage stability margin. The technique allows the determination of the complete PV curves. It has attracted a great deal of interest from researchers and engineers since it was first presented in [20]. Many algorithms have been proposed to speed up the calculation of the CPF method, such as the nonlinear predictors developed in [58-60]. In order to deal with ill-conditioned problems at and near the critical point, a fast decoupled power flow method using the reactive power injection as continuation parameters has also been presented [61].

Besides the methods based on *PV* curves a procedure called "COLLAS" has been developed for determining the voltage collapse distance [62]. The procedure can also schedule the preventive actions to be taken in an emergency state. The voltage stability margin is evaluated based on area or system-wide indicators.

Due to a large number of contingencies (i.e., a large number of operating scenarios in power systems), advanced numerical algorithms are adopted to assess the voltage stability margin in power systems. The artificial neural network (ANN)

based approaches have been applied in power systems [63]. The multilayer feedforward ANN methods have shown the advantages of robustness for real time application [64].

Since voltage instability is generally considered to be a local phenomenon, a large number of buses usually do not participate at the beginning of voltage collapse. Thus a popular approach is to find equivalents of areas that are external to the system in which the voltage stability is monitored. The Ward equivalent is one of these techniques [65]. By improving the performance of boundary matching, an extended Ward equivalent method is presented in [66]. For the purpose of online applications, significant work has been done on fast boundary matching [67]. Combining the advantages of both ANN and the Ward equivalent, a fast voltage stability assessment method has been studied in [68].

In summary, plenty of research work has been done for fast identification of the voltage stability margin in power systems. Most of the above methods work well in offline applications. However, they have a common drawback in that they require too much computation time and a good knowledge of the studied power system (the knowledge is needed to form the equivalent of the system). Such requirements bring challenges for online applications even with modern computer technologies, since the complexity of power systems has increased considerably in recent years and will be more complicated in the future.

Aimed at online applications, this chapter presents a new procedure to estimate power system voltage stability margin. First, the impedance matching theorem is applied to the coupled single-port network equivalent. The maximum power that can be transferred to each load is obtained as well as the voltage stability margin. Using the obtained voltage stability margin as the first guess, an iterative power flow method is then used to correct the voltage stability margin by considering the actions of voltage regulation devices (such as the switched shunts).

In addition to online voltage stability monitoring, identification of the weak bus(es) of the power system is essential for the design of remedial actions for preventing the approaching voltage collapse. Since it is commonly believed that voltage collapse happens when there are no solutions to power flow equations, it is essential to determine the weak buses through the analysis of the Jacobian matrix, as shown in (4.2).

$$\begin{bmatrix} \Delta\theta \\ \Delta V \end{bmatrix} = J \begin{bmatrix} \Delta P \\ \Delta Q \end{bmatrix} = R\Lambda T \begin{bmatrix} \Delta P \\ \Delta Q \end{bmatrix} \tag{4.2}$$

where J is the power flow Jacobian matrix, $\Lambda = \mathrm{diag}(\lambda_1, \lambda_2, \cdots \lambda_n)$ is the matrix with the eigenvalues of J, and R and T are the left and right eigenvector, respectively.

The eigenavlue λ is also called mode. The critical mode is the one with the smallest value. The buses are ranked based on their participation factors associated with the critical mode, which is derived from eigenvectors [69]. The bus with the highest participation factor is classified as the weakest bus. The modal analysis method has been widely adopted by utility companies to facilitate categorizing the vulnerable buses in the procedure of power system studies and planning.

The modal analysis method has limitations, however, in recognizing the critical mode. Firstly, it requires stressing the system as close to the collapse point as possible. This process needs a great deal of computation time. Secondly, when a group of eigenvalues are very close to each other, the method can hardly distinguish which one should be given more attention [70]. Moreover, the large variations of the eigenvalues when the power system is close to the nose point bring about a major challenge in identifying the weak buses [71]. Last but not least, the procedure of calculating the eigenvalues and eigenvectors involves considerable effort, especially for large-scale power systems.

This chapter presents a new method to rank the load buses based on their vulnerabilities to voltage collapse. The method relies on the coupled single-port network equivalent and the impedance matching theorem. The ratio between the equivalent impedance of the network and the impedance of the load is calculated for each coupled single-port network equivalent. Then, the critical bus is

recognized by comparing those impedance ratios. The validity of the proposed method is verified by comparison studies with the modal analysis method using several test power systems. The advantages of the proposed method lie in its simplicity, computing efficiency, and ability to identify the weakest bus without stressing power systems.

The ultimate objective of a load shedding scheme is to improve the reliability of power systems, which involve providing power to as many customers as possible. Therefore, in addition to preventing voltage collapse, in which all the customers are lost, load shedding schemes should minimize the influence to customers. In other words, the amount of load shedding should be as small as possible. In order to optimize the load shedding schemes, a novel multistage load shedding optimization algorithm is provided in this work. The performance of this method is verified by using several test power systems, including a real 2038 bus power system.

4.2 Load shedding oriented voltage stability monitoring

4.2.1 Estimation of the voltage stability margin

The impedance matching theorem used in the single-port network equivalent is particularly promising in terms of the computation speed. The single-port network

equivalent method can easily get the voltage stability margin for each load bus by using the following equation (4.1) [11, 22, and 29].

$$S_{\max} = \frac{\left|E_{eq}^2\right|\left[\left|Z_{eq}\right| - \left(\text{imag}\left(Z_{eq}\right)\sin\delta + \text{real}\left(Z_{eq}\right)\cos\delta\right)\right]}{2\left[\text{imag}\left(Z_{eq}\right)\cos\delta - \text{real}\left(Z_{eq}\right)\sin\delta\right]^2} \tag{4.3}$$

where E_{eq} and Z_{eq} are the equivalent voltage and the equivalent impedance of the single-port network equivalent, δ is the power factor angle of the load, and $\text{imag}(.)$ and $\text{real}(.)$ denote the imaginary and real part of the variables, respectively.

It is worth mentioning that the impedance matching condition is based on the matching of impedance magnitude (i.e. $\left|Z_{eq}\right| = \left|Z_L\right|$). A conjugate impedance match in the form of $Z_L^* = Z_{eq}$ cannot apply to power systems, since both the impedance of transmission network and the impedance of loads are reactive (with a positive imaginary part). The reason of magnitude matching is derived by the following equations.

The Thevenin equivalent circuit of a simple power system is depicted in Figure 4.1. The apparent power consumed by the load (Z_L) is calculated by (4.4).

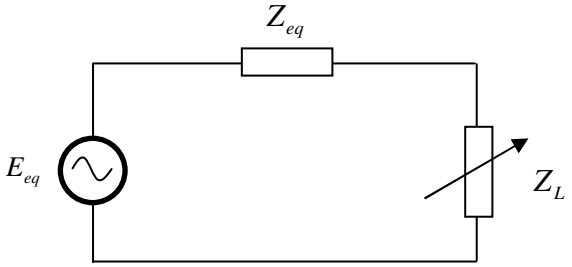

Figure 4.1 Thevenin equivalent of a simple power system

$$S_L = \left| \left(\frac{E_{eq}}{Z_{eq} + Z_L} \right)^2 Z_L \right| \tag{4.4}$$

Because the loads in power systems generally maintain a constant power factor and the network impedance does not change with the loading, the two impedances can be expressed by (4.5) and (4.6) respectively.

$$Z_{eq} = \left| Z_{eq} \right| e^{j\theta_s} \tag{4.5}$$

$$Z_L = \left| Z_L \right| e^{j\theta_L} \tag{4.6}$$

where $\left| Z_{eq} \right|$, θ_s, and θ_L are constant. $\left| Z_L \right|$ is the magnitude of the load impedance.

Substituting (4.5) and (4.6) into (4.4), we get

$$S = \frac{|Z_L|}{\left|\left|Z_{eq}\right|e^{j\theta_s} + |Z_L|e^{j\theta_L}\right|} \cdot |E_{eq}|^2 = \frac{|Z_L|}{\left|\left|Z_{eq}\right| + |Z_L|e^{j(\theta_L - \theta_s)}\right|} \cdot |E_{eq}|^2 \tag{4.7}$$

In (4.7), the only variable is $|Z_L|$. Thus the maximum apparent power is obtained when $\frac{dS}{d|Z_L|} = 0$, which gives

$$\frac{\left(|Z_{eq}|^2 + |Z_L|^2 + 2|Z_{eq}||Z_L|\cos\alpha\right) - |Z_L|\left(2|Z_L| + 2|Z_{eq}|\cos\alpha a\right)}{\left(|Z_{eq}|^2 + |Z_L|^2 + 2|Z_{eq}||Z_L|\cos\alpha\right)^2} = 0 \tag{4.8}$$

where α is the angle difference $\theta_L - \theta_s$.

Solving (4.8), the magnitude of load impedance $|Z_L|$ is equal to the magnitude of the network impedance $|Z_{eq}|$. Therefore, equation (4.3) is proved.

$$|Z_L| = |Z_{eq}| \tag{4.9}$$

The coupled single-port network equivalent with the virtual impedance model is represented by Figure 4.2. For this equivalent circuit, the impedance matching theorem states that the maximum power is achieved when the magnitude of load impedance Z_{Lj} is equal to the magnitude of the system side impedance $\left(Z_{eq,jj} + Z_{cj}\right)$.

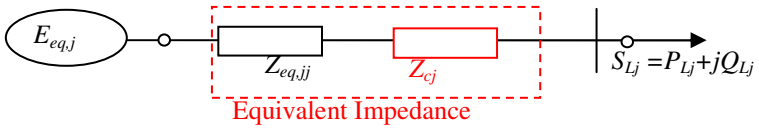

Figure 4.2 The coupled single-port network equivalent using virtual impedance model

Therefore, for load bus j, the maximum power that can be transferred is obtained from (4.10). The maximum scaling factor can be calculated by (4.11).

$$S_{\max,j}=\frac{\left|E_{eq,j}^{2}\right|\left[\left|Z_{eq,j}\right|-\left(\text{imag}\left(Z_{eq,j}\right)\sin\delta_{j}+\text{real}\left(Z_{eq,j}\right)\cos\delta_{j}\right)\right]}{2\left[\text{imag}\left(Z_{eq,j}\right)\cos\delta_{j}-\text{real}\left(Z_{eq,j}\right)\sin\delta_{j}\right]^{2}} \tag{4.10}$$

where δ_j is the power factor angle of load j.

$$\lambda_{\max,j}=\frac{S_{\max,j}}{S_{Lj}} \tag{4.11}$$

Equation (4.11) indicates that the maximum scaling factor for every load may be different. Since the load increasing pattern is usually selected so that all the loads are scaled by the same ratio, it is reasonable to choose the minimum one as the maximum scaling factor for the studied power system.

$$\lambda_{\max,system}=\min\left\{\lambda_{\max,1},\lambda_{\max,2},\cdots,\lambda_{\max,n}\right\} \tag{4.12}$$

where $\lambda_{\max,system}$ is the maximum scaling factor for the studied power system.

In addition, the voltage stability margin is determined by (4.13).

$$\text{margin} = \frac{\lambda_{\max,system} - \lambda_0}{\lambda_0} \times 100\% \tag{4.13}$$

where λ_0 is the scaling factor at the base loading level (normally $\lambda_0 = 1$).

The above procedure of voltage stability margin estimation can be represented as a flowchart, as shown in Figure 4.3. Assuming an outage event occurs, the scheme will work as follows:

- Gather system real-time operation status: admittance matrix *Y* from SCADA, synchronous generator voltage phasors V_G, and voltage and current measurements at the interested buses from PMUs. At the same time, the control devices will be considered in the equivalent network. For instance, the OLTCs (On-Load Tap Changer) will be grouped in their corresponding loads. The generators will be converted to voltage sources behind its saturated synchronous reactance when they reach the reactive power output limit.

- Calculate the equivalent voltage E_{eqj} and the equivalent impedance Z_j (*j=1, 2…n*) of the coupled single-port model by (3.12) and (3.16), respectively.

- Compute voltage stability margin for each single-port system by using impedance matching equations (4.10) and (4.13). In (4.10), the equivalent voltage E_{eq} and impedance Z_{eq} should be replaced by their corresponding E_{eqj} and Z_j.

- Find the system voltage stability margin by using (4.12).

- Load shedding is triggered based on the margin/critical results and load shedding criteria.

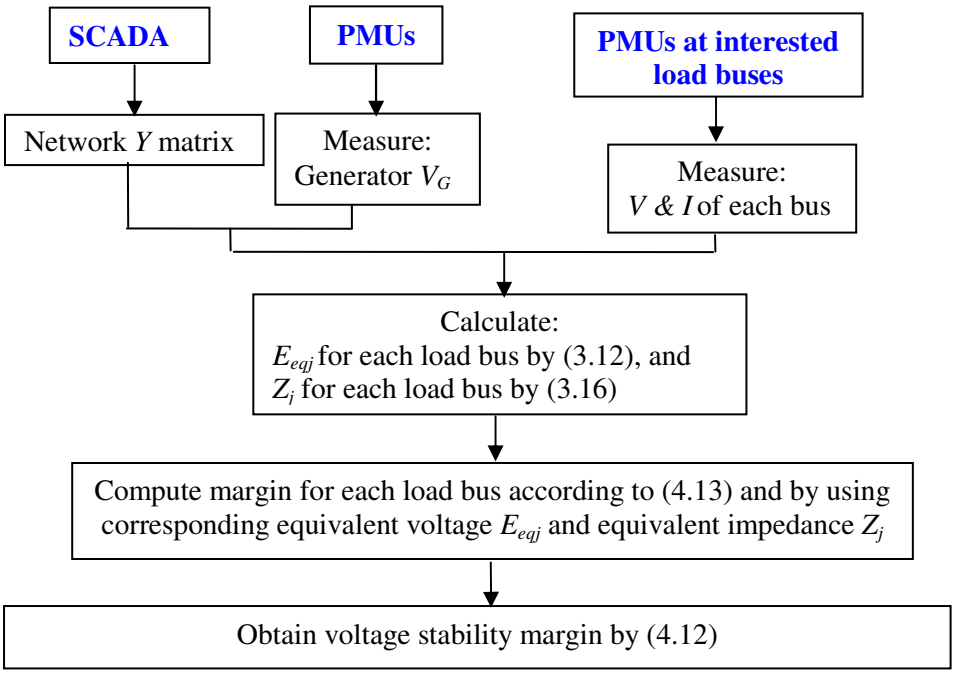

Figure 4.3 The flowchart for voltage stability margin estimation

A sample case study was conducted on a 9-bus system to illustrate how the above procedure works. It should be noted that the voltage and current phasors used in this sample are obtained from the solutions of power flow.

Step 1: Obtain the voltage and current phasors and the admittance matrix for the system at the base case

Table 4.1 Voltage and current phasors at all buses

Bus no.	Bus type	Voltage	Current
1	3	$1.06\angle 0°$	--
2	2	$1.045\angle -9.22°$	--
3	2	$1.01\angle -23.01°$	--
4	1	$0.9088\angle -22.63°$	$2.9023\angle -17.97°$
5	1	$0.9042\angle -18.15°$	$0.8602\angle -63.15°$
6	1	$0.8723\angle -24.92°$	$0.8917\angle -69.92°$

$$Y = \begin{bmatrix} 6.025 - 19.4471j & -4.9991 + 15.2631j & 0 & 0 & -1.0259 + 4.2350j & 0 \\ -4.9991 + 15.2631j & 9.5213 - 30.2721j & -1.1350 + 4.7819j & -1.6860 + 5.1158j & -1.7011 + 5.1939j & 0 \\ 0 & -1.1350 + 4.7819j & 3.1210 - 9.8224j & -1.9860 + 5.0688j & 0 & 0 \\ 0 & -1.6860 + 5.1158j & -1.9860 + 5.0688j & 10.5130 - 36.7393j & -6.8410 + 21.5786j & 4.8895j \\ -1.0259 + 4.2350j & -1.7011 + 5.1939j & 0 & -6.8410 + 21.5786j & 9.5680 - 35.5336j & 4.2574j \\ 0 & 0 & 0 & 4.8895j & 4.2574j & -8.7499j \end{bmatrix}$$

Note: Bus type 3 – swing bus; bus type 2 – PV bus; bus type 1 – PQ bus.

Step 2: Build the multi-port network equivalent

The multi-port network equivalent is built by (4.14) and (4.15).

$$E_{eq} = KV_G = -Y_{LL}^{-1} Y_{LG} V_G \tag{4.14}$$

$$Z_{eq} = Y_{LL}^{-1} \tag{4.15}$$

where Y_{LL} and Y_{LG} are the sub-matrices of Y, as shown in (3.2).

Step 3: Solve each coupled single-port network equivalent

By using the virtual impedance model, the parameters of each coupled single-port network equivalent can be obtained as shown in Table 4.2.

Table 4.2 The parameters of each coupled single-port network equivalent

Load no.	Load bus no.	Equivalent voltage	Equivalent impedance
1	4	$1.0375\angle -11.79°$	$0.0433 + 0.0640\,j$
2	5	$1.0378\angle -9.85°$	$-0.0223 + 0.2241\,j$ [1]
3	6	$1.0846\angle -10.89°$	$-0.0659 + 0.3512\,j$ [1]

[1] The impedance here is equivalent impedance. So the real part does not have to be positive.

The maximum power and the maximum scaling factor for each load can be calculated based on (4.10) and (4.11) respectively. The results are listed in Table 4.3a.

Table 4.3a The maximum scaling factor for each load

Load no.	Load bus no.	Maximum power	Maximum scaling factor
1	4	4.67	1.77
2	5	1.46	1.88
3	6	1.05	1.35

Step 4: Obtain the voltage stability margin for the system

The maximum scaling factor of the system is determined by (4.12). The voltage stability margin is calculated by (4.13).

$$\lambda_{\max,system} = \min\{1.77, 1.88, 1.35\} = 1.35$$

$$\text{margin} = \frac{\lambda_{\max,system} - \lambda_0}{\lambda_0} \times 100\% = 35\%$$

Note that the actual maximum scaling factor, which is calculated by using the CPF method in PSAT (Power System Analysis Toolbox) [72], is 1.49. The estimated margin is smaller than 1.49. The error of this estimation is about 9%,

which is relatively large. However, our further studies show that the error becomes much smaller (less than 5%) when the operating point is closer to the voltage collapse point. Therefore, the proposed method would perform well if the estimation is updated continuously during the changing of power systems. Table 4.3b shows the estimation.

Table 4.3b The results of margin estimation of different power systems

Test system	Estimation error (%)	
	Estimated at base case	Estimated when the system is stressed close to nose point (5% margin)
IEEE9 bus system	0.103	0.071
IEEE 30 bus system	8.9	4.49
IEEE 39 bus system	1.54	1.92
2038 bus AIES	0.55	2.75

4.2.2 Correction of the margin estimation using an iterative power flow method

The demonstration study in the previous section points out that there are errors in the estimated voltage stability margin when the operation point is far from the point of voltage collapse. The reason why there are errors is explained below.

Theoretically, the maximum power transfer should be calculated using the Thevenin equivalent parameters at the critical point, $E_{eq-critical}$ and $Z_{eq-critical}$ shown in Figure 4.4. However, in practice, it is usually estimated using the equivalent parameters ($E_{eq-operating}$ and $Z_{eq-operating}$) at the current operating point since $E_{eq-critical}$ and $Z_{eq-critical}$ are not available.

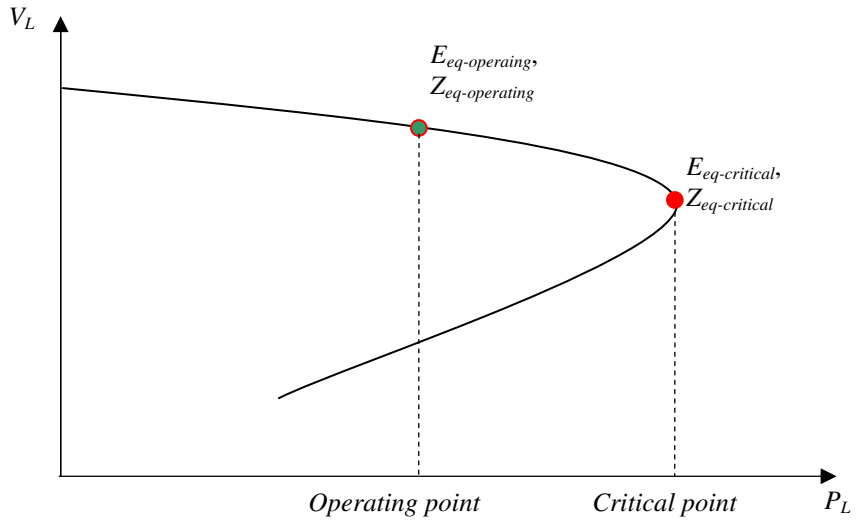

Figure 4.4 Relationship between the Thevenin equivalent parameters at the operating point and at the critical point

Due to the nonlinear characteristics of power systems, when the operating point is not close to the critical point, $E_{eq-operating}$ and $Z_{eq-operating}$ are likely to have some differences with $E_{eq-critical}$ and $Z_{eq-critical}$ respectively. This characteristic was also observed in Chapter 3.

Since the voltage regulation devices (such as the switched shunts) would be activated when the system is getting stressed, the effects of their actions should be considered when the voltage stability margins are estimated. However, the coupled single-port network equivalent is obtained using only the knowledge of current operating condition (any methods based on the measurements have the same problem). On one hand, this is the advantage of the coupled single-port network equivalent method. On the other hand, the estimated voltage stability margins may not be accurate because the influences of network changes are not taken into consideration.

A correction method is needed to make a more accurate estimation. A prediction/correction method is proposed in this chapter. It uses the scaling factor estimated from the impedance matching theorem as a predictor. The correction mechanism is completed by running a series of power flow calculations. The stop criterion consists of two conditions: 1) the power flow calculation has diverged at least once; and 2) the estimated scaling factors at two consecutive iterations are close enough. If only the second condition has been satisfied, the estimated scaling factor will be multiplied by a ratio (greater than 1.0) to ensure that the procedure does not get trapped by a local maximum. The procedure of the prediction/correction method is described in Figure 4.5. To verify the proposed method, it was applied to several test power systems. The simulation results are presented in the next subsection.

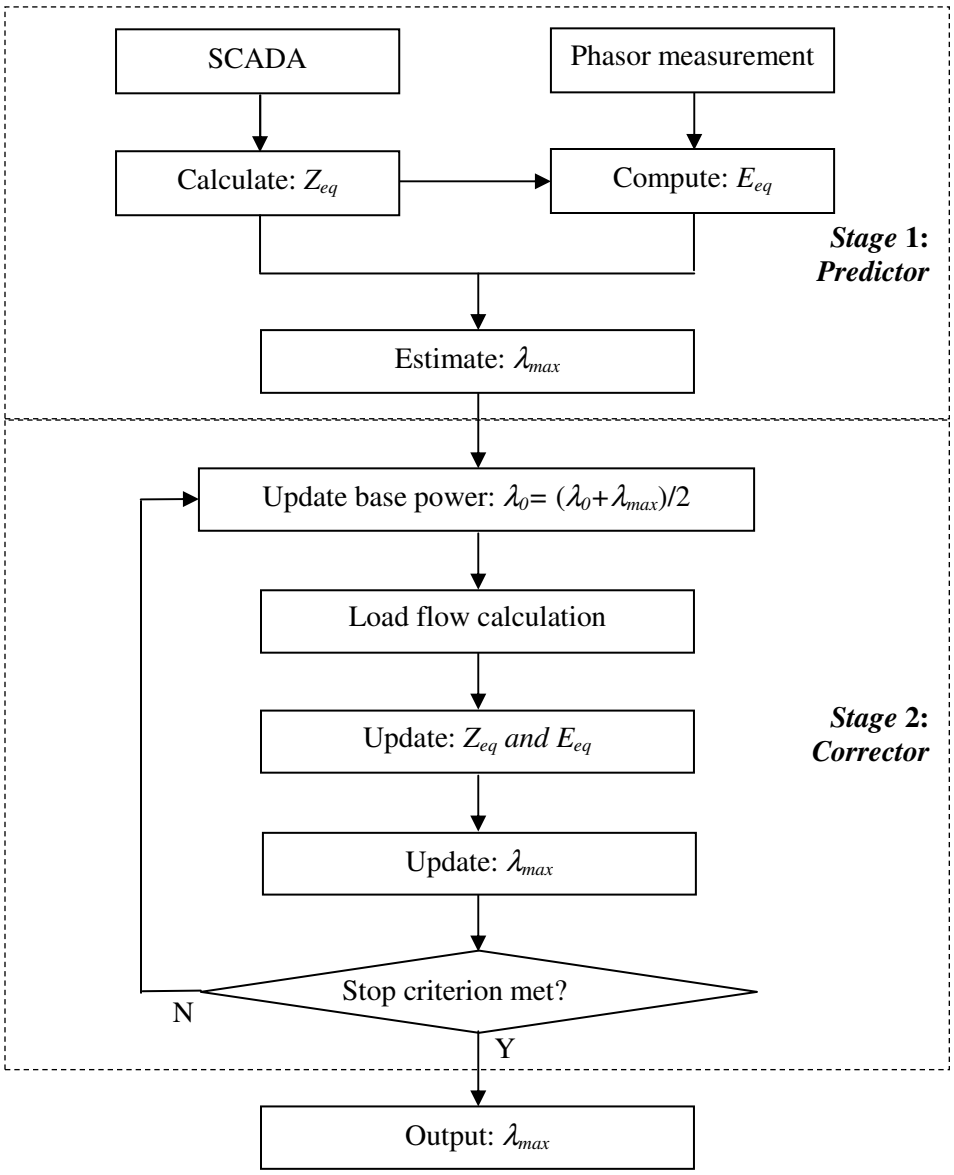

Figure 4.5 The implementation procedure of the prediction/correction method

4.2.3 Simulation results on several benchmark power systems

Several benchmark power systems [45] are studied in this subsection to examine the performance of the presented prediction/correction method. The following results are provided for this study:

a) The estimated scaling factor at each corrective action. The estimated maximum scaling factor is compared with the real maximum scaling factor, which is calculated by using PSAT.

b) The number of iterations is required for each power system. The number of power flow calculations is compared with the one required by the traditional continuation power flow method, which is used in PSAT.

1) The results on maximum scaling factor estimation

The following figures show the estimations of the maximum scaling factors. The actual maximum scaling factor (dashed line) is calculated by PSAT. The estimated maximum (solid line) is obtained by using the proposed method. The results demonstrate that the proposed method has a good accuracy with only a small number of iterations required.

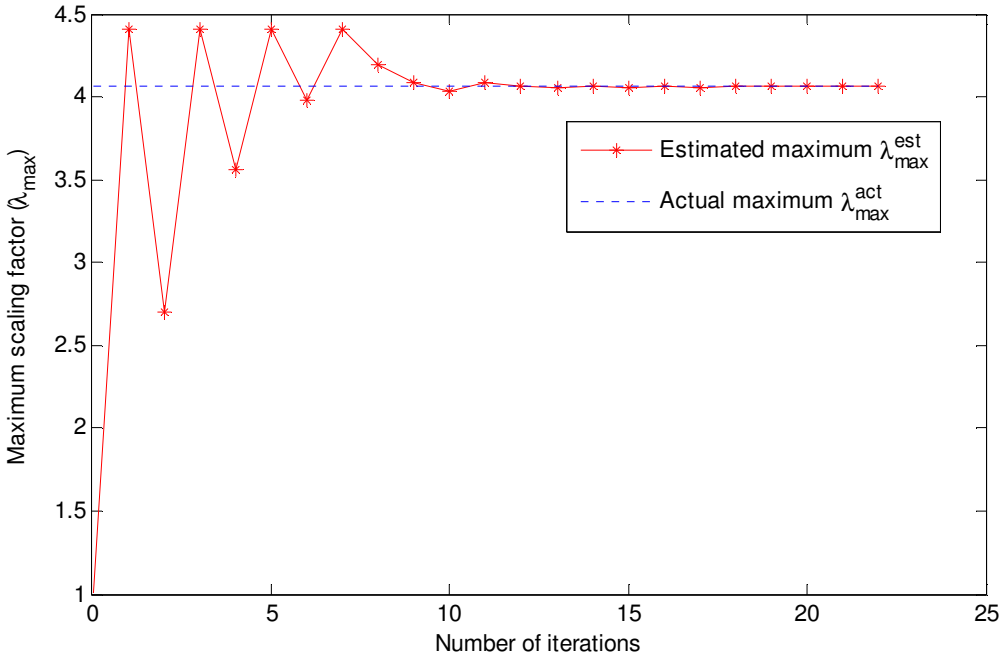

Figure 4.6 Scaling factor estimation for IEEE 14 bus system

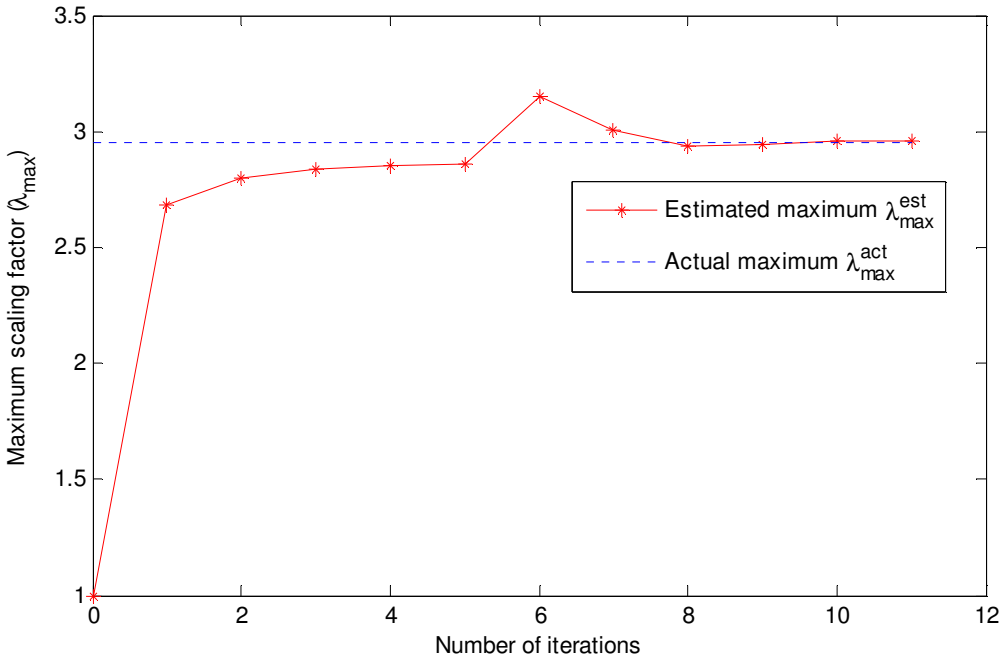

Figure 4.7 Scaling factor estimation for IEEE 30 bus system

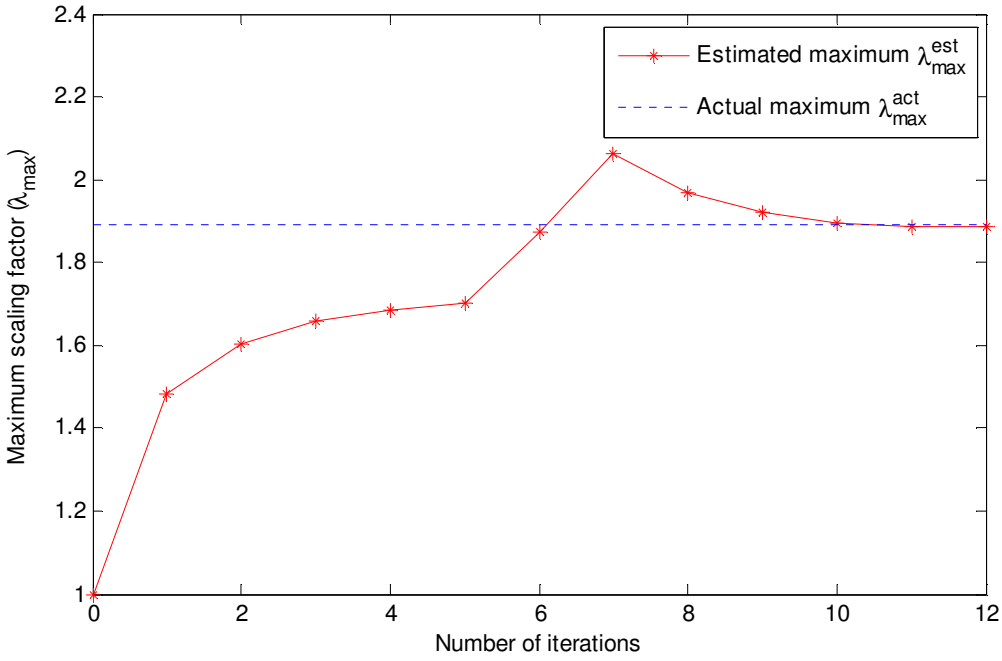

Figure 4.8 Scaling factor estimation for IEEE 57 bus system

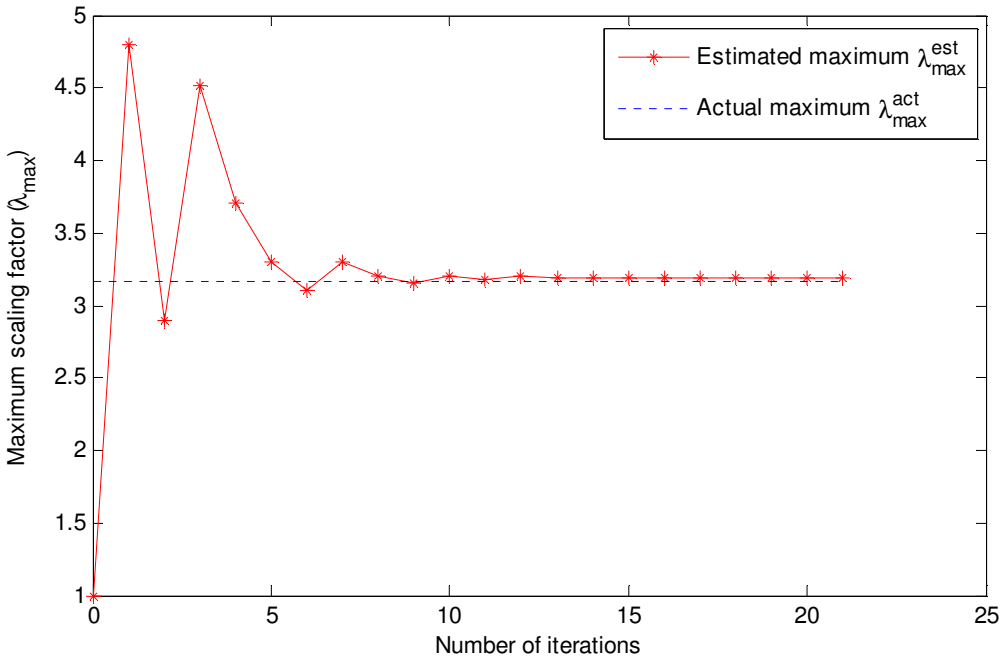

Figure 4.9 Scaling factor estimation for IEEE 118 bus system

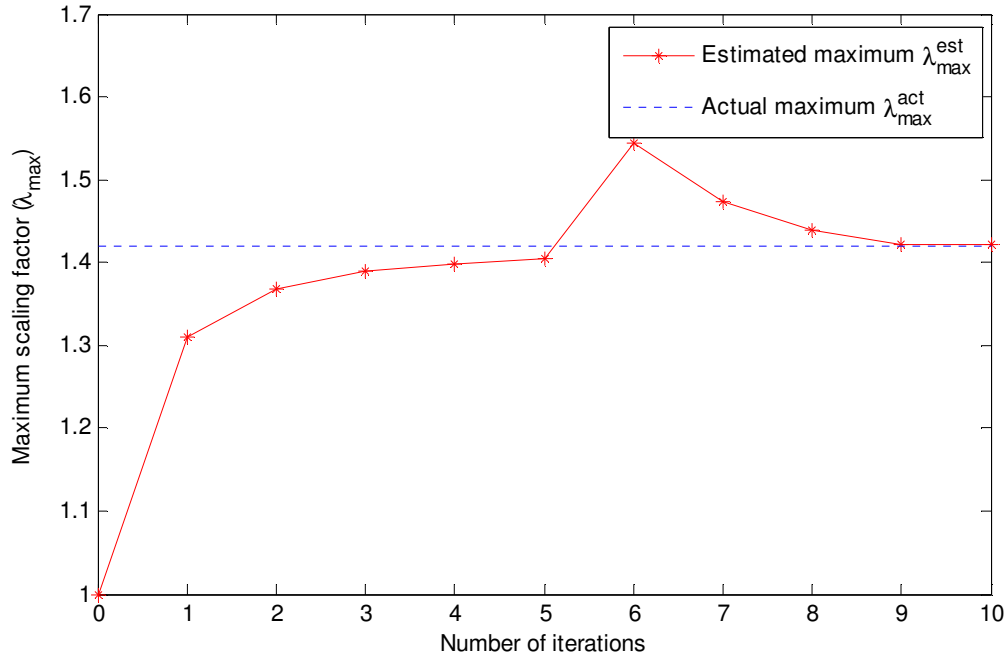

Figure 4.10 Scaling factor estimation for IEEE 300 bus system

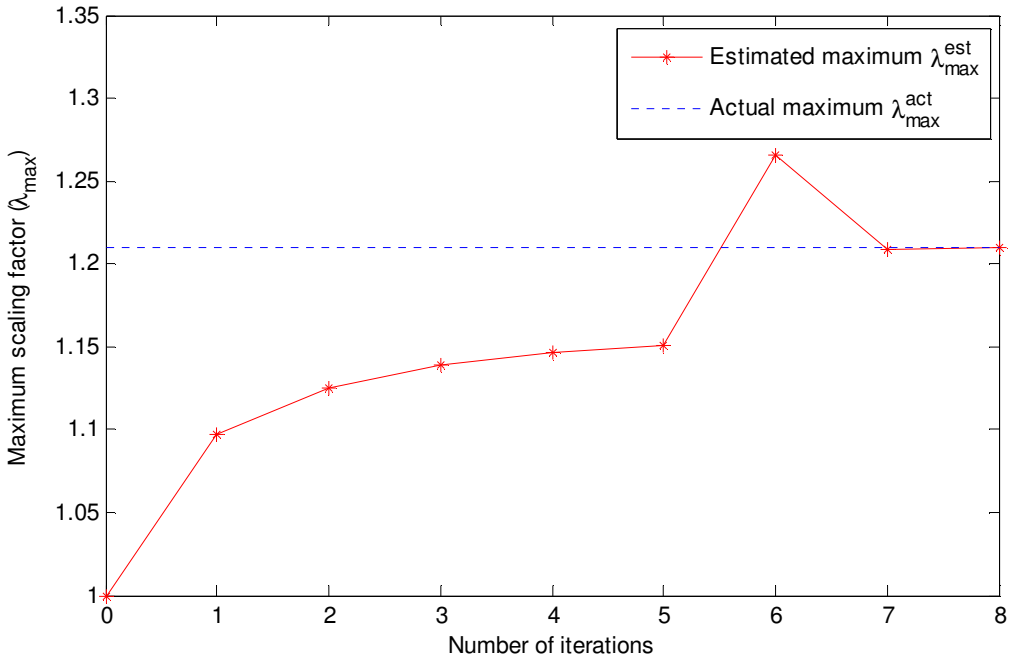

Figure 4.11 Scaling factor estimation for 2038 bus Alberta Integrated Electric System (AIES)

2) The comparison of computation efforts

Since the most computing effort on margin estimation is spent on solving the power flow equations, the number of calculating power flow equations is a very important factor in terms of evaluating the performance of voltage stability monitoring schemes. The following table lists the number required by the CPF method (in PSAT) and the one needed by the proposed method. The comparison results demonstrate the advantage of the proposed method. It can effectively speed up the process of evaluating the power system voltage stability margin. Moreover, the number of power flow calculations required for the proposed method remains almost constant in spite of the scale of power systems. In other words, it is not sensitive to the size of the system.

Table 4.4 The number of power flow calculations required

Test power systems	Number of power flow calculations	
	Conventional CPF	The proposed method
IEEE 14 bus system	16	9
IEEE 30 bus system	18	8
IEEE 57 bus system	14	9
IEEE 118 bus system	32	9
IEEE 300 bus system	52	9
2038 bus AIES	40	8

4.3 Identification of the weak bus(es)

The weakest bus is defined as the one which has the biggest influence on the voltage stability margin. It is important to recognize these buses in both power system long-term planning studies and power system operation planning studies. These buses are identified as the locations where the enhancements or remedial actions should be implemented. The modal analysis method is the widely accepted technique to identify these buses. In this subsection, a method based on the proposed multi-port network equivalent is presented. The validity of the proposed method is verified by comparing the results from the modal analysis method. The advantages of the proposed method are also discussed.

4.3.1 Ranking the load buses based on the impedance ratios

As discussed in the previous section, the coupled single-port network equivalent actually relies on the impedance matching theorem to estimate the voltage stability margin for each load bus. It is therefore reasonable to use the impedance ratio as an indicator to describe the influence of the load buses. In other words, the load buses can be ranked based on the ratio between the equivalent impedance of the coupled single-port network equivalent and the impedance of the studied load, as shown by (4.16).

$$r_{z,j} = abs\left(\frac{Z_{eq,j}}{Z_{Lj}}\right) \tag{4.16}$$

where $Z_{eq,j}$ is the equivalent impedance of the coupled single-port network; Z_{Lj} is the equivalent impedance of the load j and is calculated by (4.17).

$$Z_{Lj} = \frac{V_{Lj}}{I_{Lj}} \tag{4.17}$$

where V_{Lj} and I_{Lj} are the voltage phasor and the current phasor at load bus j.

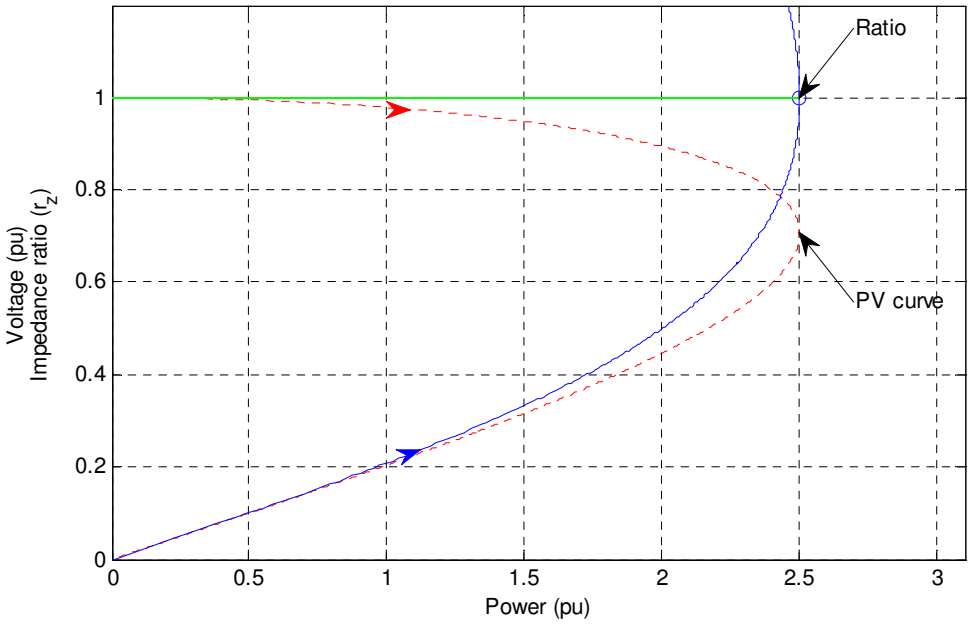

Figure 4.12 Evolution of impedance ratio with stressing power systems

The maximum power for each coupled single-port network equivalent is obtained at the condition of impedance matching, which means the ratio $r_{z,j}$ is equal to 1.

Under normal operating condition, the ratio is less than 1. When the power system is approaching the transmission limit, the ratio is increasing and finally reaches the critical value 1.0. The above process is shown by Figure 4.12.

In any operating scenario, the weakest bus can be identified as the load bus whose impedance ratio is the closest to the value of 1.0. For example, the impedance ratios for a simple power system are calculated and shown in Figure 4.13. Load bus 2 is recognized as the weakest bus among all the four load buses for the specific operating condition because the impedance ratio at load bus 2 is the closest to 1.

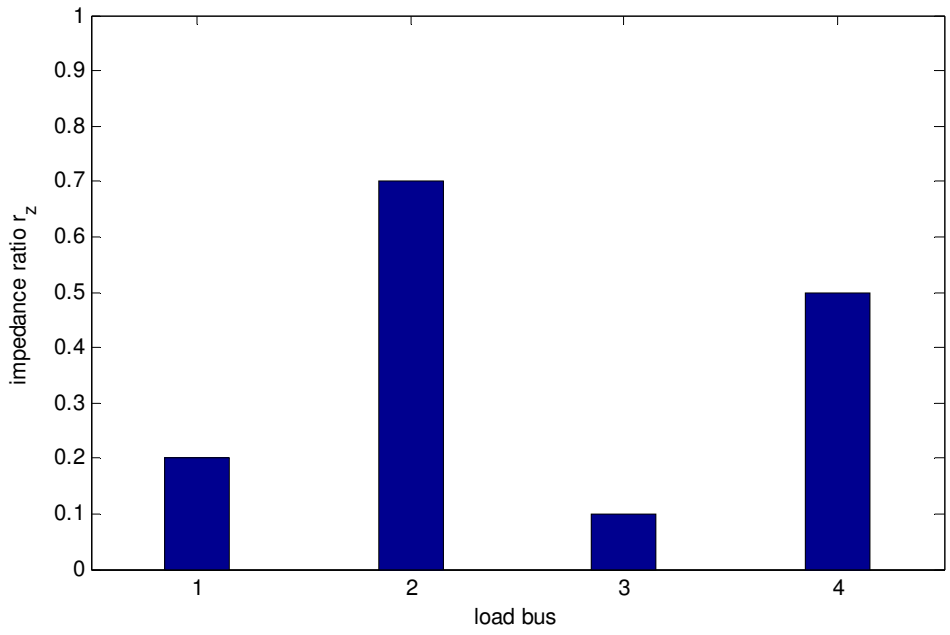

Figure 4.13 Identification of the weakest bus based on impedance ratio

At this point, there are two important questions needing to be answered.

1) Are the bus ranking results reliable?

2) Are these results sensitive to the loading level (similar to the results obtained by the modal analysis method)? Are there any sharp variations in the results with power systems approaching voltage collapse?

Since the method of modal analysis is generally accepted by both the industry and academia, it is essential to verify the results acquired by the proposed method by comparing them with those obtained from the modal analysis method. As long as both methods give similar results, the proposed method can be trusted.

As for the second question, the analysis in Chapter 3 clearly shows that the equivalent impedance of the network remains relatively constant when power systems get stressed. Meanwhile, the impedance values of the loads calculated by (4.18) remain in proportion to each other. The reason for the above observation is that the loads are scaled by the same ratio and the bus voltages are nearly proportional to each other.

$$Z_{Lj} = \frac{\left|V_{Lj}^2\right|}{S_{Lj}} \tag{4.18}$$

where V_{Lj} is the bus voltage at load bus j.

This important feature makes the proposed bus ranking method very promising. Unlike the modal analysis method, which requires stressing the system close to voltage collapse point, the proposed method can rank the load buses based only on the information at the current operating condition. System studies are conducted in the following two sections to verify the above findings.

4.3.2 Result verification by using the modal analysis method

In order to validate the proposed impedance ratio based bus ranking method, several test power systems are studied using both the proposed method and the modal analysis method. Figures 4.14-4.19 show the comparison of results. Due to the possible variations of the modal analysis method on different operating scenarios, the studied power systems are all stressed to the voltage collapse point.

Table 4.5 lists the top 5 weakest buses for each studied power system. The study shows that the results of the modal analysis method and those of the proposed method are consistent with each other. For the 2038 bus AIES, the x-axis of Figure 4.19 shows renumbered load buses in order to make the figure clearer. The load buses are renumbered in the sequence of their appearance in the power flow case. The results in Table 4.5 show the real bus numbers of the weakest locations.

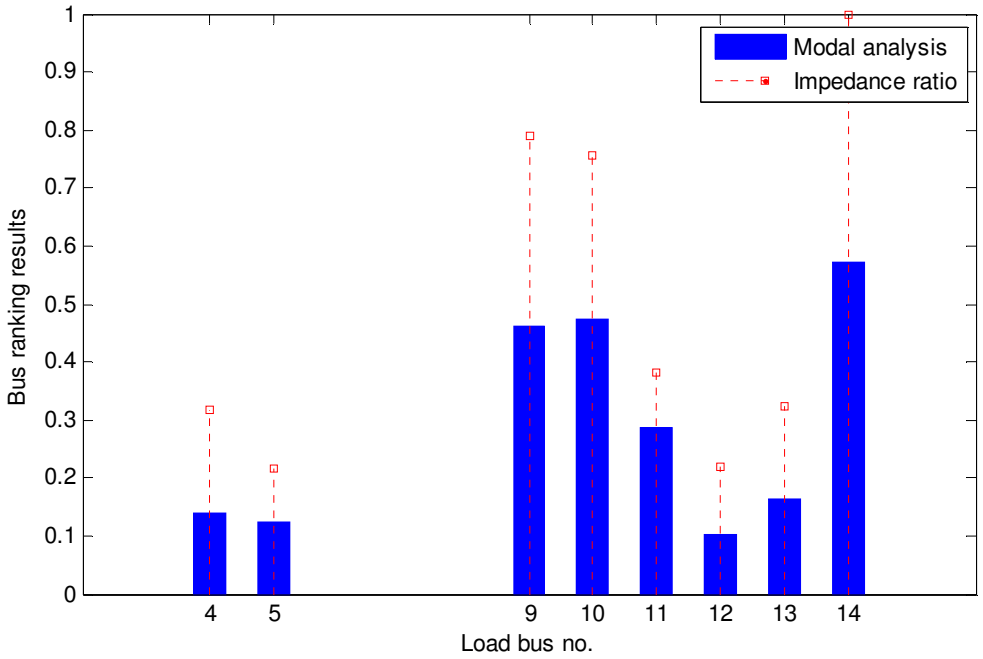

Figure 4.14 Bus ranking results for IEEE 14 bus system

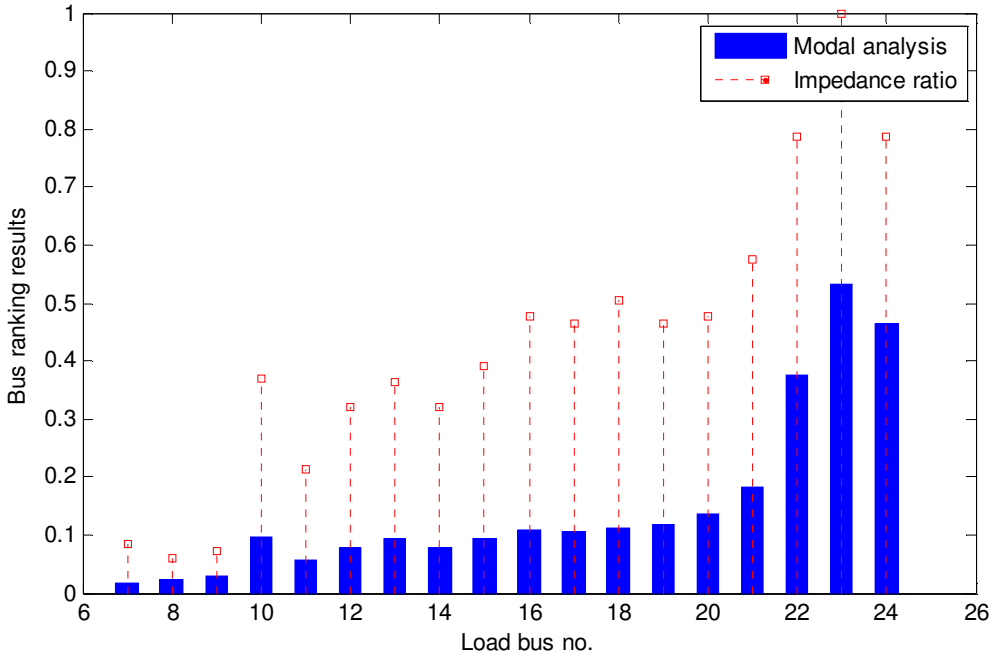

Figure 4.15 Bus ranking results for IEEE 30 bus system

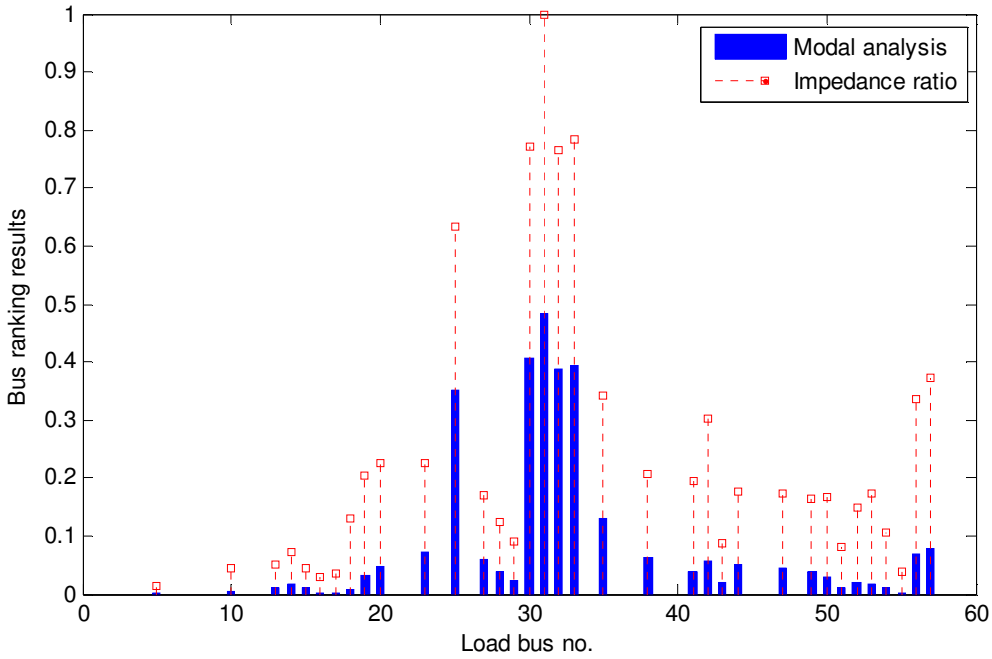

Figure 4.16 Bus ranking results for IEEE 57 bus system

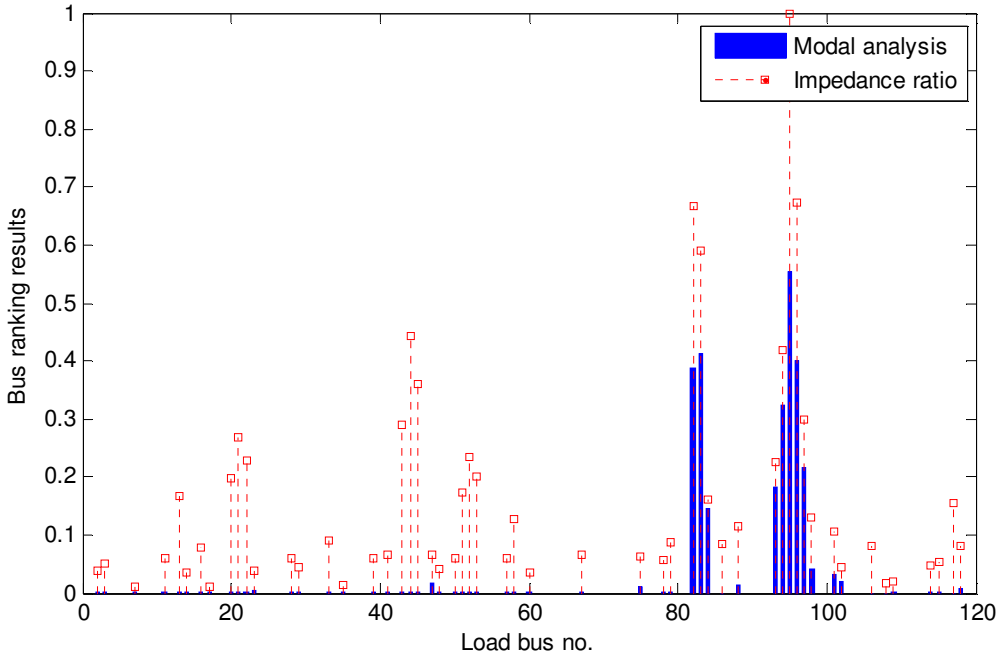

Figure 4.17 Bus ranking results for IEEE 118 bus system

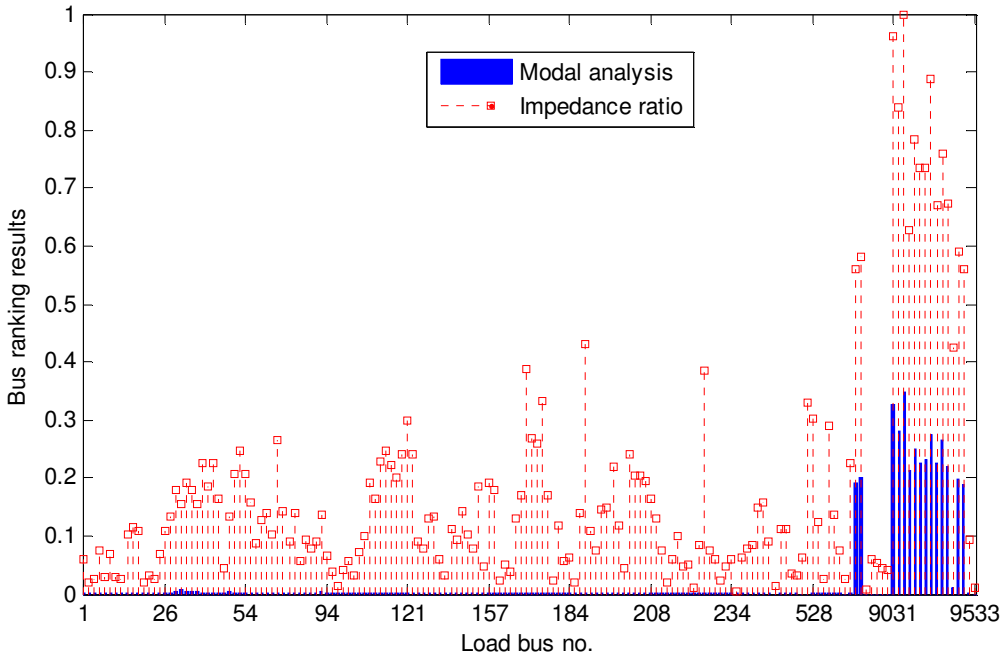

Figure 4.18 Bus ranking results for IEEE 300 bus system

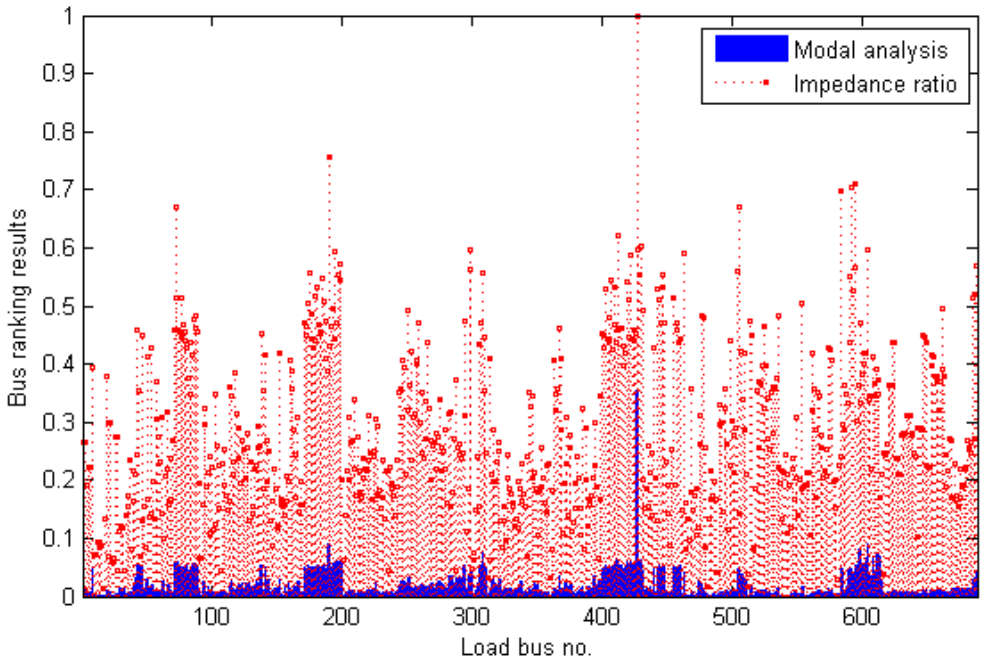

Figure 4.19 Bus ranking results for 2038 bus Alberta Integrated Electric System

Table 4.5 The top 5 weakest buses for the studied power systems

Test power systems	Top 5 weakest load buses (listed in the order of weakness)	
	The modal analysis method	The proposed method
IEEE 14 bus system	14, 10, 9, 11, 13	14, 9, 10, 11, 13
IEEE 30 bus system	23, 24, 22, 21, 20	23, 24, 22, 21, 18
IEEE 57 bus system	31, 30, 33, 32, 25	31, 33, 30, 32, 25
IEEE 118 bus system	96, 90, 97, 89, 95	96, 97, 89, 90, (74, 95)[2]
IEEE 300 bus system	9033, 9031, 9032, 9038, 9042	9033, 9031, 9038, 9032, 9035
2038 bus AIES	1435, 1886, 1161, 1877, 1895	1435, 1161, 1873, 1870, 1862

4.3.3 Sensitivity studies for the load bus ranking

To demonstrate that the proposed method is less sensitive to the operating points, the bus ranking results are traced when increasing the loading level of power systems. The top 5 weakest load buses are traced during scaling up the system loads. The results are shown in Figure 4.20 – Figure 4.25. The results clearly reveal the advantages of the proposed method. It can usually identify the weak buses under the normal operating condition (scaling factor is equal to 1.0). This

[2] They are equally weak in this case.

feature is very important in terms of designing and triggering the load shedding schemes in power systems. Equipped with this feature, the load shedding scheme can be easily optimized both in terms of load shedding locations and load shedding amounts for online applications.

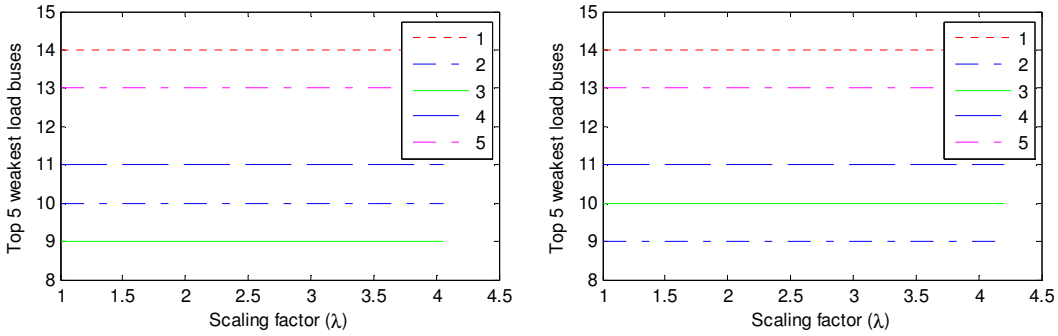

(a) Results of the modal analysis method

(b) Results of the proposed method

Figure 4.20 Tracing the bus ranking results for IEEE 14 bus system

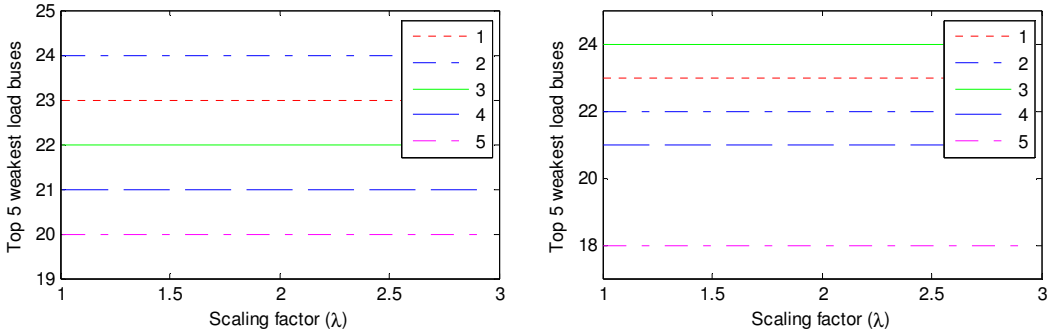

(a) Results of the modal analysis method

(b) Results of the proposed method

Figure 4.21 Tracing the bus ranking results for IEEE 30 bus system

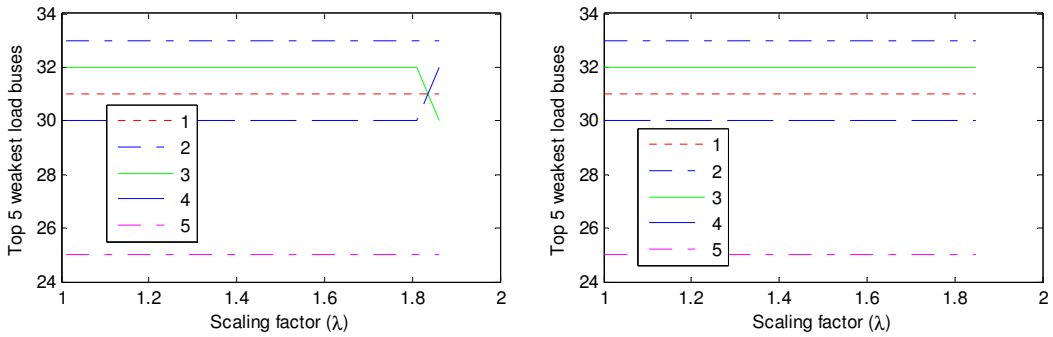

(a) Results of the modal analysis method

(b) Results of the proposed method

Figure 4.22 Tracing the bus ranking results for IEEE 57 bus system

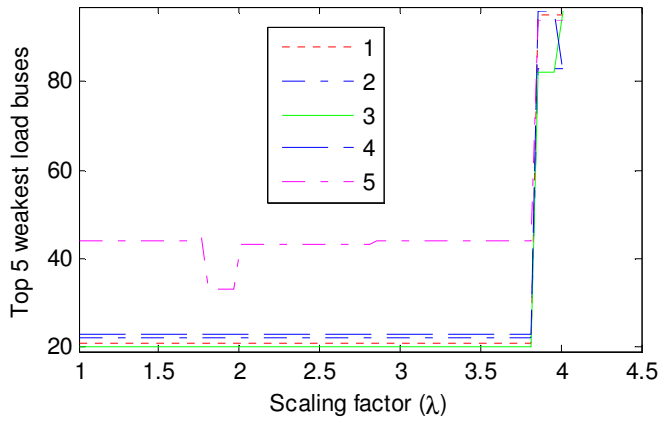

(a) Results of the modal analysis method

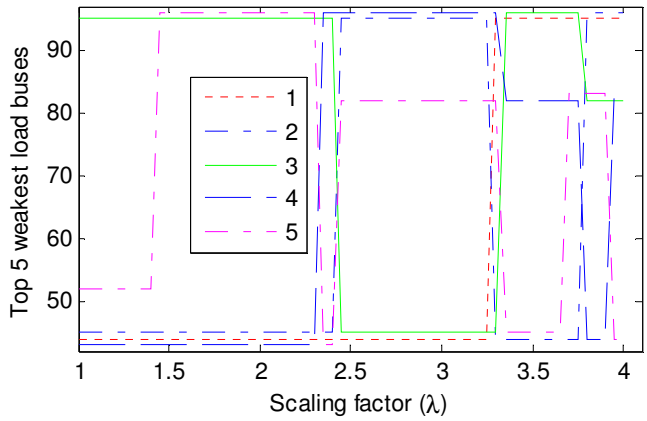

(b) Results of the proposed method

Figure 4.23 Tracing the bus ranking results for IEEE 118 bus system

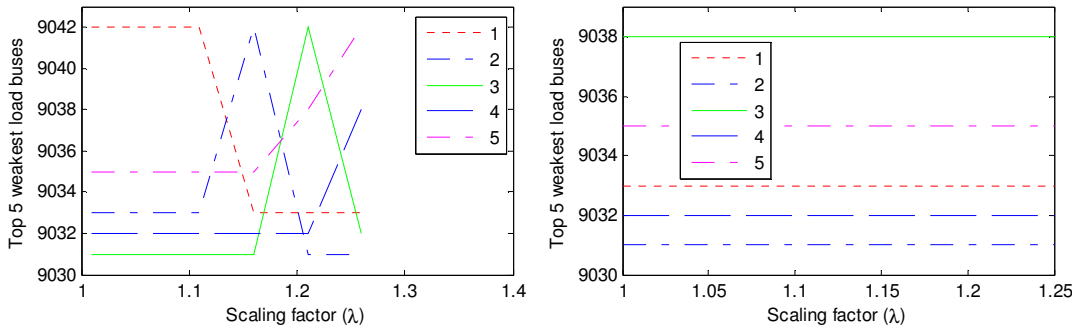

(a) Results of the modal analysis method

(b) Results of the proposed method

Figure 4.24 Tracing the bus ranking results for IEEE 300 bus system

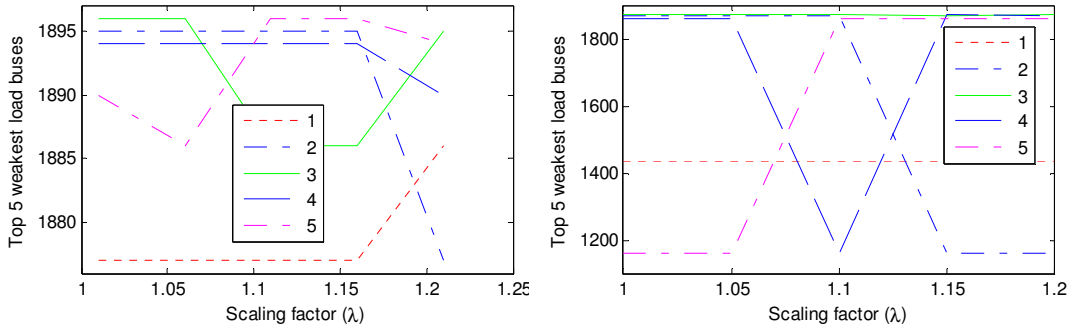

(a) Results of the modal analysis method

(b) Results of the proposed method

Figure 4.25 Tracing the bus ranking results for 2038 bus AIES

4.4 A multistage optimization algorithm

Many methods have been presented in recent years to optimize the amount of load shedding [18, 73-74]. Sensitivities of voltage stability margin and sensitivities of voltage with respect to load parameters are often used to determine the optimum

load locations. These methods use the sensitivity information to determine the necessary amount of load shedding. The voltage stability margin sensitivity with respect to load parameters can normally be defined as (4.19), which is modified from the sensitivity formula in [4].

$$Sen_j = \frac{\Delta\lambda}{\Delta S_j} \qquad j = 1,2,\cdots,n \tag{4.19}$$

where ΔS_j is the amount of load shedding at load bus j. $\Delta\lambda$ is the voltage stability margin increment after the load shedding, and n is the number of loads.

The minimum amount of load shedding to achieve the required voltage stability margin increment $\Delta\lambda^{req}$ is determined by shedding loads from the most sensitive load until the achieved margin increase $\Delta\lambda^{*}$ exceeds the required one. $\Delta\lambda^{*}$ is calculated by (4.20) [73].

$$\Delta\lambda^{*} = \sum_{j}^{m} Sen_j \times \Delta S_j \qquad m \le n \tag{4.20}$$

where $\Delta S_j = f_j \times S_j$, f_j is the shedding fraction of the selected load, S_j and ΔS_j are the load demand and the amount of shedding at load bus j respectively. As indicated in [73], the minimum amount of load shedding obtained from (4.20) relies on the following two conditions:

(1) Linearity of (4.20): the voltage stability margin increments from any single load shedding can be summed up.

(2) Constant sensitivities: the voltage stability margin sensitivities remain constant no matter how much load is shed at the selected location.

For many load shedding strategies, the validity of the above two conditions is generally assumed. However, due to the inherent nonlinear characteristics of power systems, the above two assumptions are unreliable. As a consequence, the calculated amount of load shedding may not be optimal.

In order to investigate this matter, the voltage margin sensitivities with respect to the amount of load shedding are studied by using (4.19) and (4.20). The studied power system is the IEEE 14-bus system. The investigation results on the linearity of (4.20) are shown in Figure 4.26. In this figure, $\Delta\lambda^{*}$ is calculated by using (4.20) and $\Delta\lambda^{act}$ is obtained using the power flow method in the commercial software PSS/E. Figure 4.26 clearly reveals that the validity of the linearity assumption is doubtful.

To study the second concern, the voltage stability sensitivities of the six loads in the IEEE 14-bus system are examined. For this purpose, two different operation conditions – with and without considering the nonlinear effects – are studied. The

nonlinear effects are the reactive power limit, actions of the switched shunts, and the movements of the tap changers.

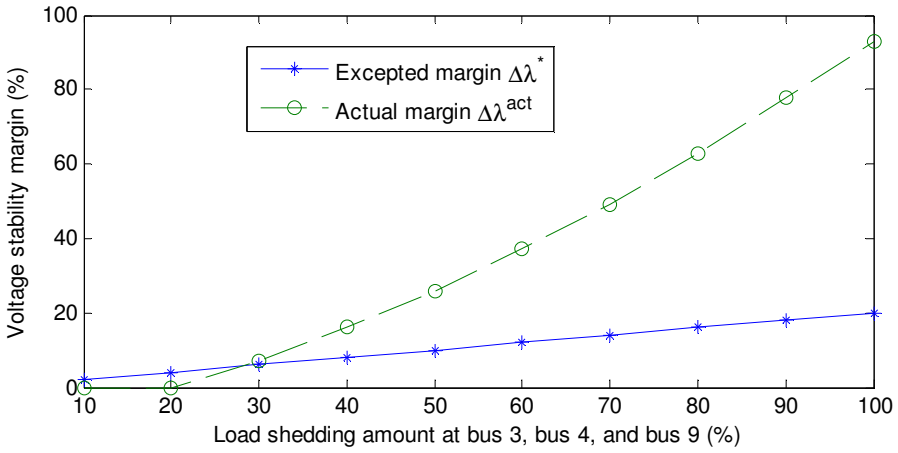

Figure 4.26 The actual and the expected voltage stability margins

The margin increment results with respect to different load shedding amounts are shown in Figure 4.27. According to Figure 4.27(a), when the nonlinear effects are not considered, the relationship between the margin increments and the load shedding amount is almost linear. In other words, without considering the nonlinear effects in the system, the sensitivities remain relatively constant. On the other hand, when the nonlinear effects are considered, these sensitivities vary significantly, as shown in Figure 4.27(b). This figure also indicates that shedding more loads does not necessarily lead to a higher margin increment.

According to what was explained above, none of the assumptions considered in (4.20) are exactly valid in power systems. Therefore, the solution obtained by (4.20) may not even be close to the optimal load shedding results. In order to

optimize the load shedding amount for voltage collapse prevention, a practical strategy called the multistage optimization method is proposed in this work.

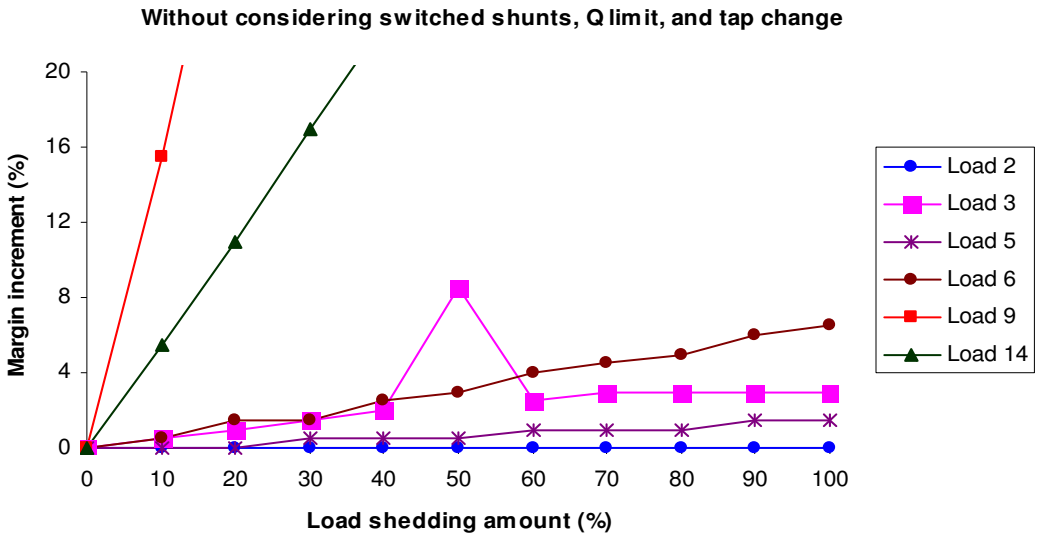

(a) Margin increments with respect to different load shedding amount (without considering the nonlinear effects)

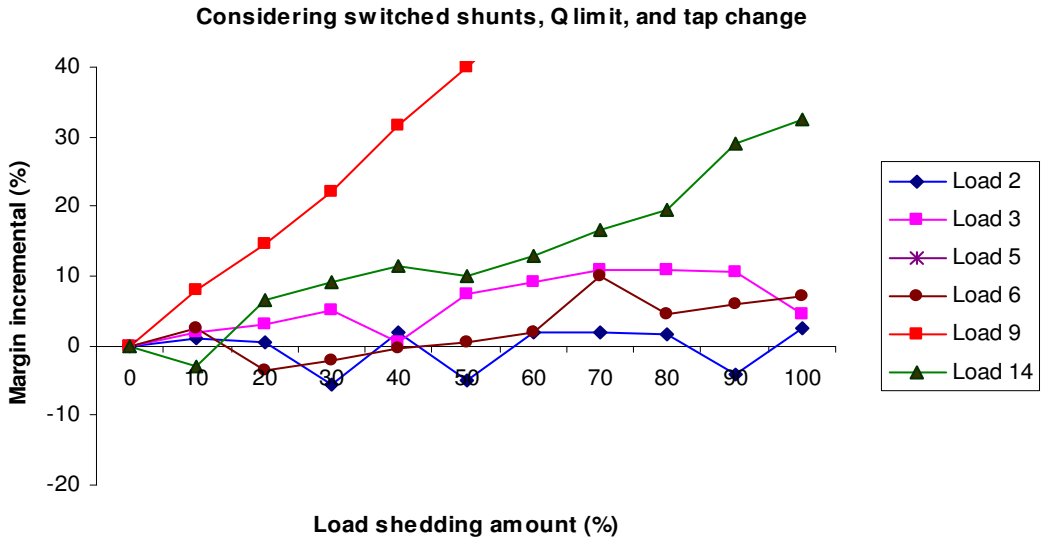

(b) Margin increments with respect to different load shedding amount (with considering the nonlinear effects)

Figure 4.27 The variation of the sensitivities under different load shedding amount

4.4.1 The proposed multistage optimization method

The above analysis indicates that a nonlinear optimization problem, as described by (4.21), needs to be solved to obtain the optimal load shedding rules.

$$\begin{aligned} \min & \left\{ S_{shed} = \sum_{i=1}^{m} \Delta S_i \right\} \\ & \Delta\lambda^* = f\left(\Delta S_1, \Delta S_2, \cdots, \Delta S_m\right) \\ & \Delta\lambda^* \geq \Delta\lambda^{req} \\ st. \quad & power\ flow\ \varphi(z, s) = 0 \\ & Power\ \ system\ \ components\ \ Limits \\ & Limits\ proposed\ by\ the\ load\ shedding\ providers \end{aligned} \tag{4.21}$$

where S_{shed} is the total load shedding amount, m is the number of available load shedding providers, z is the system state vector, and s is the vector of active and reactive powers consumed by the loads.

As seen in (4.21), several power system operation constraints including power flow equations, power system components limits, and the limits of load shedding providers are considered in the optimization problem. More factors, such as generators' cost functions and load characteristics, can also be considered as long as they are properly modeled in (4.21). However, the principle of solving this nonlinear optimization problem remains the same. In this work, we focus mainly on introducing the principles of the multistage optimization method, which is used to solve the problem described by (4.21).

Previous analysis reveals that the relationship between the margin improvement and the load shedding amounts is an unknown nonlinear function, say a function *f*. Therefore, one of the challenges in solving this nonlinear optimization problem is to get a hold of the function *f*. This function is impossible or at least very difficult to obtain since there are thousands of variables related to it.

To overcome this difficulty, a practical multistage optimization method is proposed. It is called multistage because it solves (4.21) stage by stage. For each stage, two circumstances are considered:

1) The load shedding is applied at only one location at a time.

2) The load shedding amount is limited to a small value (say 10%) so that the sensitivities can be considered constant.

Considering the above conditions, equation (4.21) can be converted to a series of linear optimization problems, i.e., the function *f* is approximated by a piecewise linear method with consideration of only one variable at a time. At each stage, the linear optimization problem can be described by (4.22). By solving these linear optimization problems one by one, the voltage stability margin is improved stage by stage. Until the last stage, the desired voltage stability margin is obtained. The

solution to the original problem is the combination of the solutions to all these linear optimization problems.

$$\begin{aligned} &Max \ \{\Delta\lambda_i\} \\ &st. \quad \Delta\lambda_i = Sen_i \times \Delta S_i \\ &\quad i = 1,2,...,n \end{aligned} \tag{4.22}$$

Since (4.22) is a linear optimization problem, it is quite easy to solve. It suffices to calculate the sensitivities and select the load with the highest sensitivity.

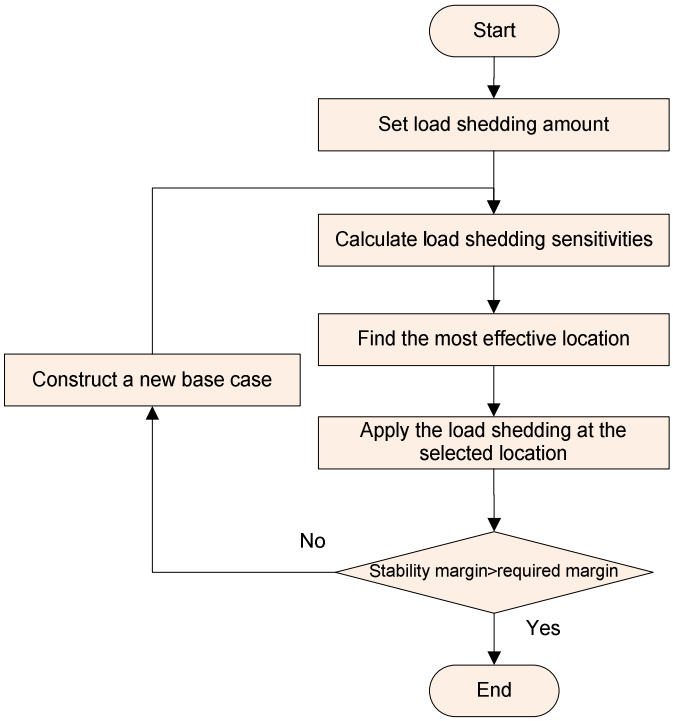

Figure 4.28 The flowchart of the proposed multistage method

The procedure of the proposed multistage method is depicted in Figure 4.28. As seen in this figure, the sensitivities are calculated at each stage and the load with

the highest sensitivity is selected as the most effective location. The load shedding is then applied at the selected location. After this load shedding, a new operation case is constructed and the next stage starts. This process will be repeated until the required margin is obtained. The final load shedding rule is the combination of the results from all stages. It is worthwhile to mention that the term "multistage" is used to describe the design procedure, not to reflect the load shedding stages in implementation.

The load shedding sensitivities can be calculated by using any existing method such as that proposed in [4]. The main problem of this group of methods is that they are very time-consuming. This problem becomes more important in the proposed multistage method because the sensitivities need to be calculated at each stage, and a large number of stages might be necessary for a large-scale power system. A new algorithm is required in order to make the proposed multistage method more practical. The new algorithm should be able to find the most effective location for the load shedding with little computing effort. In this study, the weak bus ranking application presented in Section 4.3 is used.

Combined with the procedure of identification of the weak load buses, the proposed multistage method can be implemented by following the procedure depicted in Figure 4.29. In the new procedure, the multiport network equivalent is constructed at each stage. Then, the impedance ratio is used to find the most sensitive (weak) load bus. Finally, the optimum load shedding amount is obtained.

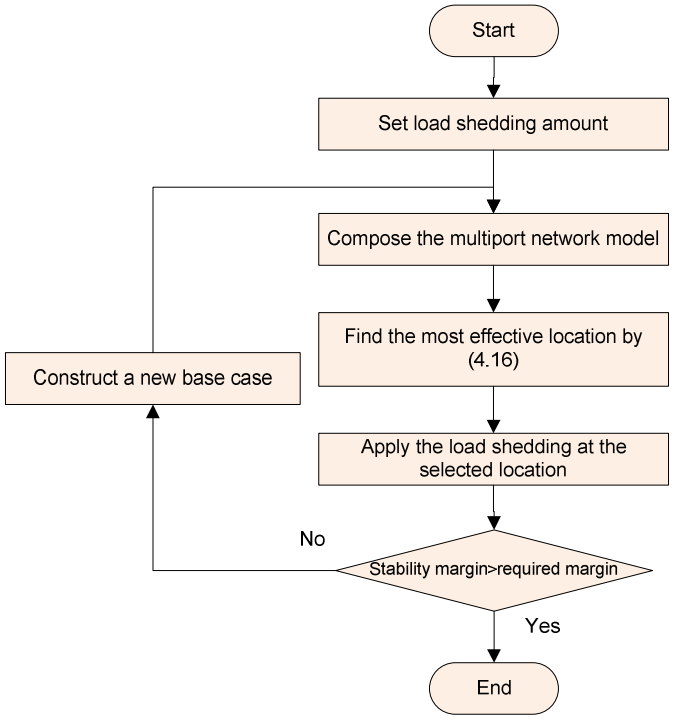

Figure 4.29 The flowchart of the proposed strategy with weakest bus identification

In the next subsection, the procedure described in Figure 4.29 will be illustrated by using the IEEE 14-bus system, the IEEE 118-bus system, and a real 2038-bus power system.

4.4.2 Illustration studies of the selected power systems

The proposed multistage optimization strategy is applied to several test power systems and the results are investigated in this subsection. Both the proposed method and the conventional method described by (4.20) are used in this study.

The results obtained from the conventional method are used as comparison references. The detailed information regarding the conventional method can be found in [73]. The load shedding step size is defined as 10% of the selected load for both methods.

IEEE 14-bus system: This test power system is a stressed system from the base IEEE 14-bus system. The studied case has 1.85 times more load demand than the base system. The voltage stability margin of the studied case is 42%. After a selected N-2 contingency, i.e. two transmission lines outages (the branch between bus 2 and bus 4, and the branch between bus 2 and bus 5), the power system loses its power flow solvability. The load shedding strategy is then applied to ensure that the voltage stability margin is no less than the required 5% (WSCC standard [46]).

Based on the bus ranking results, load bus 14 will be chosen at the first stage and the load shedding amount is 10% for this stage. This procedure is then repeated until the required voltage stability margin is obtained. Table 4.6 lists the load shedding results obtained from the proposed strategy and those obtained by the conventional strategy. As seen in this table, in order to restore the system, the proposed method shed 0.43MW less active power and 2.28 Mvar less reactive power.

Table 4.6 Results of the load shedding rules for IEEE 14-bus system

<table>
<tr><th>Methods</th><th colspan="3">Load shedding rules</th><th>Total shedding amount</th><th>Margin after shedding</th></tr>
<tr><td rowspan="14">The proposed strategy</td><td>Stage</td><td>location</td><td>Amt (%)</td><td rowspan="14">29.36 MW,

11.84 MVar</td><td rowspan="14">5%</td></tr>
<tr><td>1</td><td>14</td><td>10</td></tr>
<tr><td>2</td><td>14</td><td>10</td></tr>
<tr><td>3</td><td>9</td><td>10</td></tr>
<tr><td>4</td><td>9</td><td>10</td></tr>
<tr><td>5</td><td>9</td><td>10</td></tr>
<tr><td>6</td><td>14</td><td>10</td></tr>
<tr><td>7</td><td>14</td><td>10</td></tr>
<tr><td>8</td><td>9</td><td>10</td></tr>
<tr><td>9</td><td>14</td><td>10</td></tr>
<tr><td>10</td><td>10</td><td>10</td></tr>
<tr><td>11</td><td>14</td><td>10</td></tr>
<tr><td>12</td><td>9</td><td>10</td></tr>
<tr><td>13</td><td>4</td><td>10</td></tr>
<tr><td rowspan="4">The conventional method</td><td colspan="2">Location</td><td>Amt (%)</td><td rowspan="4">29.79 MW,
14.12 MVar</td><td rowspan="4">6%</td></tr>
<tr><td colspan="2">14</td><td>100</td></tr>
<tr><td colspan="2">10</td><td>100</td></tr>
<tr><td colspan="2">9</td><td>20</td></tr>
</table>

IEEE 118-bus system: The test system is a stressed IEEE 118-bus system. The studied case has 2 times more load demand than the base IEEE 118-bus system. The stability margin of the studied case is 6%. After an N-1 contingency, i.e. the loss of the line between bus 74 and bus 75, the system voltage stability margin shrinks to 4.0%. The results for the load shedding rules are listed in Table 4.7. In this case, the results of the proposed strategy are the same as the conventional

method. The reason is that this contingency is not severe and very small amount of load shedding is enough to restore the system. As a result, as seen in Table 4.7, the proposed strategy is completed in only one stage. In this situation, the performance of the proposed strategy might be improved by reducing the percentage of the load shedding amount at each stage.

Table 4.7 Results of the load shedding rules for IEEE 118-bus system

Methods	Load shedding rules			
	Location	Amt (%)	Total shedding amount	Margin after shedding
The proposed strategy	Bus 44	10	1.6 MW, 1.2 Mvar	5%
The conventional method	Bus 44	10	1.6 MW, 1.2 MVar	5%

A real 2038-bus power system: A 2038-bus power system is studied here. After an N-1 contingency, i.e. loss of the line between bus 74 and bus 814, the system loses its power flow solvability. To save space, only the final results of the load shedding rules are listed in Table 4.8, which shows that the proposed method shed 1.67 MW less active power and 1.05 Mvar less reactive power.

In order to further verify the advantage of the proposed multistage method, another N-1 contingency, which is the loss of the line between bus 1164 and bus 1165, is studied. After this contingency, the system again loses its power flow

solvability. The top 5 weakest load buses for this case are the buses 1169, 19156, 19185, 4590, and 19371.

Table 4.8 Results of the load shedding rules for a real large system (outage of the line from bus 74 to bus 814)

Methods	Load shedding rules			
	Location	Amt (%)	Total shedding amount	Margin after shedding
The proposed strategy	4220	100	34.89 MW, 15.49 MVar	5.0%
	4219	30		
	99393	10		
The conventional method	4220	100	36.56 MW, 16.54 MVar	6.0%
	4219	40		

Table 4.9 Results of the load shedding rules for a real large system (outage of the line from bus 1164 to bus 1165)

Methods	Load shedding rules			
	Location	Amt (%)	Total shedding amount	Margin after shedding
The proposed strategy	1169	60	6.85 MW, 2.4 MVar	8.0%
	19185	10		
The conventional method	1169	100	9.5 MW, 3.7 MVar	8.0%

Both the conventional method and the proposed multistage method are studied to determine the optimal load shedding rules. The results are listed in Table 4.9. As

seen in this table, the proposed method shed 38.6% less active power and 54.1% less reactive power.

The above case study results confirm the advantages of the proposed multistage method. Compared to the conventional load shedding amount calculation algorithms, the required load shedding amount calculated by the proposed multistage optimization method is much less.

4.5 Summary and conclusions

In this chapter, the impedance matching theorem was applied to the coupled single-port network equivalent. By modeling the coupling effects as virtual impedance, the maximum power which can be transferred to each load bus was obtained at the condition of impedance matching. Thus the maximum scaling factor was obtained, and so was the voltage stability margin.

The voltage stability margin calculation method mentioned above only utilizes the information from current operating condition. However, when the system is getting stressed, the movements of voltage controlling devices (such as the switched shunts, OXLs, and so on) should be taken into account. In order to consider the actions of voltage controlling devices, a prediction/correction method was presented. The predictor is the voltage stability margin estimated above. The

correction procedure includes running a couple of power flows, which would take the voltage controlling devices into consideration.

Several test power systems were studied to verify the presented methods. The results showed that the proposed method has the following advantages:

1) The voltage stability margin estimated by the impedance matching theorem at the base case is very close to the actual one. This makes it promising in terms of fast protection.

2) The prediction/correction method can converge to the actual voltage stability margin with little computing effort. This feature makes it more suitable for online applications.

Since proper selection of load shedding locations is critical to optimize the load shedding amount, it would be very useful to rank the load buses based on their weaknesses. Traditionally, voltage level is used to evaluate the weakness of the load buses and to trigger the designed load shedding schemes. Due to the heavy use of reactive power support, the limitations of using voltage level as the indicator become more and more obvious. This chapter presented a method to rank the load buses for the purpose of selecting suitable load shedding locations, based on the impedance ratio between the equivalent impedance of the transmission network and the equivalent impedance of the load.

The impedance matching theorem expresses that the maximum power is reached (voltage collapse point) when the impedance ratio is equal to 1. Therefore, it is reasonable to use the impedance ratio as an indicator to rank the load buses. Several power systems were studied by using the modal analysis method and by using the proposed method. The comparison of bus ranking results confirmed the validity of the proposed method. Furthermore, an interesting feature of the proposed method has been discovered during the case studies. Unlike the modal analysis method, by which the results obtained show sharp variations during the system getting stressed, the results calculated by the proposed method are usually consistent. This unique feature makes it very promising in terms of online load shedding applications.

Last but not least, the load shedding amount is another important parameter of the load shedding schemes. Because of the nonlinear relationship between the voltage stability margin and the load shedding amount, a nonlinear optimization problem needs to be solved for optimizing the load shedding rules. A practical multistage optimization method to solve such a nonlinear optimization problem was proposed in this chapter. By using the piecewise linear method, the multistage method converts the original nonlinear problem into a series of linear programming problems and solves these linear problems one by one. At each stage, the voltage stability margin is improved and the desired margin is obtained at the last stage.

Chapter 5

The event-driven load shedding scheme

Load shedding schemes can be generally classified into two types based on their triggering mechanism: response-based schemes and event-driven schemes. A comparison of these two triggering mechanisms is conducted in this chapter in order to clarify the advantages of the event-driven schemes. Following the comparison, a comprehensive review of the event-driven load shedding schemes currently implemented in power systems is made, then a new event-driven load shedding scheme is proposed. The new event-driven load shedding scheme utilizes the three applications presented in the previous chapter for fast calculating the load shedding rules.

The proposed event-driven load shedding scheme involves the following actions:

1) Compute a lookup table of load shedding actions for various credible and critical events. This table will be updated periodically or driven by events. The table is stored in the EMS (Energy Management System) as a special protection scheme.
2) The EMS collects the status of the power system by using the SCADA (Supervisory Control and Data Acquisition) system.
3) The load shedding action is triggered when an event in the lookup table is

detected.

The advantages of the proposed event-driven load shedding scheme are its speed of operation and ease in obtaining the optimal load shedding locations and amounts. With the increasing observability of modern power systems, the proposed scheme can easily be integrated into the EMS and perform a good protection against voltage collapse.

5.1 The triggering strategies of load shedding schemes

Two types of strategies are generally used to activate the protection schemes in power systems: response-based strategy and event-driven based strategy [73].

5.1.1 Response-based strategy

When the operation condition of the system changes, such as with the loss of a transmission line (*an event*) or change in electrical quantities (*the responses*), they are always manifested in the voltage or frequency at some locations. The response-based schemes, such as undervoltage load shedding schemes, use these voltage or frequency fluctuation signals to determine whether or not the power system is in an emergency condition. Table 5.1 presents an example of the response-based load shedding scheme.

Due to the limited communication ability in the past decades, response-based schemes gained more attention than the event-driven based schemes and many were implemented, such as the prevailing undervoltage load shedding schemes. However, the response-based technique is difficult to use nowadays as discussed in Chapter 2. First of all, it is difficult to establish the settings (i.e. when to trigger the load shedding actions) at various locations of the load shedding participants. The response-based actions also take more time than the event-driven based actions to kick in due to lack of coordination. Moreover, it is hard to optimize the amount of load shedding since only information at the local area is generally taken into consideration.

Table 5.1 Comparison of response-based schemes and event-driven schemes

Algorithm	Sample protection rules	
	Trigger	Action
Response-based	Voltage at bus #*i* less than 0.9 pu	α MW Load deduction at bus #*j*
Event-driven based	Transmission line #*k* is out of service	β MW load deduction at bus #*h*

5.1.2 Event-driven based strategy

The event-driven based schemes directly detect the changes of network topology or operation conditions of power components, which would push the power

system into emergency condition. For example, if the outage of a line might lead to an emergency condition, the event-driven based schemes directly triggers the protection actions based on whether the line is connected in the system or not.

The advantages of the event-driven based algorithms are that they can directly detect the cause of the emergency condition in a power system's control centre, compute the required load shedding actions, and then distribute these actions to the corresponding locations. These algorithms are much faster than the response-based schemes and can be easily implemented and optimized. The event-driven approach has become more and more attractive with the development of modern communication technology and the greater availability and reliability of detective sensors.

In general, an event-driven based strategy can be described by a flowchart such as in Figure 5.1. The flowchart indicates that three main tasks are involved in the design of an event-driven based load shedding scheme:

- **Events detection**: detect the changes of the monitored components in the power system by using the SCADA and/or PMUs, which are generally available.
- **Computation of the load shedding lookup table:** this is the core part of the event-driven load shedding schemes. The load shedding lookup tables are calculated through offline planning studies. They are updated either

periodically (daily or hourly depending on necessity) or by event-triggered tuning studies at the System Control Center (SCC).

- **Load shedding operation**: when a critical event is detected, the load shedding scheme will evaluate whether a specific load shedding job is needed. If a load shedding task is needed, the amount, location, and time delay of the load shedding (obtained from the lookup tables) will be sent to the operation station through either SCADA or some other dedicated communication path. The load shedding action can be done automatically or manually.

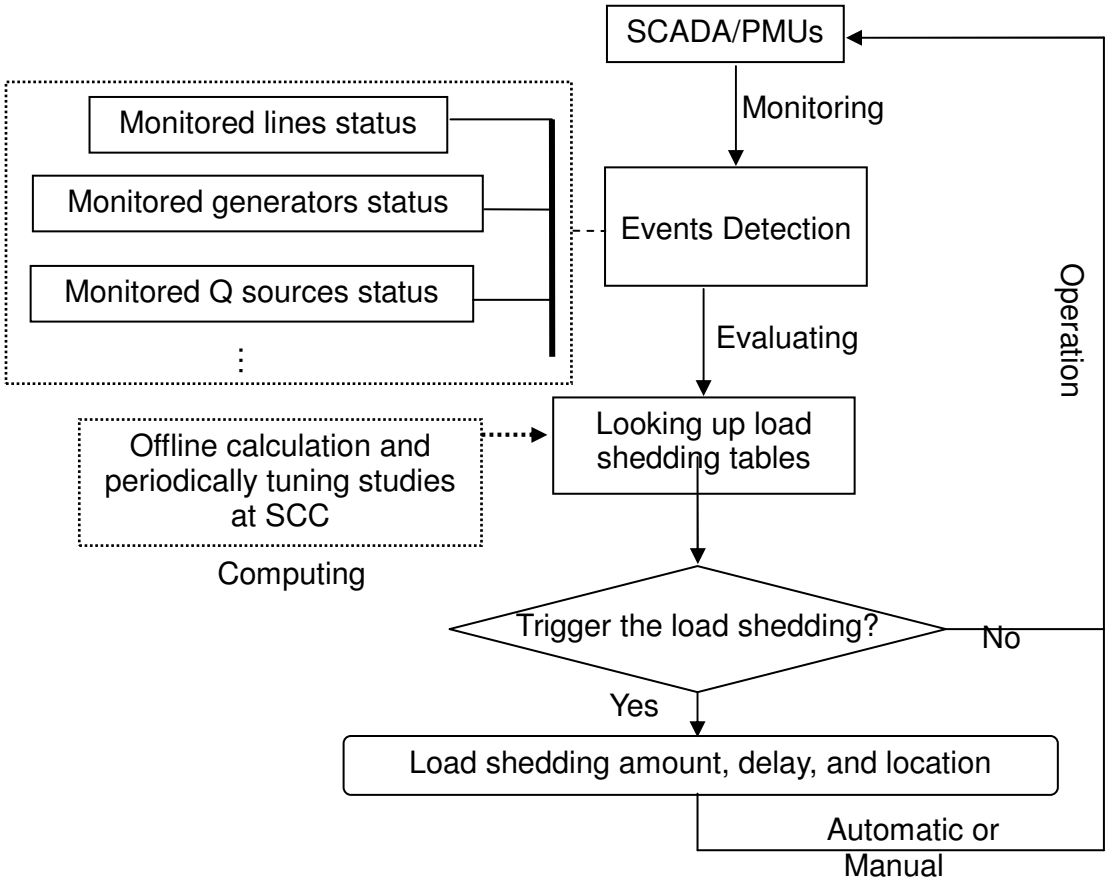

Figure 5.1 The flowchart of event-driven based load shedding schemes

The above three tasks describe the general procedure to design an event-driven load shedding scheme. An extensive review of the implemented event-driven load shedding schemes was conducted and the findings are presented in the next subsection. The experiences obtained from the literature review are adopted in the proposed event-driven load shedding scheme.

5.2 Literature review on the implemented event-driven load shedding schemes

During this research, the following load shedding schemes were studied in detail:

- Fast acting load shedding scheme (FALS) for Florida Power and Light, 1982 [75]

  As an EMS function, the scheme acts as a protective relay scheme to prevent the approaching blackout. It was installed at the system control center (SCC) and used the statewide SCADA communications to control the load shedding in the south Florida area. There are two reasons to choose the SCC. The first is that the SCC was already a central collection point of the power system measurements which needed to be monitored to determine if a serious disturbance had occurred. In addition, the communication system can bring measurements into the SCC every two seconds. The second reason is that

there was an existing load shedding program used manually. It could easily be modified to accept a new design.

Considering several requirements, such as operational speed (determined by the offline system studies), the scheme needs a six by six matrix of alarm condition of individual telemetered points. At least one point in each row (level) had to be in the alarm condition to set a flag for that level. All six level flags had to be set, at the same time, to immediately trigger a load shedding action. A delayed load shedding is initiated if four specific levels are set and verified in the alarm condition for a specific delay period.

The design philosophy of the matrix is that the measurements in level one and level two are used to determine that a loss of sufficient magnitude has occurred within the state, such as in generation changes. On the other hand, the measurements in level three to level five are used to determine if a loss of generation leads to the system instability. The measurements in level six are to monitor the interchanges with other systems.

- Three event-driven based load shedding schemes for Entergy System [76]

The purpose of the fast acting load shedding scheme (VSHED) is to develop an automated process that could detect instability in the region and trigger the predefined load shedding. It obtains information directly from the SCADA

system. It also needs a communication path, which is from the problem location to the transmission operation center.

In order to trigger the predefined load shedding actions, three conditions have to be simultaneously satisfied: 1) the load level on the Franklin auto is greater than 360MW; 2) voltage at three of four critical buses should drop below 0.92 pu simultaneously (these buses and voltage level were selected based on steady state and dynamic simulations); and 3) the Franklin transformer should be off-line.

The load shedding is applied in blocks in order to provide operational flexibility and minimize impact on customers. The load shedding locations are selected based on the voltage stability sensitivity and the priority of the loads. The amount of load shedding is increased until the voltages in the region recover to the acceptable level.

The VSHED performs its function without a dispatcher's intervention. It monitors the system condition every two seconds and checks whether the load shedding criteria are being met and whether the load shedding command should be issued. A user-defined delay may be specified between load shedding groups to allow voltages to settle down, but there will be no delay between breaker operations within one group; trip command is issued to all breakers within one group at the same time.

- Two event-driven protection schemes for Hellenic System [73]

For the projected load of 2007 and assuming a reasonably pessimistic weakened Hellenic system, voltage collapse may be encountered for two critical contingencies involving loss of generation in Attica and Peloponnese. These two critical contingencies are: 1) loss of both circuits of the Lavrio-Pallini 400 kV line; 2) loss of two generation units at a particular power station.

The system study shows that all other credible contingencies always have acceptable voltage stability margins. Thus, an event-driven load shedding scheme is only designed to protect the system against these two specific contingencies. The protection scheme, event-driven, is manually armed from the control centre, when the system is considered insecure for the corresponding contingency based on the online voltage stability analysis and operational experience.

The validity of the two load shedding schemes is examined through quasi-steady state simulation studies concerning the actual and projected stressed system conditions. The load shedding location and amount are determined by using the sensitivities between the expected voltage increase and the load shedding amount. The experience of the load shedding scheme indicates that

the wide-area, open loop load shedding strategy is the most effective in terms of shedding amount.

- Load shedding and generation shedding for BC System [77]

The remedial action scheme (RAS) presented in this paper has been used extensively in the BC power grid to mitigate the impact of certain credible contingencies in the systems. This scheme involves both generation shedding and load shedding actions. It has been used to enable the BCTC system operator to operate the system closer to the transfer limit, hence the system capability will increase significantly.

The arming adjustment of the RAS is made centrally at the system control centre. It is armed automatically by the EMS at the SCC every four minutes or immediately following a change in network configuration based on the prevailing system conditions. Network configuration, equipment status, actual power flows, area load levels, and post contingency operation constraints are all taken into account. The reason to choose the EMS based RAS is that the system information is already available at the SCC and it ensures the coordination of RAS control actions.

The actions corresponding to different operation scenarios and different events are listed in a group of lookup tables. There is one lookup table for each

operation scenario. Each row in the lookup table indicates the actions that should be taken for a specific event. These lookup tables are obtained through operation planning studies.

- Defence plan against extreme contingencies in Hydro-Quebec power system [78]

In order to increase the system's ability to withstand some extreme contingencies, Hydro-Quebec developed a number of special defensive measures, called "defence plan against extreme contingencies." The purpose of this plan is to detect and confine incidents that exceed the system's strength automatically. Due to the large number of possible extreme contingencies, the defence plan is designed to detect the consequence of the contingency on the power system rather than to detect the contingency itself. In other words, the defence plan is basically triggered by the response of the system after an extreme contingency occurs. At the same time, the defence plan also aims to make the greatest possible use of the local measurements and to perform the remedial actions locally.

Since the defence plan is developed to protect the system against a set of extreme contingencies, it involves a set of measures corresponding to the list of contingencies as well. One of the main problems encountered is ensuring the coordination of these various measures. The solution is to clearly define

the operation condition for a specific task of each measure. Thus, during complex contingencies involving a number of measures, no outside coordination is required. Each measure must be able to act as a function of its own protection range (list of contingencies), and the combination of actions should ensure preserve the power system's stability.

Based on the above investigation special attention needs to be paid to the following concerns:

- Distinguish between **sudden and slow loss** of components, especially generators.

- Operation conditions: **peak periods and off peak periods**. This consideration is necessary to prevent a load shedding for the same event, but at off peak periods.

- **Time issues**: line fault clearance time, capacitor banks switching time, and load shedding execution time.

- **Import limit on the interconnections**: the available transfer capability (ATC) limits have a big influence on the system operating condition. They may change daily or even hourly. Therefore, the status of ATC limits should be monitored.

- **Available amount to be shed**: even if the load shedding scheme is perfectly designed and the circuit breakers are opened as required, voltage collapse could still happen if the selected shedding locations do not have sufficient load amount to be shed. Thus, monitoring of the available amount of load at the candidate load shedding locations should be considered in the load shedding logic.

- **Coordination** of the load shedding rules. The coordination is particular for the events which may happen chronologically in a short period, in which the load shedding action for the first event has not settled down. In this case, if the next load shedding action takes place as usual, some unexpected problems may occur. Therefore, coordination between the load shedding actions needs to be considered.

- **Failure detection**: Besides the failure of SCADA, the load shedding scheme should detect the failure of circuit breaker, relay, communication link, etc. It should also inform the system operator about the failure, to be prepared to perform manual load shedding, and when to initiate manual load shedding.

Besides overcoming the above issues, a load shedding scheme should also have the following additional features:

- **Accurately detect the approaching voltage instability**: many implemented load shedding schemes, such as the single-port impedance match based load shedding scheme, suffer from the difficulties that the approaching voltage instability problems cannot be detected in a timely manner.

- **Ease of setting the parameters**: due to the fast changing of the power consumption pattern and large amount of power integrated from the distributed generations, the pattern of power flow for an interconnected power system may experience big changes every day or even every hour. Under this condition, the designed load shedding scheme should be able to easily change the load shedding rules to protect the system under the new power flow pattern.

- **Ease of implementation**: another very important feature of the designed load shedding scheme is that it should be easy to implement, and especially it should be able to be embedded in the EMS. It should utilize the existing infrastructure as much as it can, rather than install new ones.

Since the load shedding decision is made at the SCC, it has the same challenges as other centralized load shedding schemes. The main challenge is the time delay, especially the communication delay of SCADA. This is the particular reason why

the time delay has to be calculated and verified in task 3 mentioned in Section 5.1.

5.3 The proposed event-driven based load shedding scheme

The literature review demonstrates the advantages of the event-driven based load shedding schemes as they are adopted by many utility companies. However, although many event-driven load shedding schemes have been implemented, there are no general procedures that power system engineers can follow in designing their specific load shedding actions. Moreover, there are no well-accepted methods to optimize the load shedding amount. The findings in the literature review can help people to prepare the necessary information about the power system, but they cannot guide the design. Therefore, there is a need to come out with a new load shedding scheme, which can be easily implemented by the power system engineers.

A new event-driven load shedding scheme, shown in Figure 5.2, is proposed in this thesis. It is based on the findings from the literature review and the collected information from the utility companies, which represent state-of-art modern power systems. The proposed event-driven load shedding scheme is intended to be an application of the EMS. The calculation of load shedding rules is automatically triggered if the system status violates any of the user-defined criteria. A criterion can be a period of time (i.e. the calculation is called daily or hourly), or big changes of some monitored variables (such as the changes of

reactive power reserve at a particular area), and/or a command from the SCC.

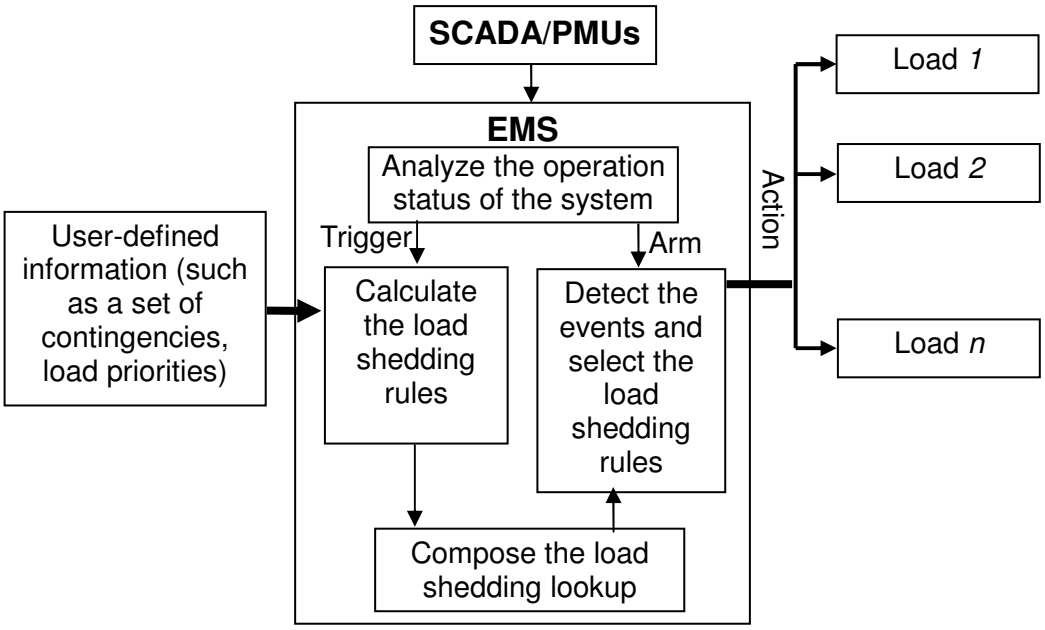

Figure 5.2 Implementation of the proposed event-driven load shedding scheme

When the calculation is activated, a set of user-defined information such as a list of contingencies will be studied. During this study, the current load shedding rules will be evaluated against these contingencies. If one or more of the contingencies cannot be protected by their corresponding load shedding rules, then new load shedding rules for them will be computed by calling a function block ("Calculate the load shedding rules"), which is preinstalled in the EMS. Once the new load shedding rules are obtained, the load shedding lookup table will be updated in the EMS.

The role of the second block ("Detect the events and select the load shedding rules") is to detect the events, to select the right load shedding rules, and to send the load shedding commands to the individual load shedding locations.

The EMS monitors the status of power system components through SCADA. Selected events will be passed to this block. If an event is recognized as one of the events listed in the lookup table, the EMS will put the corresponding load shedding rules into action. A typical lookup table looks like Table 5.2. In the following subsections, the three main tasks discussed in section 5.1 are discussed in detail.

Table 5.2 A sample event-driven based load shedding lookup table

Event no.	Load *1*	Load *2*	…	Load *n*
Event *1*	1.2MW, 0.3Mvar	None	…	5.0MW
Event *2*	None	2.3MW, 1.2MVar	…	None
…	…	….	….	…
Event *m*	2.4MW, 0.6Mvar	1.15MW, 0.6MVar	…	2.5MW

5.3.1 Task 1: Event detection

This task is aimed to extract information from data collected by SCADA. It will detect the failure of SCADA and also deal with the issues related to bad data. The

data extracted will be stabilized. It will then be used to trigger the application of calculating load shedding rules and to arm the load shedding actions. One example is shown by Table 5.3. To effectively protect the power system, it should be as fast as possible.

Table 5.3 Event detection (*Template*)

Event No. / **System status**	Event 1	Event 2	…	Event n
Line outage	Specific line *x*	…	…	…
Generator status (outage, reactive power limit, …)	On (Off)			
Var reserves	*y* Mvar			
Breaker status	On (off)			
Load amount (at the load shedding locations)	*a* MW, *b* MVar			
User-defined criteria	…			

5.3.2 Task 2: Computation of the load shedding lookup table

This task focuses mainly on the identification of the potential voltage collapse risks and finding the load shedding rules to prevent voltage collapse. A list of

contingencies (events) is provided at the beginning of this task. By examining the post-contingency voltage stability margin which is evaluated by the quasi-steady state analysis, another list of critical events is obtained. These events indicate the possible combinations of outages that would result in extremely low voltage or voltage collapse. Using the multistage strategy, the load shedding rules for each critical event can be calculated. One simple example is shown in Table 5.4.

Table 5.4 Load shedding rules (*Example*)

Event ID	Load shedding	
	Load shedding locations	Load shedding amount
1	Load bus 4220, ID 99 Load bus 4219, ID 99	27.4 MW, 11.9 MVar 9.16 MW, 4.64 MVar
2	Load bus 1169, ID 99 Load bus 19185, ID 99	9.5 MW, 3.7 MVar 1.15 MW, 0.18 MVar
3	Load bus 18234, ID 99 Load bus 19234, ID 99 Load bus 19281, ID 99	12.9 MW, 4.2 MVar 8.04 MW, 2.64 MVar 9.18 MW, 0.78 MVar
4	Load bus 19281, ID 99	1.53 MW, 0.13 MVar

As mentioned earlier in the chapter, the time delay of operating a specific load shedding rules is very important in preventing the approaching voltage collapse. According to the final report on Northeast USA-Canada blackout of August 14, 2003, it could have been averted if manual or automatic load shedding of 1,500

MW had occurred within the Cleveland-Akron area before the outage of Samis-Star 345 kV line [2]. Therefore, a load shedding rule should also indicate the maximum time-delay to complete the load shedding. The time-delay should be designed for the purpose of protection cooperation as well. This time delay information is obtained through performing time-domain simulations on the studied power system. Adding the time delay information to the load shedding rules, a complete load shedding rule should look like the ones in Table 5.5.

Table 5.5 Load shedding rules (*Example*)

Event ID	Load shedding		Maximum time delay (s)
	Load shedding locations	Load shedding amount	
1	Load bus 4220, ID 99 Load bus 4219, ID 99	27.4 MW, 11.9 MVar 9.16 MW, 4.64 MVar	0.5
2	Load bus 1169, ID 99 Load bus 19185, ID 99	9.5 MW, 3.7 MVar 1.15 MW, 0.18 MVar	0.8
3	Load bus 18234, ID 99 Load bus 19234, ID 99 Load bus 19281, ID 99	12.9 MW, 4.2 MVar 8.04 MW, 2.64 MVar 9.18 MW, 0.78 MVar	0.2
4	Load bus 19281, ID 99	1.53 MW, 0.13 MVar	39.0

5.3.3 Task 3: Load shedding operation

Load shedding operation focuses mainly on monitoring the communication

between the SCC and the load shedding locations to make sure that the signal for action is sent out correctly. It also collects the feedback from those locations to make sure that the right action has been performed.

Among the above three tasks, the second one (Task 2: Computation of the load shedding lookup table) is not only the most important but also is the one requiring more technical guidelines for power system engineers. For task 1, the commercial EMSs have already done a great deal of it. Meanwhile, the experiences on power system protection can be directly used to fulfill task 3. In the next chapter, a general procedure to complete task 2 is presented to facilitate the design of such an event-driven load shedding scheme.

5.4 Summary and conclusions

In this chapter, a comparison study of the two triggering strategies (response-based and event-driven based) of load shedding schemes was conducted. With modern technology, fast and reliable communications are usually available, which makes the event-driven load shedding scheme very attractive. A complete literature review of the implemented event-driven based load shedding schemes indicates that there is a need to develop a general procedure, which power system engineers can easily follow when designing their specific load shedding schemes. The proposed scheme aims to provide such a solution. The main tasks related to designing such a load shedding scheme are described in detail. The multi-port

network equivalent, the bus ranking algorithm, and the multistage optimization method provide an integrated support to complete these tasks.

In order to have a better understanding of the proposed event-driven load shedding scheme, a sample load shedding scheme will be provided in the next chapter. Chapter 6 will detail the design procedure, which includes the static power flow studies and the dynamic time-domain studies. The power flow studies are to determine the system voltage stability margin. The time-domain studies are used to find the critical load shedding operation time. The detailed design methodology is also given in the next chapter.

Chapter 6

Design methodology of the proposed event-driven load shedding scheme

In the previous chapter, the main tasks of the event-driven load shedding were clarified. Among all those three tasks, the second task (finding the load shedding rules) is most difficult and essential, since the amount of load shedding has a vital influence on the system's reliability and security.

This chapter describes the design methodologies of computing those load shedding rules. The load shedding rules are optimized in terms of reliability (minimum load shedding amount) and security (desired voltage stability margin). The overall design procedure includes two parts: power system planning studies and operation planning studies. In order to obtain the third parameter of load shedding rules, i.e., the time-delay, a bisection search method is used to determine the most suitable value during the time-domain simulations. The rest of the chapter details the procedures involved in the above studies. In order to have a better understanding of the described design methodologies, a sample event-driven load shedding scheme designed for the Alberta Integrated Electric System (AIES) is presented in this chapter.

6.1 Introduction

As a general principle, the proposed design procedure is intended to compute the load shedding locations and amounts for the credible contingencies based on power system planning studies on representative operation cases. Thereafter, the load shedding locations and amounts will be adjusted periodically (hourly, daily, or weekly) according to the corresponding operations planning case. The overall framework is described by Figure 6.1.

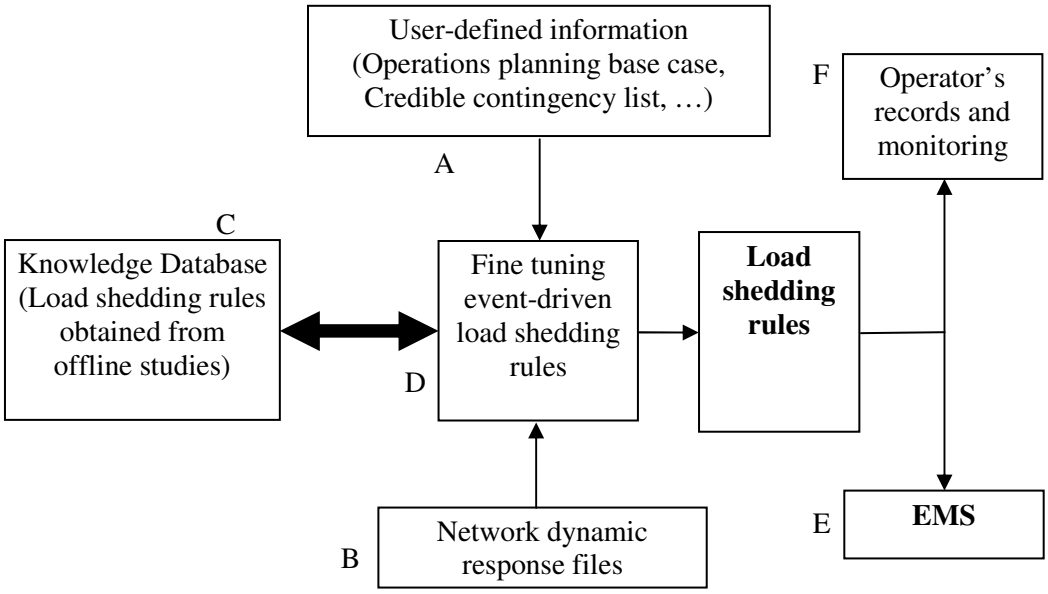

Figure 6.1 Framework of the proposed advanced event-driven load shedding scheme

In Figure 6.1, the dark blocks C, D, E, and F are the main functional blocks for this scheme. The knowledge database (Block C) records the load shedding rules obtained from power system planning studies. Block D will accept the user-

defined information (such as weekly operations planning base case) and the network dynamic response files as input. By evaluating the current load shedding rules, which are stored in the knowledge database, it indicates whether the current load shedding rules are still able to protect the system. If not, it tunes the load shedding rules based on the new case file. The new load shedding rules will be stored in the knowledge database and marked as the current load shedding rules. Thereafter, the load shedding rules are uploaded to the EMS system (Block E), which will detect the events and shed the required loads when the events occur in power systems.

Block F plays an important role in operators' interaction with the load shedding scheme. It not only shows the current load shedding rules, but also gives out the warning messages and recommended actions if the current load shedding rules cannot fully protect the system from any of the credible contingencies.

6.2 Power system planning studies to determine the candidate load shedding locations

Power system planning studies will use representative operations scenarios to calculate the load shedding rules, as shown in Figure 6.2. Those load shedding rules are used to determine the candidate load shedding locations, where the equipment should be installed or configured.

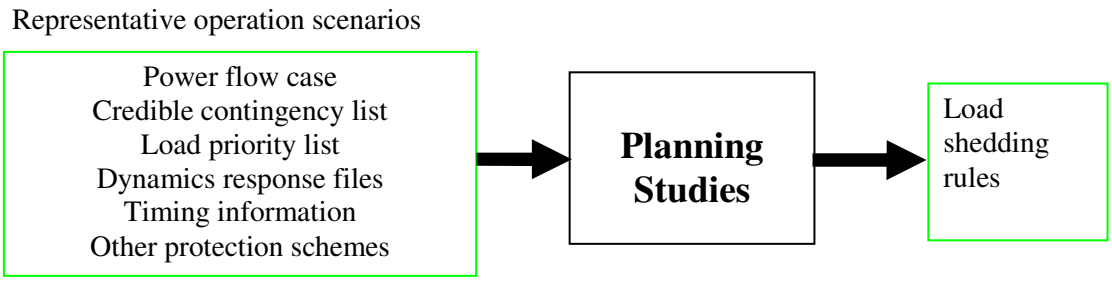

Figure 6.2 Basic input/output of the planning studies

After the input has been finalized, the following steps will be done to determine the load shedding rules. The whole procedure is shown in Figure 6.3. The steps are as follows:

- The first step is to identify the critical contingencies. All the credible contingencies will be evaluated by the standard PV curve method and the critical ones will be identified by their PV curve margin.

- At the second step, a set of load shedding locations will be selected based on their effectiveness and their priorities; then, an optimization method, which is the multistage method, is performed to minimize the load shedding amount.

- At the third step, the maximum operation time will be investigated by time-domain simulation.

- The final step is to fine-tune the implementation logic of the designed load shedding rules by using the system timing information and the information about other protection schemes.

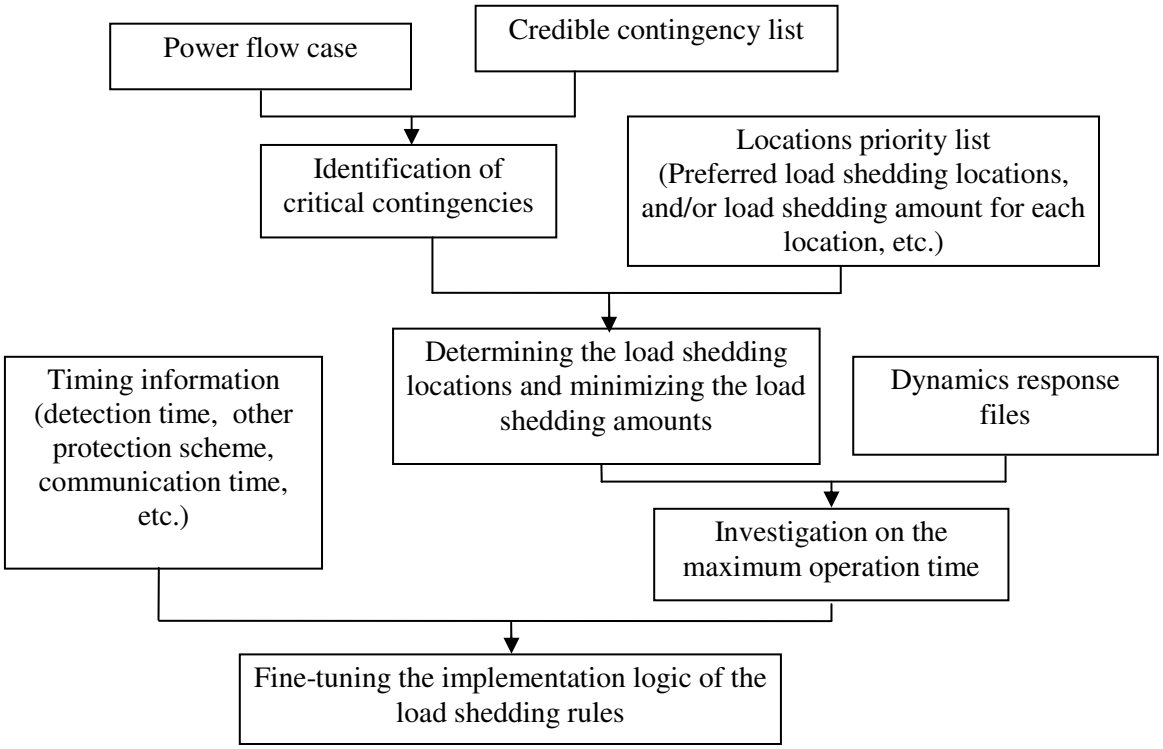

Figure 6.3 The procedure of planning studies on the event-driven load shedding

6.3 Operation planning studies on load shedding rules

The load shedding rules calculated by power system planning studies are workable for most of the representative operating scenarios. To make the load shedding rules more specific, a tuning study needs to be performed. In this work,

the weekly operating base case is used as an example to describe the procedure of operation planning studies. The load shedding rules are optimized weekly, as shown in Figure 6.4. The power system engineers can use daily or monthly operating base cases as their tuning objects based on their practical needs.

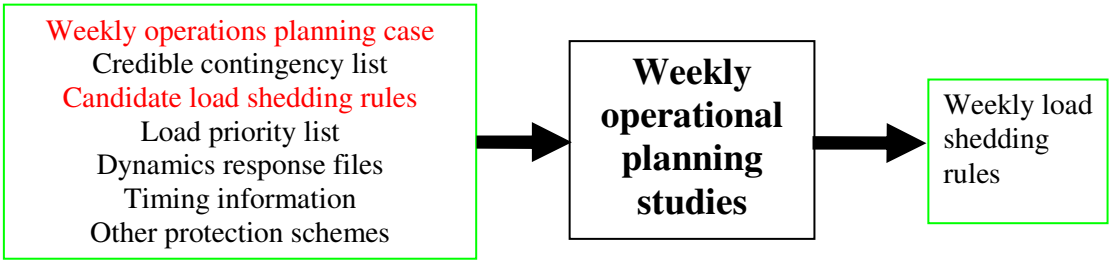

Figure 6.4 Basic inputs/outputs of weekly operation planning studies

The weekly operation planning study mainly performs the following tasks:

- Evaluate the credible contingency events recommended by utilities and identify the critical contingency events by using the industry standard PV curve method on the studied weekly operations planning case.

- Evaluate the current load shedding rules. If there are any critical contingency events unprotected, then the multistage optimization method will be used to determine the new weekly load shedding rules.

- Depending on results obtained in the above step, the study of identification

of the weakest load buses may be needed.

- Investigate the maximum allowed operation time of the designed load shedding scheme by performing time-domain simulations.

- Fine tune the weekly load shedding rules based on the results obtained from time-domain simulations.

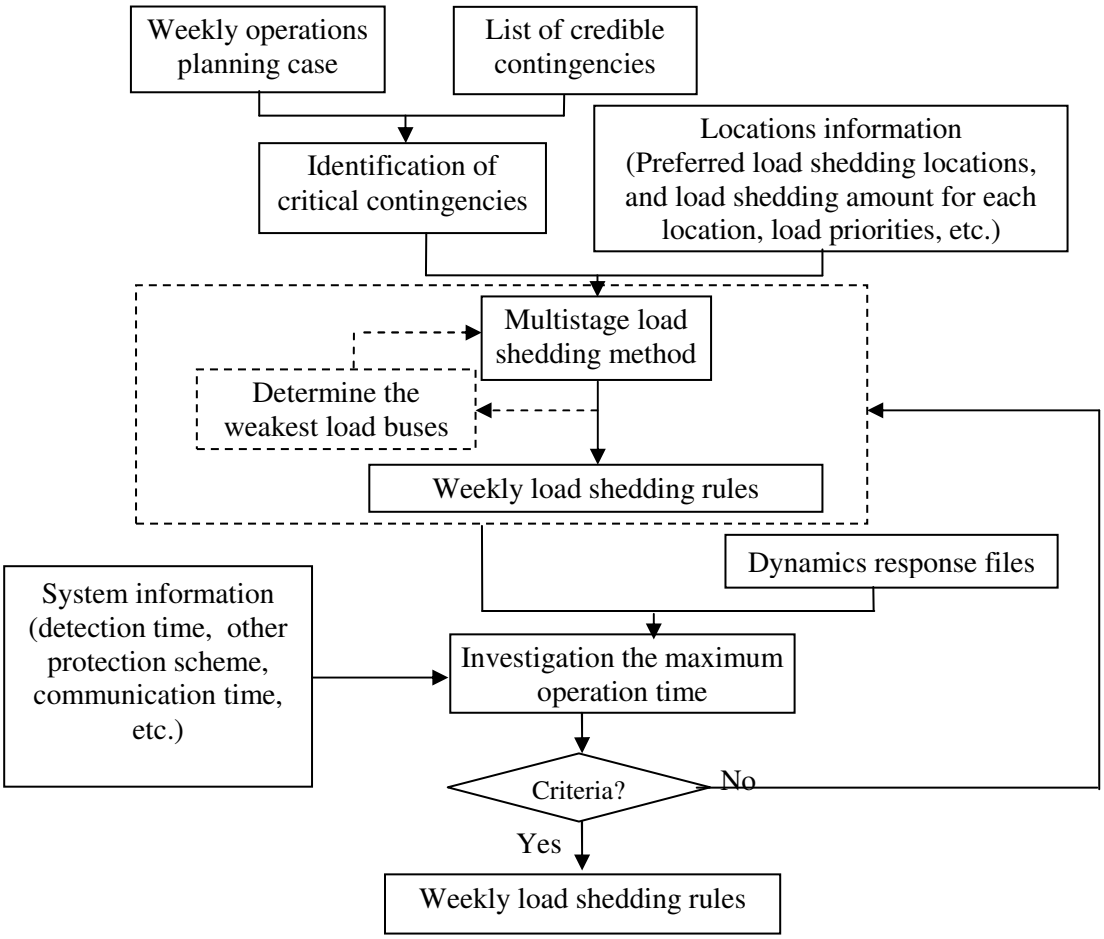

Figure 6.5 The procedure of the weekly operation planning studies

The overall design procedure is shown in Figure 6.5. The methods, including contingency scan, multistage load shedding method, and determination of the maximum operation time by bisection method, are all described in the later sections.

6.4 The Methodologies

The above subsections show the procedures of the system planning study and the operation planning study. The methodologies associated with them are described in this subsection.

a) Identification of critical contingencies

   The study performs the **industry standard PV-curve technique** to evaluate the credible contingencies and screens the critical contingencies based on their voltage stability margin (WECC standard can be applied here).

b) Determination of the load shedding locations and amount

   After the selected critical contingency is applied on the operation base case, the top 10 weakest load buses are determined by using the proposed bus ranking method.

The proposed **multistage optimization method** is implemented to finalize the load shedding locations and to minimize the load shedding amount. It takes the user-defined load locations and priorities as input. Using the multistage optimization method, it outputs the optimal load shedding rules for each critical contingency (event).

c) Investigation of the maximum operation time

After the load shedding locations and load shedding amount are determined, theoretically, the load shedding rule has been found because the event-driven load shedding is aimed to operate at the instant that the event occurs. However, there are always some delays in practice, such as event detection delay and communication time.

The proposed **bisection based algorithm** is used to find the maximum time delay, which is defined as when the designed load shedding rule can still fulfill its performance even the load shedding rules is operated with such a delay after the event occurs.

6.4.1 Task 1: Identification of critical contingencies

The objective of task 1 is to find the critical contingencies, which are defined by their post-contingency power transfer margin (normally less than 5% for N-1 contingency, less than 2.5% for N-2 contingency).

After the system operators prepared a list of credible contingencies associated with the weekly operation planning case, this task would scan all those credible contingencies and screen out the critical contingencies by using the industry standard PV-curve method. It is worth mentioning that the system operators also had to define how the system is stressed, not only because it has a big impact on the post-contingency power transfer margin, but also because it affects the load shedding rules.

6.4.2 Task 2: Determine the weekly load shedding rules

After the critical contingencies are found, task 2 will use the proposed multistage optimization method to determine the load shedding rules.

The main idea of the multistage method is to obtain the load shedding rules through several stages. At each stage, the most effective location is selected and a small amount of load is shed at the selected location (the sensitivities of voltage stability margin with respect to the amount of load shedding can be assumed constant). If the stability margin is not high enough after this load shedding, a new base case which is the old base case but with the current load shedding is constructed. Then the above process will go over on the new base case. This procedure is repeated until the desired stability margin is achieved. The application procedure of the multistage method is shown in Figure 6.6.

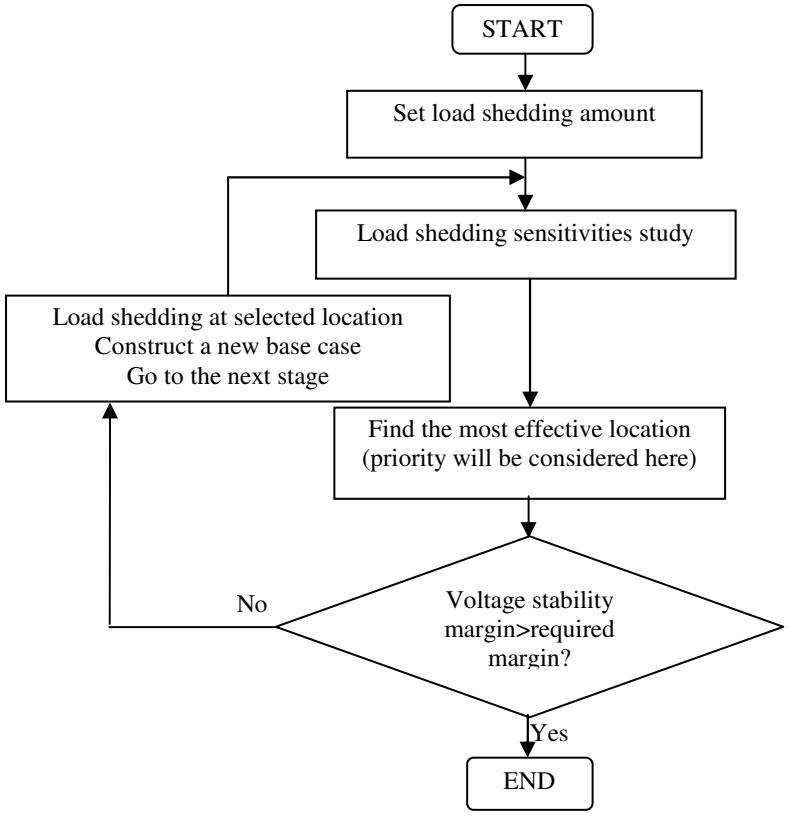

Figure 6.6 Procedure of determining locations and minimizing amounts

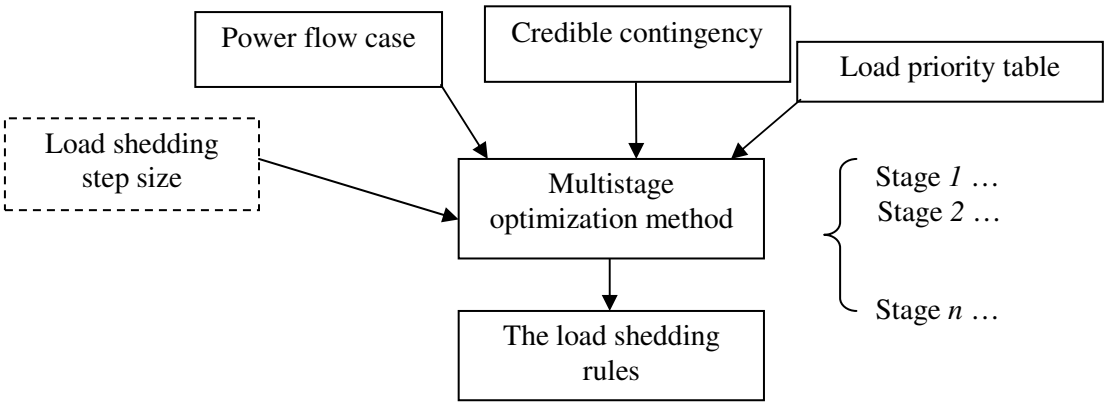

Figure 6.7 Using the multistage method to calculate the load shedding rules

For a practical load shedding scheme, the load priority has to be considered at each stage, as seen in Figure 6.7. As a result, identifying the most effective location becomes a two-objective optimization problem, in which the objectives are the maximization of the stability margin and the load priority. In order to be able to solve this optimization problem, the load priority should be considered as a weighting factor to the load shedding sensitivities. This will convert the problem into a one-objective optimization problem with the objective function (OF) as shown in (6.1).

$$
\begin{aligned}
&OF = Max\left(\sum_{i=1}^{n} k_i\right) \\
&\text{where } \mathrm{k_i} = c_i x_i \\
&\qquad S_i = \frac{\mu_{\mathrm{load,i}} - \mu_0}{\mu_0} \times 100\% \\
&\qquad x_i = \frac{S_i}{L_{load,i}} \\
&\qquad c_i = load\ priority\ [0,1] \qquad \mathrm{i} = 1, 2, ..., \mathrm{n}
\end{aligned}
\tag{6. 1}
$$

The load shedding sensitivity S_i is defined as the voltage stability margin improvement after the load shedding amount $L_{load,i}$ applied at load *i*. The scaling factor μ is the one used in the standard PV curve studies. The load priority c_i for load *i* is defined as follows: The load priority is 0 if the load cannot be shed and will be a value between 0 and 1 if the load can be shed but with some penalty.

The procedure to solve the problem described by (6.1) is shown in Figure 6.7. Since the multistage method selects the most effective locations for each stage and sheds small amount of load at each stage, it would theoretically give the optimal load shedding rules for each critical contingency. It is important to mention that the meaning of "multistage" here is ***only to describe the design procedure, not to reflect that the load shedding has stages in its implementation***.

Because there are numerous loads in a large-scale power system, it would take a great deal of time and effort to evaluate the effectiveness of those loads at each stage. Moreover, it may need various stages to obtain the final load shedding rules. There is a need to develop a fast scan method to speed up the calculation. The bus ranking method presented in Chapter 4 perfectly fits here.

Therefore, at the beginning of each stage the bus ranking method is called. The top 10 weakest load buses corresponding to each critical contingency are identified. Thereafter these weakest buses will be studied in detail and the rest of the load buses are ignored. Since only the top 10 weakest load buses are considered in each critical contingency, the set of feasible solutions to the multistage method at each stage is significantly reduced. Thus, the computation efforts are reduced. By using the bus ranking technique, the procedure described here can ensure that the load shedding rules are updated quickly even for large-scale interconnected power systems.

6.4.3 Task 3: Investigation of the maximum operation time

The operation time is important to any power system protections. There is no exception for the event-driven load shedding scheme. Although the event-driven load shedding scheme is designed to be operated immediately after the events are detected, the time required for detection of the event, transmission of the signals, and operation of the system breakers still delays the load shedding actions. If this time delay is longer than a certain value called maximum time delay, then the designed load shedding will not be able to prevent the voltage instability.

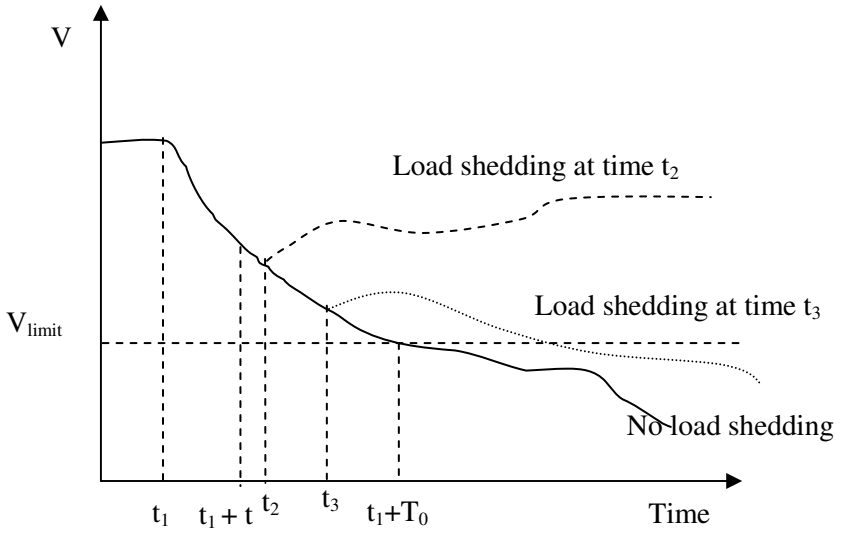

Figure 6.8 The influence of different time delays

As an example, the voltage profiles of a power system with the load shedding applied at different instants are shown in Figure 6.8. As seen in this figure, when

the load shedding is applied at t_3 which is higher than the maximum time delay, the load shedding is not able to prevent the coming voltage instability. As a result, it is important to determine the maximum time delay of any designed load shedding scheme. This study will use the time-domain simulations to investigate the system performance after application of the designed weekly load shedding rules. The maximum time delay is determined based on the following criteria (the system operators should modify these criteria based on their own operation conditions):

- No bus voltage is out of the desired voltage (in this study, we assume [0.8 1.2]pu).

- System voltage stable, no over-limit voltage oscillations (we assume the limit is that the peak-to-peak of the voltage RMS value is less than 0.2 pu in one second).

In this work, a bisection method is proposed to find the maximum allowable time delay. The procedure of the bisection method is shown in Figure 6.9. In Figure 6.9, T_0 is selected as the instant that the voltage is out of the desired voltage range. The load shedding is firstly applied at $t=T_0$. If the simulation results show the load shedding works, the maximum time delay is defined as T_0. Otherwise, the load shedding will be applied at the right middle of t=0 and $t=T_0$. This procedure will

be repeated until the difference between two time instants obtained from previous steps and current step is small enough.

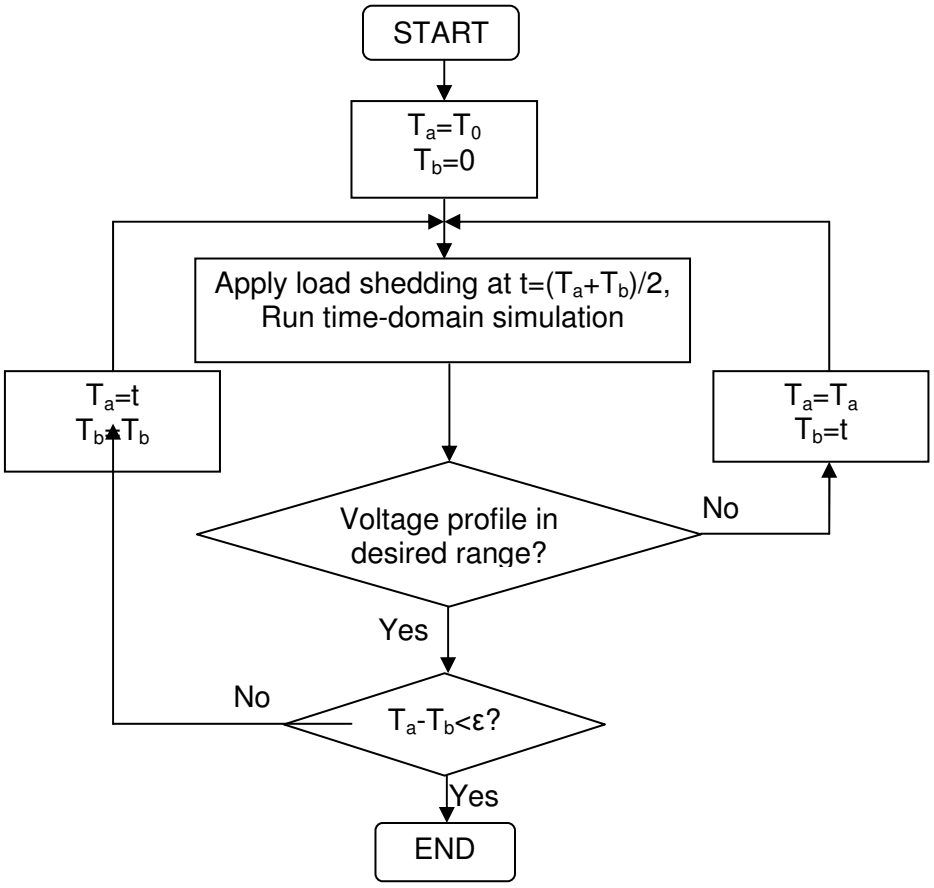

(a) Flowchart of the proposed method

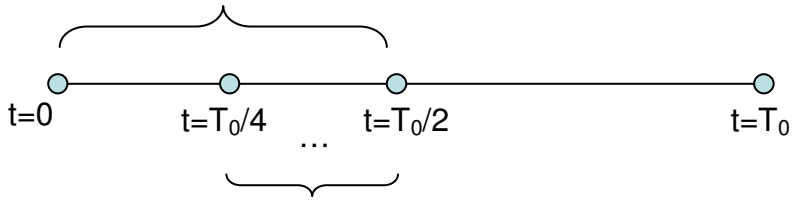

(b) Bisection search algorithm

Figure 6.9 The bisection search method to determine the maximum time delay

For some cases, even the maximum operation time is equal to zero (which means the immediate load shedding); the system may not be able to meet the required criteria. In this case, new load shedding has to be calculated by revisiting task 2. By increasing the requirement on the post-contingency power transfer margin, a new load shedding rule can be found. Through reiteratively running task 2 and task 3, a set of weekly load shedding rules will be obtained, which meets the requirement on both static power flow margin and dynamic performance.

6.5 An example of the proposed event-driven load shedding scheme

In this section, an example of the event-driven load shedding scheme is presented. The example is based on the Alberta Integrated Electric System (AIES). It firstly calculates the load shedding rules by using static voltage stability analysis, after which the load shedding rules would be examined by using the time-domain simulation. In this example, only the N-1 contingencies (for transmission lines) are studied. All the three tasks described in section 6.4 are used to complete the example.

6.5.1 Static studies: calculation of the load shedding rules

In this subsection, the load shedding rules will be calculated based on the static studies, which involves completing task 1 and task 2. The calculation follows the

procedure described in previous section and is performed by the commercial power system analysis software PSS/E.

6.5.1.1 Identification of the critical contingencies

All the N-1 transmission line contingencies are studied. The critical contingencies and their post-contingency margin are listed in Table 6.1.

Table 6.1 The critical N-1 transmission line contingencies

Event ID	From bus	To bus	Branch ID	Post-contingency margin (%)
1	74	814	49	<0.0
2	1164	1165	57	<0.0
3	1229	1234	49	<0.0
4	1235	1281	99	4.0

6.5.1.2 Identification of the top ten weakest load buses

For each critical contingency (event), the top 10 weakest load buses are obtained by using the bus identification method presented in Chapter 4. The following figures show the results. The impedance ratios for all load buses are plotted on the left and the top ten weakest load buses ranked based on their respective impedance ratio are plotted on the right. These results are obtained at the base loading level with the corresponding contingency applied.

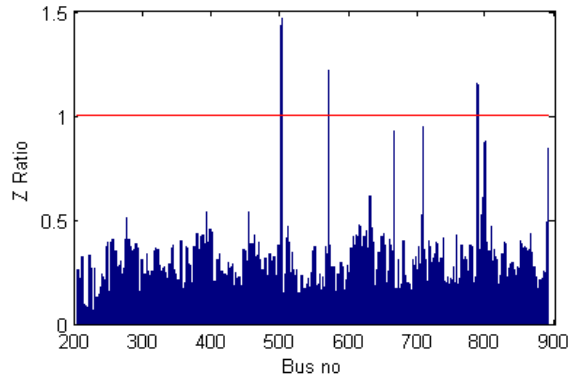

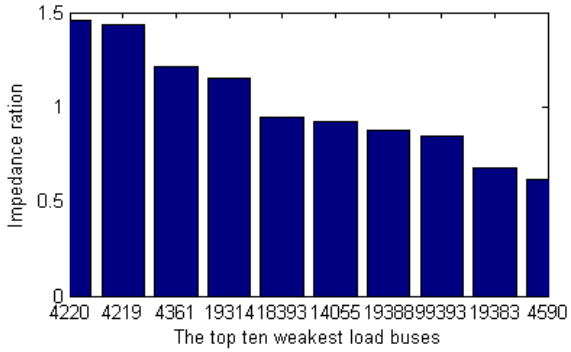

(1) B74_B814_ID49

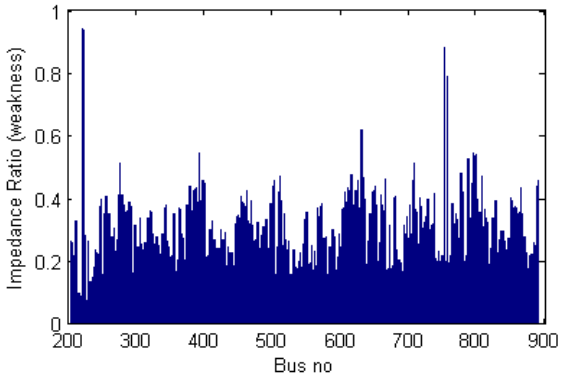

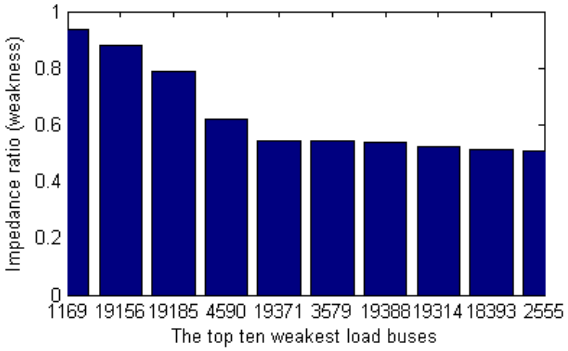

(2) B1164_B1165_ID57

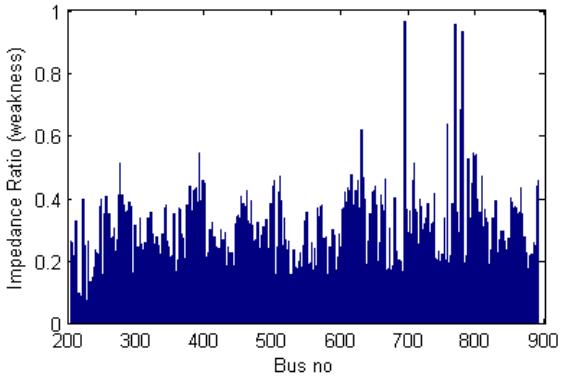

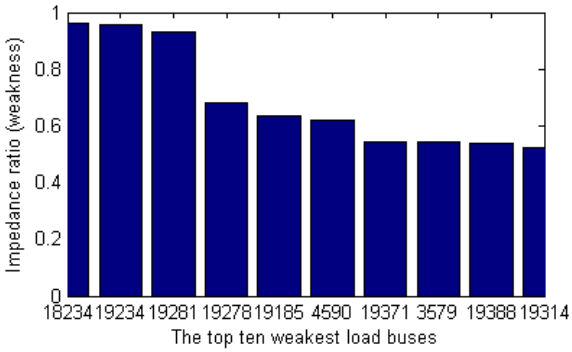

(3) B1229_B1234_ID49

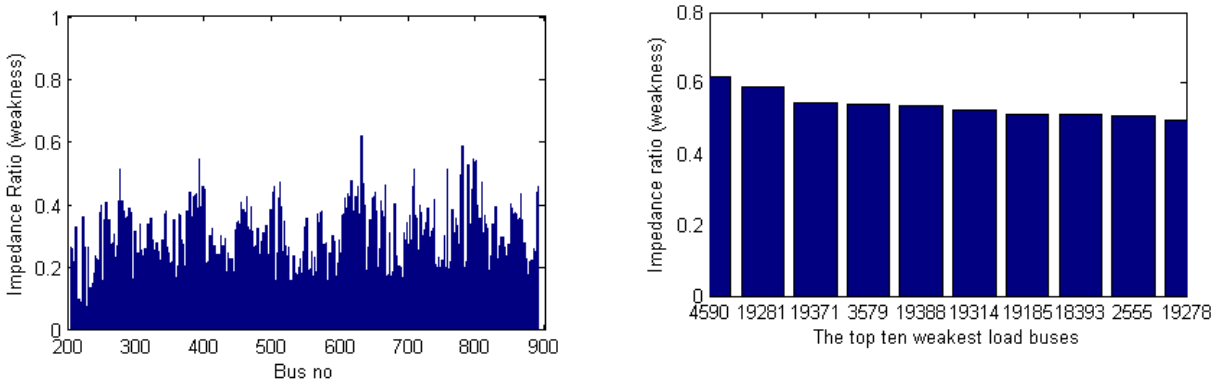

(4) B1235_B1281_ID99

Figure 6.10 The weakest loads corresponding to each critical contingency

6.5.1.3 Determining the load shedding rules

Using the ten weakest load buses of each critical contingency as the feasible solution set, the multistage optimization algorithm is applied to compute the load shedding rules. The calculated load shedding rules are listed in Table 6.2. After the load shedding, the static system voltage stability margins are all improved to a value higher than 5.0% (which is the requirement of WECC) for all these N-1 contingencies.

In order to further evaluate these load shedding rules, the time-domain simulation is conducted to benchmark them. The performance on the dynamic studies is provided in the next subsection.

Table 6.2 Load shedding rules for each identified critical contingency

Event ID	$Margin_{pre\text{-}load\ shedding}$ (%)	$Margin_{post\text{-}load\ shedding}$ (%)	Load shedding rules	
			Load	Amount (%)
1	<0.0	6.0	At bus 4220, ID 99	100.0
			At bus 4219, ID 99	40.0
2	<0.0	8.0	At bus 1169, ID 99	80.0
			At bus 19185, ID 99	10.0
3	<0.0	9.0	At bus 18234, ID 99	100.0
			At bus 19234, ID 99	40.0
			At bus 19281, ID 99	60.0
4	4.0	10.5	At bus 19281, ID 99	10.0

6.5.2 Dynamic studies: establishing the maximum time delay

The dynamic study is conducted to establish the maximum time delay, which is defined as when the designed load shedding rule can still fulfill its performance even though the load shedding rules are operated with such a delay after the event occurs.

6.5.2.1 Event ID 1: B74_B814_ID49

The simulation results show that the system voltage becomes less than the lower limit (assumed at 0.80 pu) at the instant when the contingency happens. Thus the

load shedding should be implemented immediately after the outage. In other words, the maximum time delay is 0 seconds.

Simulation results without load shedding:

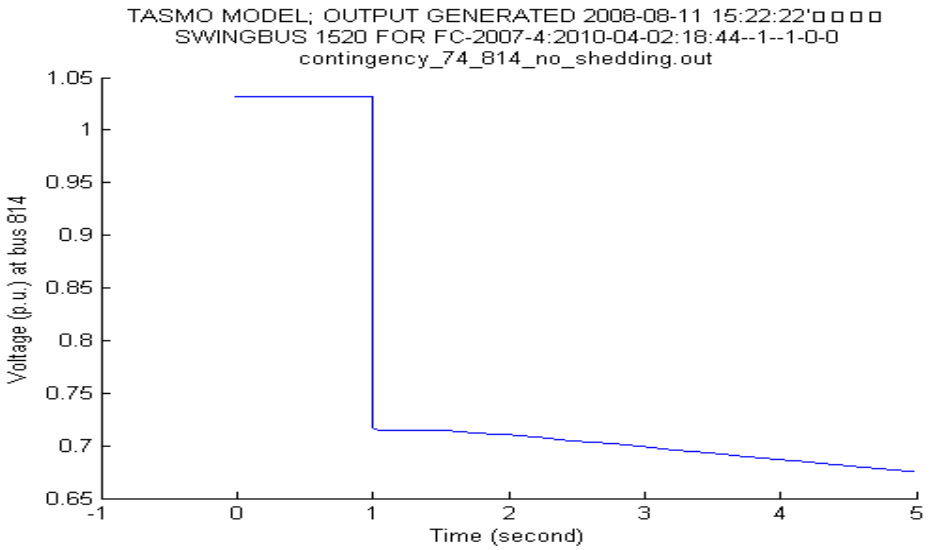

Figure 6.11 Simulation results for event ID 1 (without load shedding)

Simulation results with immediately load shedding:

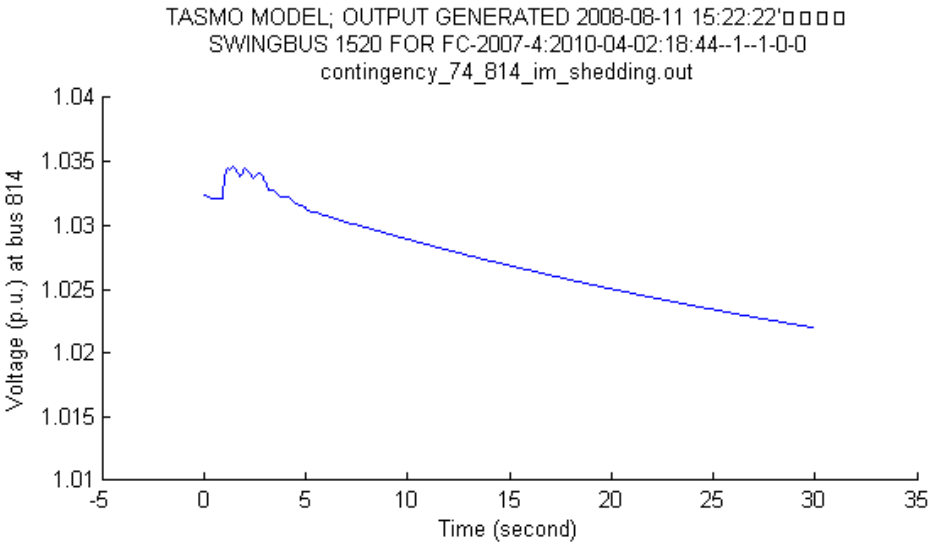

Figure 6.12 Simulation results for event ID 1 (with immediate load shedding)

6.5.2.2 Event ID 2: B1164_B1165_ID57

The simulation results (see Figure 6.13) show that immediate load shedding is required. However, even with the immediate load shedding, the simulation results (see Figure 6.14) show that the voltage profile cannot be recovered to the satisfactory value. A new load shedding rule is required. By setting the margin requirement as 10%, a new load shedding rule is calculated by the multistage method. The new load shedding rule for this contingency is

At bus 1169, ID 99 100.0%; At bus 19185, ID 99 10.0%

Figure 6.15 shows the voltage profile with the new load shedding rules. The new voltage profile satisfied the voltage criteria. The maximum delay is 0 second.

Simulation results without load shedding:

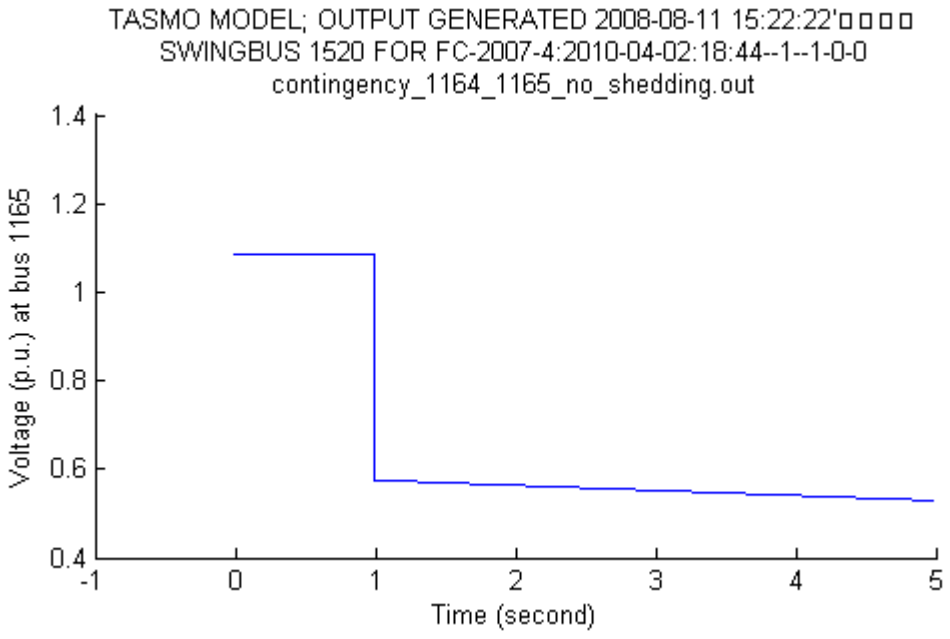

Figure 6.13 Simulation results for event ID 2 (without load shedding)

Simulation results with immediate load shedding with the old load shedding:

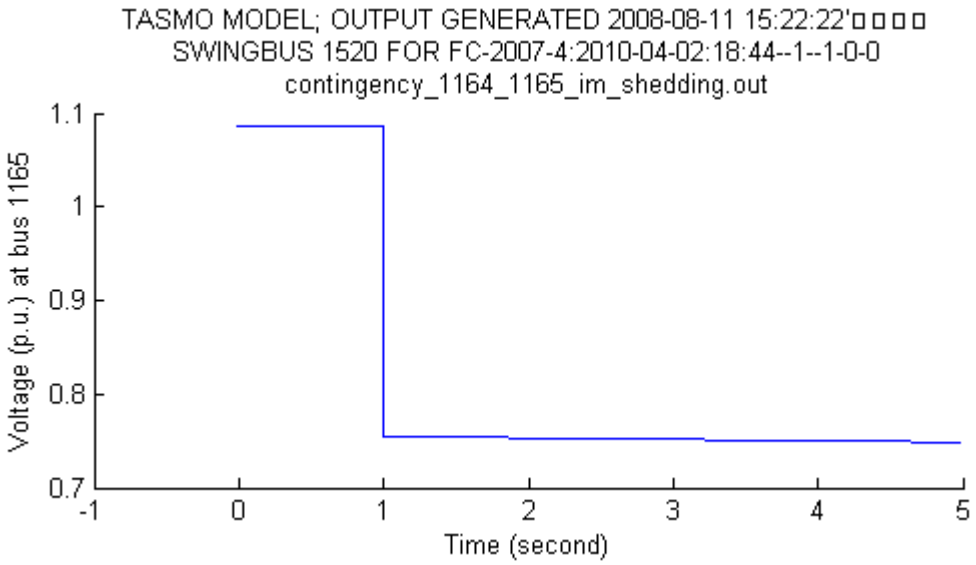

Figure 6.14 Simulation results for event ID 2 (with immediate load shedding – old rule)

Simulation results with immediate load shedding with the new load shedding:

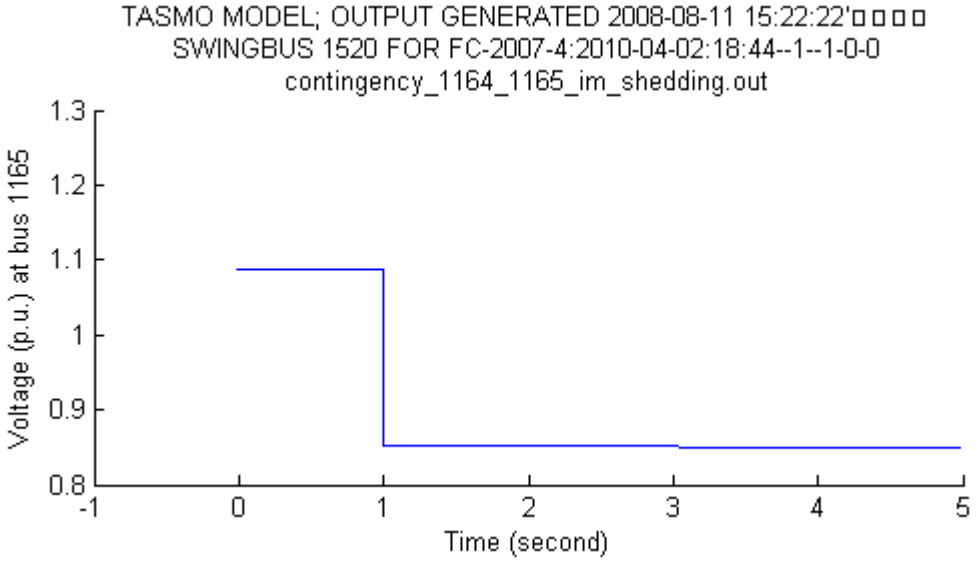

Figure 6.15 Simulation results for event ID 2 (with immediate load shedding – new rule)

6.5.2.3 Event ID 3: B1229_B1234_ID49

The simulation results (Figure 6.16) indicate that immediate load shedding is required. However, with the immediate load shedding, the voltage profile still cannot be recovered to the satisfactory value (see Figure 6.17). Additional load shedding is required. By increasing the margin requirement to 10%, a new load shedding rule for this contingency is calculated as follows,

At bus 18234, ID 99	100.0%
At bus 19234, ID 99	60.0%
At bus 19281, ID 99	60.0%

Figure 6.18 shows the voltage profile with the new load shedding rules. The new voltage profile satisfied the voltage criteria. The maximum delay is 0 seconds.

Simulation results without load shedding:

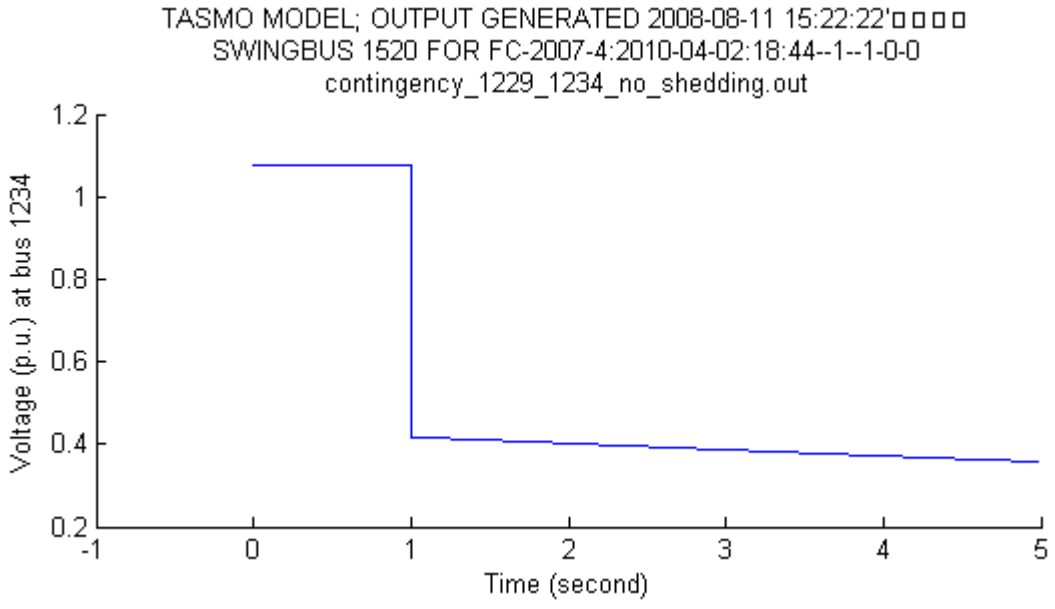

Figure 6.16 Simulation results for event ID 3 (without load shedding)

Simulation results with immediate load shedding with the old load shedding:

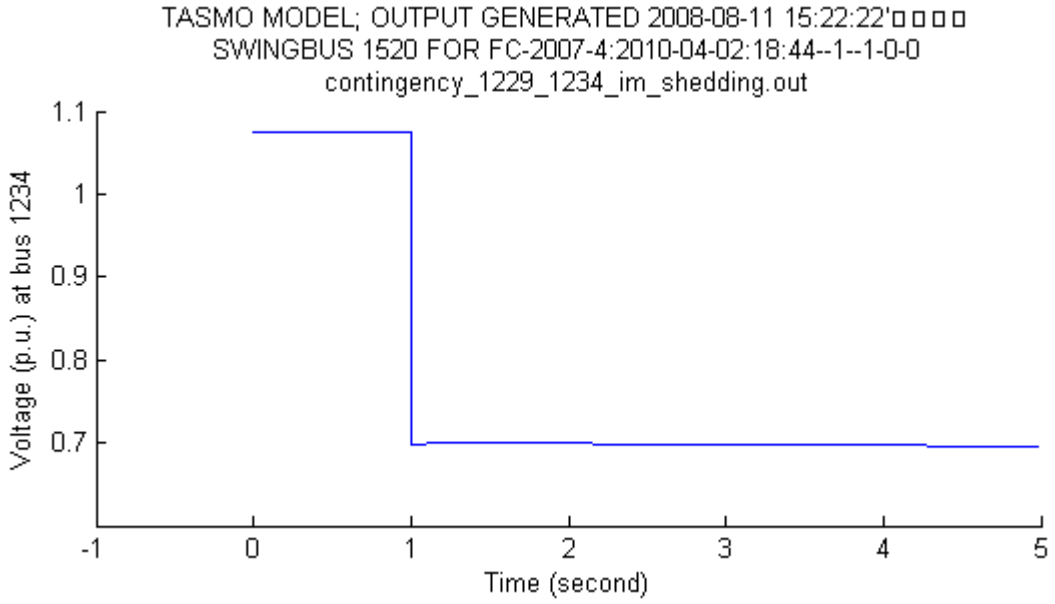

Figure 6.17 Simulation results for event ID 3 (with immediate load shedding – old rule)

Simulation results with immediate load shedding with the new load shedding:

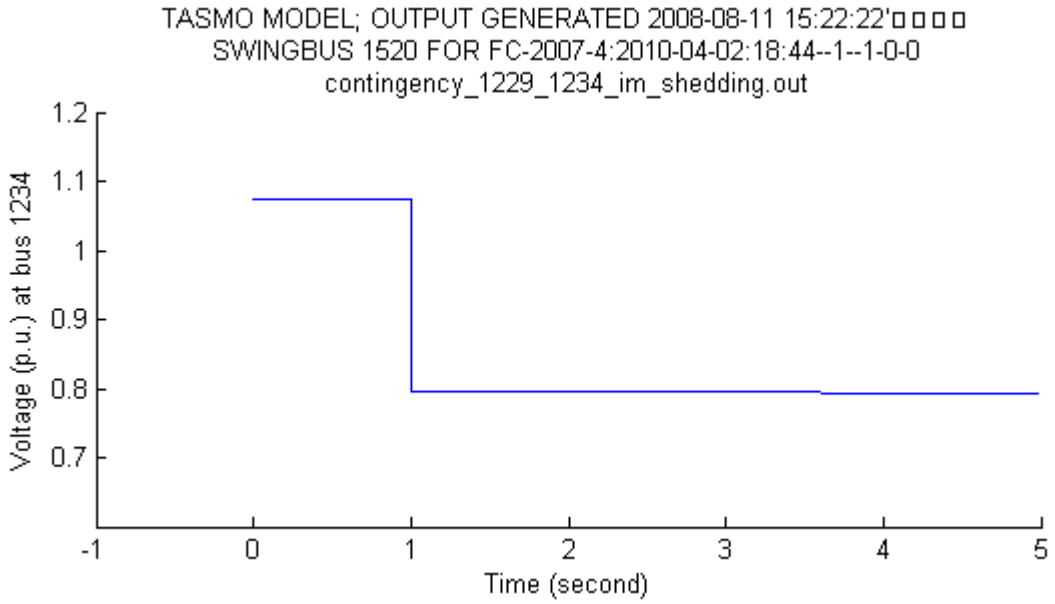

Figure 6.18 Simulation results for event ID 3 (with immediate load shedding – new rule)

6.5.2.4 Event ID 4: B1235_B1281_ID99

The simulation results show that the maximum time delay is 39 second.

Simulation results without load shedding:

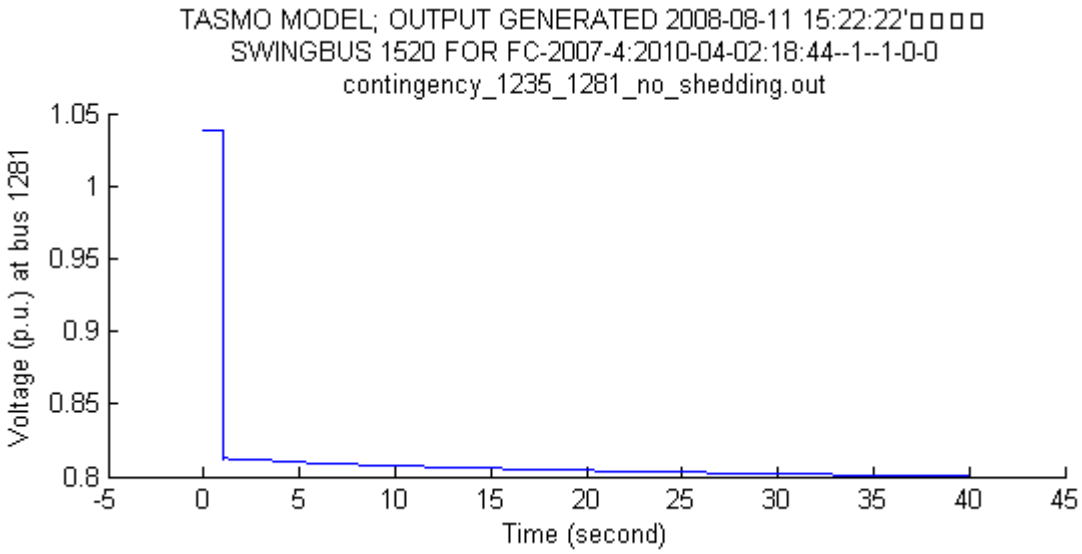

Figure 6.19 Simulation results for event ID 4 (without load shedding)

Simulation results with load shedding at T_0:

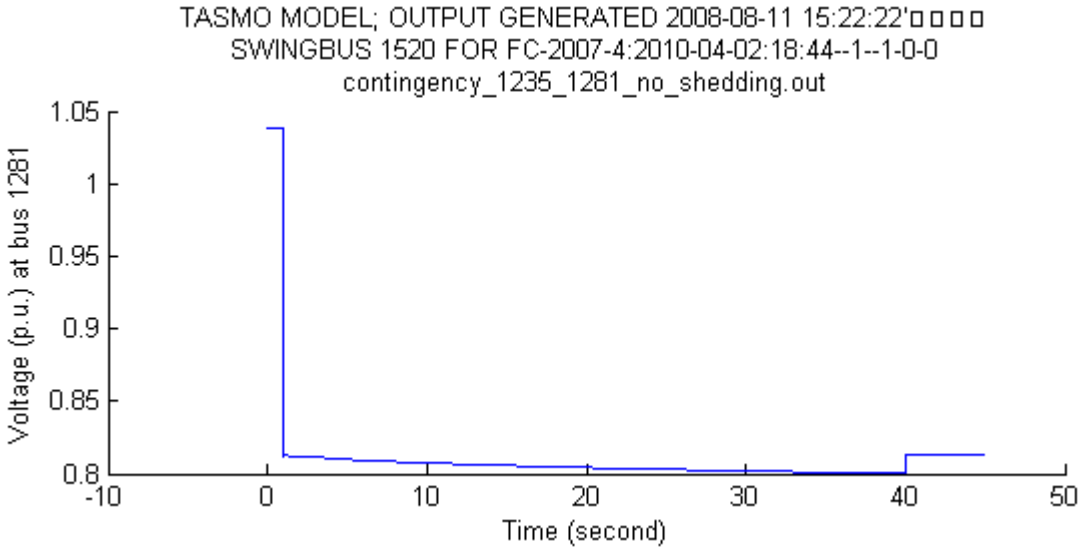

Figure 6.20 Simulation results for event ID 4 (with load shedding at t=T_0)

6.5.3 The event-driven load shedding rules

The event-driven load shedding rules for all critical N-1 contingencies have been obtained. The load shedding rules are shown in Table 6.3, which clearly indicates what the system operators should do when a particular event occurs in the power system.

Table 6.3 The load shedding rules for the example event-driven load shedding scheme

Event ID	Load shedding		Maximum time delay (s)
	Load shedding locations	Load shedding amount	
1	At bus 4220, ID 99 At bus 4219, ID 99	27.4 MW, 11.9 MVar 9.16 MW, 4.64 MVar	0.0
2	At bus 1169, ID 99 At bus 19185, ID 99	9.5 MW, 3.7 MVar 1.15 MW, 0.18 MVar	0.0
3	At bus 18234, ID 99 At bus 19234, ID 99 At bus 19281, ID 99	12.9 MW, 4.2 MVar 8.04 MW, 2.64 MVar 9.18 MW, 0.78 MVar	0.0
4	At bus 19281, ID 99	1.53 MW, 0.13 MVar	39.0

Although the maximum time delay of the load shedding rules listed above may not be very practical since most of them are zero, the procedure on how to obtain

them is clearly illustrated. Power system engineers should be able to follow the presented design methodologies to design a practical useful event-driven load shedding scheme.

6.6 Summary and conclusions

In order to facilitate the development of a practical event driven load shedding scheme, this chapter described the overall design procedure, which generally involves two parts of study: system planning study and operation planning study. The purpose of system planning study is to find the best (both economical and technical) locations to install or configure the necessary equipment used to perform the load shedding actions. Thus the system planning study is based on the representative operating cases to optimize the selection of those load shedding locations, while the operation planning study is mainly to tune the load shedding rules.

Both the system planning study and the operation planning study engage in three main tasks: identification of the critical contingencies, computing the best load shedding rules (locations and amounts), and determining the maximum operation time delay. The methodologies proposed in this chapter are to complete these three tasks. With the detailed design procedure explained in this work, it is hoped that power system engineers can design their own event-driven load shedding schemes.

Chapter 7

Conclusions and future work

7.1 Thesis conclusions and contributions

This thesis has approached topics related to voltage stability monitoring and design of an advanced load shedding scheme to prevent voltage collapse. An extensive investigation of the applicability of the single-port impedance matching method on the power systems was conducted. Based on the findings, a new and original multi-port network equivalent is proposed. The characteristics of the multi-port network equivalent were analyzed. Three applications of the multi-port network were proposed. Following these applications, an advanced event-driven load shedding scheme was developed. The design methodology of this scheme was also presented in detail.

The main conclusions and contributions of this thesis are summarized as follows:

- A comprehensive study on the voltage stability monitoring schemes was conducted. The difficulties faced by the traditional undervoltage load shedding schemes and the single-port network equivalent based load shedding schemes were discussed. By using a simple power system as an example, the investigation showed that substantial estimation errors could occur when applying the single-port network equivalent on a multi-load

power system. In the process of converting power systems to a single-port network equivalent, an assumption is required that power systems remain unchanged during two or more consecutive measurements at the studied bus. Such an assumption can hardly be satisfied during a voltage collapse process, since the power system would experience continuous changes.

- In order to overcome the difficulties encountered by the single-port impedance matching method, a new concept of network equivalent was proposed. The new equivalent is called multi-port network equivalent. Using the multi-port network equivalent, the reason that the single-port impedance matching method cannot be used to estimate voltage stability margin was discovered. It is closely related to the improper treatment of the coupling effects among load buses. The multi-port network equivalent does not rely on the assumption required by the single-port network equivalent since it takes wide-area measurements from the prevailing devices (PMUs).

- A comprehensive literature review was conducted to locate and analyze theorems of multi-port impedance matching. The review revealed that no such theorem existed. A new voltage stability monitoring technique had to be developed. The characteristics of the multi-port network equivalent were thoroughly investigated. It was found that the coupling effect of each load is a summation of the weighted currents from other loads. This

coupling effect increases dramatically when the loads increase or some disturbances occur in power systems.

- By explicitly separating the coupling terms from the voltage drops on the transmission network, a concept called coupled single-port network equivalent was developed. The coupled single-port network equivalent consists of one voltage source (calculated from the PV bus voltage), one system side impedance (obtained from system admittance matrix), the coupling term, and the load. In order to use the impedance matching theory, three different models were intended to represent the coupling terms. Both the theoretical analysis and the simulation results confirmed that modeling the coupling terms as dependent impedance is legitimate.

- Three main applications of the multi-port network equivalent were developed. They are: load shedding oriented voltage stability monitoring, the weakest load bus identification, and a multistage optimization algorithm for minimizing the amount of load shedding. Several test power systems were studied to demonstrate and to verify the proposed applications. For the purpose of comparison, the methods widely accepted by utility companies were used as reference.

- Combining the applications described above, a practical event-driven load shedding scheme was designed. After a study of the two main categories

of load shedding schemes (response-based and event-driven), the event-driven strategy was chosen due to its overwhelming advantages in modern power systems. The review of the industrial load shedding schemes was also carried out to facilitate the design. The topology and the main tasks related to the proposed scheme were carefully described.

- A set of design methodologies was developed to facilitate power system engineers to develop such an event-driven load shedding scheme. It involves power system planning studies for determining the best locations to install the load shedding action devices, and operation planning study for tuning the load shedding rules. Both studies use the bus ranking method, the multistage optimization method, and a bisection search method for settling the maximum time delay. In order to have a better understanding of these methods, an example was provided.

7.2 Suggestions for further work

The problem identified in this research has a significant impact on modern power systems since they are generally operating close to their security limits. The proposed multi-port network equivalent presents a framework for more applications. Extensions of this thesis can be explored. It is also possible that other methods to estimate the voltage stability margin and to calculate the load shedding rules could be developed. Some of the future work is as follows:

- During the process of the voltage collapse, power systems experience constant changes. These changes include generators hitting their reactive power limit, the actions of reactive power compensation devices, and the movement of OLTCs. The influences of those changes, especially when the generators hit their reactive power limits, on the applications of the multi-port network equivalent need to be further investigated.

- The contribution of the generators in terms of improving voltage stability of power systems can be evaluated after the weakest load bus is identified. The coupled single-port network model provides a way to calculate the contributions of each generator to the weakest load. Intuitively, the generator that supplies most to the load would be the most effective one to prevent voltage collapse. However, it could not be confirmed without further studies.

- Using a reduced network to represent a full-scale network is usually used to allow larger areas of major interconnected systems to be represented in studies and to achieve improved computational speed in simulation by removing buses and branches that have no major influences on the interested area. It is always a hard task to find a proper boundary of the interested area. The proposed multi-port network equivalent might be able to provide an easy way to define the boundary by examining the

dependability between the coupling effects at the boundary buses and the buses inside the interested area.

References

[1] L. L. Grigsby, *Power system stability and control*, CRC Press, Taylor & Francis Group, 2007, pp. 7.1-7.8.

[2] S. Corsi and C. Sabelli, "General blackout in Italy Sunday September 28, 2003, h. 03:28:00", *IEEE PES General Meeting,* vol.2, June 2004, pp. 1691-1702.

[3] IEEE/CIGRE Joint Task Force on Stability Terms and Definitions, "Definition and classification of power system stability", *IEEE Trans. on Power Systems,* vol. 9, no. 2, May 2004, pp. 1378-1401.

[4] T. Van Cutsem and C. Vournas, *Voltage stability of electric power systems.* New York: Springer, 2007.

[5] J. Machowski, J. W. Bialek, and J. R. Bumby, *Power system dynamics – stability and control*. 2nd Edition, John Wiley & Sons, Ltd. 2008.

[6] W. Xu and Y. Mansour, "Voltage stability analysis using generic dynamic load models", *IEEE Trans. on Power Systems*, vol. 9, no. 1, Feb. 1994, pp. 479-493.

[7] D. J. Hill, "Nonlinear dynamic load models with recovery for voltage stability studies", *IEEE Trans. on Power Systems,* vol. 8, no. 1, Feb. 1993, pp. 166-176.

[8] G. K. Morison, B. Gao, and P. Kundur, "Voltage stability analysis using static and dynamic approaches", *IEEE Trans. on Power Systems,* vol. 8, no. 3, Aug. 1993, pp. 1159-1171.

[9] T. Van Cutsem and C. D. Vournas, "Emergency voltage stability controls: an overview", *IEEE PES General Meeting*, June 2007, pp. 1-10.

[10] C. Moors, D. Lefebvre, and T. Van Cutsem, "Design of load shedding schemes against voltage instability", *IEEE PES Winter Meeting,* vol. 2, Jan. 2000, pp. 1495-1500.

[11] U.S.-Canada Power System Outage Task Force, *Final report on the August 14, 2003 Blackout in the United States and Canada: Causes and Recommendations,* April 2004.

[12] K. Vu, M. M. Begovic, D. Novosel, and M. Mohan Saha, "Use of local measurements to estimate voltage-stability margin", *IEEE Trans. on Power Systems,* vol. 14, no. 3, Aug. 1999, pp. 1029-1035.

[13] I. Smon, G. Verbic, and F. Gubina, "Local voltage-stability index using Tellegen's theorem", *IEEE Trans. on Power Systems,* vol. 2, no. 3, Aug. 2006, pp. 1267-1275.

[14] F. Gubina and B. Strmcnik, "A simple approach to voltage stability assessment in radial networks", *IEEE Trans. on Power Systems,* vol. 12, no. 3, Aug. 1997, pp. 1121-1128.

[15] J. Medanic, M. Ilic-Spong, and J. Christensen, "Discrete models of slow voltage dynamics for under load tap-changing transformer coordination", *IEEE Trans. on Power Systems,* vol. 2, no. 4, Nov. 1987, pp. 873-880.

[16] C. D. Vournas and N. G. Sakellaridis, "Tracking maximum loadability conditions in power systems", *Bulk power system dynamics and control – VII Revitalizing Operational Reliability, 2007 IREP Symposium,* Aug. 2007, pp. 1-12.

[17] C. D. Vournas and T. Van Cutsem, "Local identification of voltage emergency situation", *IEEE Trans. on Power Systems,* vol. 23, no. 3, Aug. 2008, pp. 1239-1248.

[18] C. J. Mozina, "Undervoltage load shedding", *60th Annual Conference for Protective Relay Engineers,* March 2007, pp. 16-34.

[19] Y. Yuan, X. Wen, and C. Zhou, "Comparison of load margin analysis for steady-state voltage stability", *UPEC 2007,* Sept. 2007, pp. 592-596.

[20] V. Ajjarapu and C. Christy, "The continuation power flow: a tool for steady state voltage stability analysis", *IEEE Trans. on Power Systems,* vol. 7, no. 1, Feb. 1992, pp. 416-423.

[21] N. Yorino, H. Li, and H. Sasaki, "A predictor/corrector scheme for obtaining Q-limit points for power flow studies", *IEEE Trans. on Power Systems,* vol. 20, no. 1, Feb. 2005, pp. 130-137.

[22] A. Wiszniewski, "New criteria of voltage stability margin for the purpose of load shedding", *IEEE Trans. on Power Delivery,* vol. 22, no. 3, July 2007, pp. 1367-1371.

[23] M. Moghavvemi and O. Faruque, "Real-time contingency evaluation and ranking technique", *IEE Proc-Gener. Transm. Distrib.,* vol. 145, no. 5, Sept. 1998, pp. 517-524.

[24] M. Larsson, C. Rehtanz, and J. Bertsch, "Real-time voltage stability assessment of transmission corridors", presented at the *IFAC Symp. Power Plants and Power Systems Control,* Seoul, Korea, 2002.

[25] V. Balamourougan, T. S. Sidhu, and M. S. Sachdev, "Technique for online prediction of voltage collapse", *IEE Proc. Generation, Transmission, and Distribution,* vol. 151, no. 4, July 2004, pp. 453-460.

[26] M. Moghavvemi and F. M. Omar, "Technique for contingency monitoring and voltage collapse prediction", *IEE Pro. Generation, Transmission, and Distribution,* vol. 145, no. 6, Nov. 1998, pp. 634-640.

[27] I. Musirin and T. K. Abdul Rahman, "Novel fast voltage stability index (FVSI) for voltage stability analysis in power transmission system", *IEEE SCOReD 2002,* July 2002, pp. 265-268.

[28] P. Kessel and H. Glavitsch, "Estimating the voltage stability of a power system", *IEEE Trans. on Power Delivery,* vol. 1, no. 3, July 1986, pp. 346-354.

[29] Y. Gong, N. Schulz, and A. Guzman, "Synchrophasor-based real-time voltage stability index", *IEEE PES 2006,* Oct. 2006, pp. 1029-1036.

[30] B. Venkatesh, R. Ranjan, and H. B. Gooi, "Optimal reconfiguration of radial distribution system to maximize loadability", *IEEE Trans. on Power Delivery,* vol. 19, no. 1, Feb. 2004, pp. 260-266.

[31] G. Verbic and F. Gubina, "A new concept of voltage-collapse protection based on local phasors", *IEEE Trans. on Power Delivery,* vol. 19, no. 2, April 2004, pp. 576-581.

[32] Undervoltage load shedding taskforce, *Undervoltage load shedding guidelines*, Technical studies subcommittee, Western Systems Coordinating Council (WSCC), July 1999.

[33] North American Electric Reliability Council Report, *Survey of the voltage collapse phenomenon*, North American Electric Reliability Council, 1990.

[34] W. Li, Y. Wang, and T. Chen, "Investigation on the Thevenin equivalent parameters for online estimation of maximum power transfer limits", *IET Generation, Transmission, & Distribution*, vol. 4, no. 10, Oct. 2010, pp. 1180-1187.

[35] S. Corsi and G. N. Taranto, "A real-time voltage instability identification algorithm based on local phasor measurements", *IEEE Trans. on Power Systems*, vol. 23, no. 3, Aug. 2008, pp. 1271-1279.

[36] A. Sudhakar and S. S. Palli, *Circuits and networks: analysis and synthesis*, Boston: McGraw-Hill higher education, 2008.

[37] S.-J.S. Tsai and K.-H. Wong, "Adaptive undervoltage load shedding relay design using Thevenin equivalent estimation", *IEEE PES General Meeting,* July 2008, pp. 1-8.

[38] M. Vidvasagar, "Maximum power transfer in *n* ports with passive loads", *IEEE Trans. on Circuits and Systems,* vol. 21, no.3, May 1974, pp. 327-330.

[39] K.K. Nambiar, "A generalization of the maximum power transfer theorem", *Proceedings of IEEE*, vol. 57, no. 7, July 1969, pp. 1339-1340.

[40] H. Baudrand, "On the generalization of the maximum power transfer theorem", *Proceedings of IEEE*, vol. 58, no. 10, Oct. 1970, pp. 1780-1781.

[41] B.A. Mathis and H.F. Mathis, "Maximum power transfer from a multiple terminal network to a single impedance", *Proceedings of IEEE,* vol. 60, no.6, June 1972, pp. 746.

[42] P. Lin, "Determination of available power from resistive multi-ports", *IEEE Trans. on Circuit Theory*, vol. 19, no. 4, July 1972, pp. 385-386.

[43] F. Spinei, "On generalization of the maximum power transfer problem", *Proceedings of IEEE,* vol. 60, no. 7, July 1972, pp. 903-904.

[44] C. Desoer, "The maximum power transfer theorem for *n*-ports", *IEEE Trans. on Circuit Theory,* vol. 20, no. 3, May 1973, pp. 328-330.

[45] Http://ee.washington.edu/research/pstca/

[46] A.M. Abed, "WSCC voltage stability criteria, undervoltage load shedding strategy, and reactive power reserve monitoring methodology", *IEEE PES Summer Meeting 1999*, vol. 1, July 1999, pp. 191-197.

[47] Y.-H. Moon, H.-S. Ryu, J.-G. Lee, and B. Kim "Uniqueness of static voltage stability analysis in power systems", *IEEE PES Summer Meeting 2001,* vol. 3, July 2001, pp. 1536-1541.

[48] Alberta Electric System Operator (AESO), *Independent system operator operating policies and procedures – OPP 303 Alberta-BC interconnection operation,* Feb. 19, 2009, pp. 59-76.

[49] *BPA voltage security assessment,* EPRI, Palo Alto, CA, Bonneville Power Administration, Vancouver WA: 2000, TE-114725.

[50] L. Wang, R. Howell, A. Moshref, M. Mueller, E. Viray, C. Yang, and J. Qiu "Real-time voltage security assessment system (VSAS) at Alberta Electric System Operator", *CIGRE Canada Conference on Power Systems,* Oct. 2008.

[51] A. Moshref, R. Howell, G. K. Morison, H. Hamadanizadeh, and P. Kundur, "On-line voltage security assessment using distributed computing architecture", *Proceedings of the International Power Engineering Conference,* May 1999.

[52] B. Stott and O. Alsac, "Fast decoupled power flow", *IEEE Trans. on Power Apparatus and Systems,* vol. PAS-93, no. 3, May 1974, pp. 859-869.

[53] S. Iwamoto and Y. Tamura, "A fast load flow method retaining nonlinearity", *IEEE Trans. on Power Apparatus and Systems,* vol. PAS-97, no. 5, Sept. 1978, pp. 1586-1599.

[54] S. C. Tripathy, N. D. Rao, and A. Kumar, "Real-time monitoring of power systems using fast-decoupled load flow", *Proceedings of IEE*, vol. 124, no. 7, July 1977, pp. 602-606.

[55] M. Enns, "An improved version of the fast decoupled load flow", *Proceedings of IEEE,* vol. 65, no. 2, Feb. 1977, pp. 278-279.

[56] R. K. Gajbhiye, D. Naik, S. Dambhare, and S. A. Soman, "An expert system approach for multi-year short-term transmission system expansion planning: An Indian experience", *IEEE Trans. on Power Systems,* vol. 23, no. 1, Feb. 2008, pp. 226-237.

[57] R.A.M. van Amerongen, "A general-purpose version of the fast decoupled load flow", *IEEE Trans. on Power Systems,* Vol. 4, no. 2, 1989, pp. 760-770.

[58] S.-H Li and H.-D Chiang, 'Nonlinear predictors and hybrid corrector for fast continuation power flow", *IET Generation, Transmission & Distribution,* vol. 2, no. 3, May 2008, pp. 341-354.

[59] S.-H Li and H.-D Chiang, "Continuation power flow with nonlinear power injection variations: A piecewise linear approximation", *IEEE Trans. on Power Systems,* vol. 23, no. 4, Nov. 2008, pp. 1637-1643.

[60] H. Mori and K. Seki, "Continuation Newton-GMRES power flow with linear and nonlinear predictors", *2007 Large Engineering Systems Conference on Power Engineering,* Oct. 2007, pp. 171-175.

[61] D.A. Alves, L.C. P. da Silva, C. A. Castro, and V.F. da Costa, "Continuation fast decoupled power flow with secant predictor", *IEEE Trans. on Power Systems,* vol. 18, no. 3, Aug. 2003, pp. 1078-1085.

[62] A. Berizzi, P. Bresesti, P. Marannino, G.P. Granelli, and M. Montagna, "System-area operating margin assessment and security enhancement against voltage collapse", *IEEE Trans. on Power Systems,* vol. 11, no. 3, Aug. 1996, pp. 1451-1462.

[63] M. La Scala, M. Trovato, and F. Torelli, "A neural network-based method for voltage security monitoring", *IEEE Trans. on Power Systems,* vol. 11, no. 3, Aug. 1996, pp. 1332-1341.

[64] K.C. Hui and M.J. Short, "A neural networks approach to voltage security monitoring and control", *Proceedings of the First International Forum on Applications of Neural Networks to Power Systems*, July 1991, pp. 89-93.

[65] R.A.M. van Amerongen and H.P. van Meeteren, "A generalized ward equivalent for security analysis", *IEEE Trans. on Power Apparatus and Systems,* vol. PAS-101, no. 6, June 1982, pp. 1519-1526.

[66] External Network Modeling Task Force, “External network modeling - recent practical experience”, *IEEE Trans. on Power Systems,* vol. 9, no. 1, Feb. 1994, pp. 216-228.

[67] K.L. Lo, L.J. Peng, J.F. Macqueen, etc. “Hybrid approach using counter-propagation neural network for power-system network reduction”, *IEE Generation, Transmission and Distribution,* vol. 144, no. 2, Mar. 1997, pp. 169-174.

[68] T.S. Chung and Y. Fu, “A fast voltage security assessment method via extended Ward equivalent and neural network approach”, *IEEE Power Engineering Review,* vol. 19, no. 10, Oct. 1999, pp. 40-43.

[69] B. Gao, G.K. Morison, and P. Kundur, “Voltage stability evaluation using modal analysis”, *IEEE Trans. on Power systems,* vol. 7, no. 4, Nov. 1992, pp. 1529-1542.

[70] C.A. Canizares, A.C.Z. De Souza, and V.H. Quintana, “Comparison of performance indices for detection of proximity to voltage collapse”, *IEEE Trans. on Power Systems,* vol. 11, no. 3, Aug. 1996, pp. 1441-1450.

[71] A.C.Z. de Souza, “Discussion on some voltage collapse indices”, *Electric Power Systems Research,* vol. 53, no. 1, Jan. 2000, pp. 53-58.

[72] F. Milano, “An open source power system analysis toolbox”, *IEEE Trans. on Power Systems,* vol. 20, no. 3, Aug. 2005, pp. 1199-1206.

[73] V.C. Nikolaidis and C.D. Vournas, “Design strategies for load-shedding scheme against voltage collapse in the Hellenic system”, *IEEE Trans. on Power Systems,* vol. 23, no. 2, May 2008, pp. 582-591.

[74] T. Van Cutsem, "An approach to corrective control of voltage instability using simulation and sensitivity", *IEEE Trans. on Power Systems,* vol. 10, no. 2, May 1995, pp. 616-622.

[75] S.A. Nirenberg, D.A. McInnis, and K.D. Sparks, "Fast acting load shedding", *IEEE Trans. on Power Systems,* vol. 7, no. 2, Aug. 1992, pp. 873-877.

[76] S. Kolluri, K. Tinnium, and M. Stephens, "Design and operating experience with fast acting load shedding scheme in the Entergy system to prevent voltage collapse", *IEEE PES Winter Meeting,* vol. 2, Jan. 2000, pp. 1489-1494.

[77] S.C. Pai and J. Sun, "BCTC's experience towards a smarter grid – increasing limits and reliability with centralized intelligence remedial action schemes", *Proceedings of IEEE Canada Electrical Power and Energy Conference 2008*, 6-7 October, Vancouver, BC.

[78] G. Trudel, S. Bernard, and G. Scott, "Hydro-Quebec's defence plan against extreme contingencies", *IEEE Trans. on Power Systems,* vol. 14, no. 3, Aug. 1999, pp. 958-966

[79] W. Li, M. Shaaban, Z. Yan, Y. Ni and F.F. Wu, "Available transfer capability calculation with static security constraints", *IEEE PES General Meeting 2003*, vol. 1, July 2003, pp. 306-310.

[80] J. H. Doudna, "Overview of California ISO summer 2000 demand response programs", *IEEE PES Winter Meeting,* vol. 1, Feb. 2001, pp. 228-233.

[81] J. H. Eto, etc. "Demand response spinning reserve demonstration", Ernest Orlando Lawrence Berkeley National Laboratory, Berkeley CA, LBNL-62761. [Online]. Available: http://certs.lbl.gov/pdf/62761.pdf.

[82] R. Tyagi and J.W. Black, "Emergency demand response for distribution system contingencies", *IEEE PES Transmission and Distribution Conference and Exposition 2010*, April 2010, pp. 1-4.

[83] E. Shayesteh, A. Yousefi, M. Parsa Moghaddam, and M.K. Sheikh-El-Eslami, "ATC enhancement using emergency demand response program", *IEEE PES PSCE'09*, March 2009, pp.1-7.

[84] D.J. Lawrence and B.F. Neenan, "The status of demand response in New York", *IEEE PES General Meeting*, vol. 4, July 2003, pp. 2270-2274.

[85] L. Goel, Q. Wu, and P. Wang, "Reliability enhancement of a deregulated power system considering demand response", *IEEE PES General Meeting*, Oct. 2006, pp. 1-6.

[86] R.B. Burke and M.I. Henderson, "Incorporating demand response in operating reserve in New England", *IEEE PES General Meeting*, vol. 2, June 2005, pp. 1570-1574.

[87] F. Rahimi and A. Ipakchi, "Demand response as a market resource under the smart grid paradigm", *IEEE Trans. on Smart Grid,* vol. 1, no. 1, June 2010, pp. 82-88.

[88] M. Parvania and M. Fotuhi-Firuzabad, "Demand response scheduling by stochastic SCUC", *IEEE Trans. on Smart Grid*, vol. 1, no. 1, June 2010, pp. 89-98.

[89] C. Su and D. Kirschen, "Quantifying the effect of demand response on electricity markets", *IEEE Trans. on Power Systems,* vol. 24, no. 3, Aug. 2009, pp. 1199-1207.

[90] S. Valero, M. Ortiz, C. Senabre, C. Alvarez, F.J.G. Franco and A. Gabaldon, "Methods for customer and demand response policies selection in new electricity markets", *IET Generation, Transmission & Distribution,* vol. 1, no.1, Jan. 2007, pp. 104-110.

[91] D.S. Kirschen and G. Strbac, *Fundamentals of Power System Economics*, Chichester, West Sussex, England: John Wiley & Sons, 2004.

[92] M.H. Albadi and E.F. El-Saadany, "Demand response in electricity markets: An overview", *IEEE PES General Meeting 2007*, June 2007, pp. 1-5.

[93] D.-H. Kim, D.-M. Kim, and J.-O. Kim, "Determination of the optimal incentives and amount of load reduction for a retailer to maximize profits considering demand response programs", *2nd IEEE International conference on Power and Energy (PECon 08)*, Dec. 2008, pp. 1290-1295.

Appendix A

An event-driven demand response scheme for power system security enhancement

Demand response has become a key feature of the future smart grid. In addition to having advanced communication and computing infrastructures, a successful demand response program must respond to the needs of a power system. In other words, the efficiency and security of a power system dictate the locations, amounts, and speeds of the load reductions of a demand response program.

Using the same principle as the one used for the event-driven load shedding scheme, an event-driven emergency demand response scheme is proposed to enhance power system security. The main difference between these two schemes lies in their different objectives. The event-driven load shedding is to prevent voltage collapse and to minimize the load shedding amount. The demand response program is to enhance the voltage stability and to minimize the social cost. A technique to design such a scheme is presented here. This technique is able to provide key setting parameters such as the amount of demand reductions at various locations to arm the demand response infrastructure. The validity of the proposed technique has been verified by using several test power systems.

A. 1 Introduction

Due to economic and environmental constraints, power systems are currently being operated closer to their limits than they were previously [79]. Various techniques have been proposed to manage this situation. An emergency demand response program, also called a demand relief program by some utilities, can play an important role in meeting the challenges involved [80].

The use of demand-side resources to respond to the operating reserves deficiency or major emergencies in power systems has attracted a great deal of attention to the smart grid due to its feasibility and quick action [81]. Significant progress has been made in the research on and implementation of demand response programs during the past decade [80-87]. Three types of demand response programs—an emergency demand response program (EDRP), a special case resources program (SCR), and a day-ahead demand response program (DADRP)—have been implemented in the New York Independent System Operator (ISO) [84]. Two demand response programs—a participating load program and a demand relief program—have been implemented by the California ISO [80]. In Pennsylvania, a voluntary Emergency Load Response and a Mandatory Interruptible Load are used for reliability programs [82].

Since the objective of all these demand response programs is focused on the economic security–constrained unit commitment (SCUC), many researchers have

proposed methods for optimizing the SCUC and to obtain the maximum social welfare [88-90]. In order to obtain these objectives, the load demand is generally modeled as an economic load model [83, 91]. By using this model, an auction dispatch problem can be formulated and solved [83]. These demand response techniques concentrate mainly on normal system conditions [92], but exploring the potential value of the demand response in managing power system security constraints under unexpected disturbances, especially given the demand response program's current prevalence, is equally important. Ref. [85] and [93] investigate the impact of the demand response on system reliability. However, the issue of how to obtain an adequate demand response in terms of improving the operating reserves has not been completely addressed. As well, the question of how to activate the demand response participants if an emergency demand response program is to be adopted needs to be answered.

This work proposed an event-driven based EDRP scheme as a solution to the above needs. A credible contingency is called an "event". A table of demand response actions is created for various events. For a given event, the table may contain parameters such as the locations and amount of demand reductions needed and is updated either hourly or daily. If an event does materialize as detected by the SCADA system, the demand response is triggered immediately according to the action table. While this scheme is simple in concept, establishing the demand response parameters is a complex technical problem. For this purpose, the multistage optimization method is used to tune the action table continuously.

Under the paradigm of the smart grid, the centralized monitoring and controlling abilities provide an excellent platform to implement the proposed event-driven based demand response scheme.

A. 2 The event-driven emergency demand response program

The proposed event-driven based EDRP aims to protect power systems in the emergency conditions caused by critical contingencies. The following problem needs to be solved in the first place:

(a) How to identify the critical contingencies which have severe impacts on the operating reserves.

As well, the event-driven based EDRP should minimize its impact on the customers and thus limit its cost. Therefore, another problem needs to be solved:

(b) For each recognized critical event, how to provide the key setting parameters such as the amount of demand reduction at various locations in order to minimize the cost.

Finally, in order to verify the designed demand response rules, especially the performance under the specific operation time, time-domain simulation studies need to be conducted. If the performance cannot satisfy the requirement, a new

demand response rule needs to be obtained by revisiting problem *(b)* and adjusting some constraints when solving it. This procedure might need to be repeated several times until a satisfactory performance can be achieved. The details of this procedure will be explained later in this section.

In summary, the proposed EDRP is designed to improve the power systems' operation reserves by the means of demand reduction when the power systems are under emergency operating scenarios, such as severe transmission line outages. This process consists of:

Step 1: Evaluate the credible contingencies recommended by operators and identify the critical contingency events by using the industry standard PV curve technique on the hour-ahead operating base cases. The critical contingency events are those in which the operating reserve is less than the desired safe value.

Step 2: For each critical contingency (event), choose the proper demand response participants and minimize the amount of demand interruptions to achieve the desired level of operation reserves. Several constraints need to be considered when performing this step: the cost of demand reduction, the priority of the demand, and the available load amount at a specific demand response provider. Some other constraints might be also considered if required by particular utility companies.

The above diverse requirements lead to a nonlinear optimization problem. The objective function is to minimize the total cost. The constraint is that the operation reserve after the demand reduction should be larger than the desired one. Other constraints, such as power flow equations and safety operation constraints are also considered. Combining the objective function and all these constraints, the nonlinear optimization problem is depicted by (A.1):

$$\begin{aligned} \min & \sum_{i=1}^{m} \int_{\Delta s_i=0}^{\Delta S_i} c_i d\Delta s_i \\ & \Delta\lambda^* = f\left(\Delta S_1, \Delta S_2, \cdots, \Delta S_m\right) \\ & c_i = g\left(\Delta s_i\right) \\ st. & \Delta\lambda^* \geq \Delta\lambda^{req} \\ & \text{power flow } \varphi(\mathrm{z}, \mathrm{s}) = 0 \\ & \text{Power system components Limits} \\ & \text{Limits by demand response participants} \end{aligned} \tag{A.1}$$

where ΔS_i is the total load reduction at the selected location *i*, m is the number of available demand response providers, $\Delta\lambda^*$ is the operation reserves after a certain amount of demand reduction, $\Delta\lambda^{req}$ is the desired operation reserve, c_i is the cost for reducing demand Δs_i at load bus *i*, z is the system state vector, and s is the vector of the active and reactive powers consumed by the loads, f and g are two unknown functions.

Step 3: Evaluate the performance of the selected demand response participants by using time-domain simulations. The emergency demand response schemes are designed for each recognized critical contingency based on steady-state PV curve

analysis. The time-domain simulation test has to be performed to check the impact of the operation time of the selected demand response participants. The desired system operation conditions may not be obtained due to some slow-acting demand response providers.

Step 4: Fine-tune the designed EDRP based on the time-domain simulation results. If the time-domain simulation performed in step 3 indicates that the desired performance (all the bus voltage is within desired limit, enough operation reserves are available, etc.) cannot be met, then the emergency demand response scheme has to be redesigned by repeating the procedure described in step 2. Since the problem is caused by the operation time of some demand response providers, the new design should try to avoid those slow-acting demand response participants. By eliminating them from the list of available demand response providers ($m-n$), a new demand response scheme can be obtained. Step 2 and step 3 might need to be repeated several times until satisfactory results are obtained.

The above design procedure is shown in Figure A.1.

An implementation scheme for the proposed event-driven based EDRP is also presented in this work (see Figure A.2). The steps described above can be implemented in the system control center. After receiving the required data from the data-collecting centre, the computing centre will perform the steps depicted in

Figure A.1. At the computing centre, the desired emergency demand response scheme will be calculated continuously. Thereafter, the schemes are uploaded to the Energy Management System (EMS) to automate the operation. The EMS will monitor the system status by receiving data from the Supervisory Control and Data Acquisition system (SCADA). If a recognized event happens in the system, the EMS will trigger the demand reductions based on the action table. The designed action table will be similar to the one shown in Table A.1.

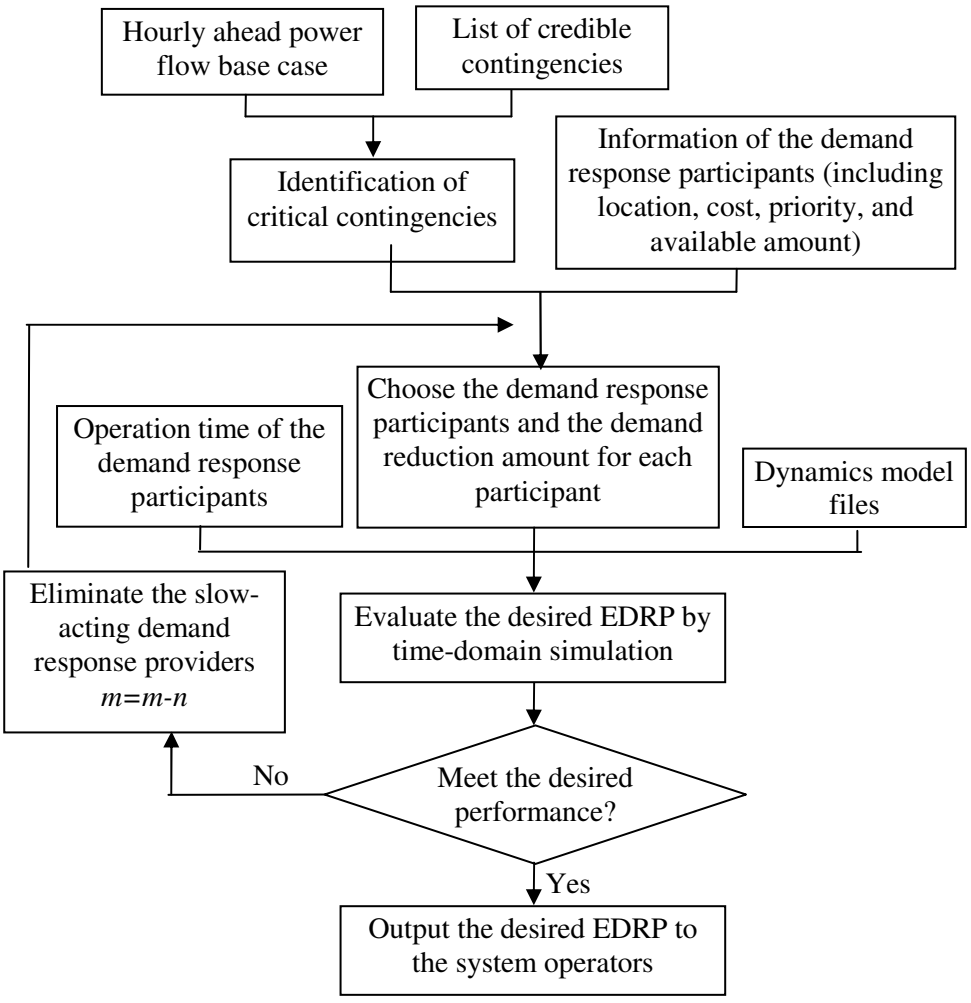

Figure A.1 The overall design procedure of the event-driven based EDRP

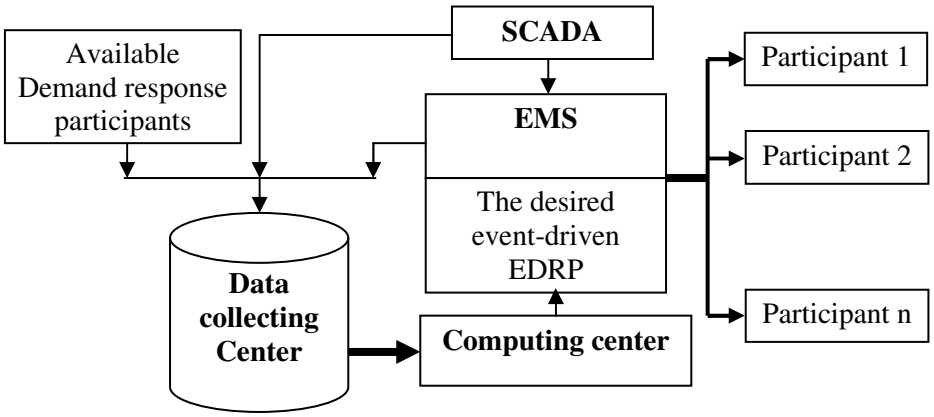

Figure A.2 The implementation scheme of the event-driven based EDRP

Table A.1 One sample of the designed action table

Events	Emergency demand response actions			
	Location	Deduction Amount (MW)	Cost ($ per hour)	Operation reserve
Event no. 1: loss of line #*k*	Participant 1	1.5	65	5%
	Participant 2	0	0	
	…	…	…	
	Participant n	0.2	5	
Event no. 2: loss of line #*m*	Participant 1	0.5	20	6%
	Participant 2	2.0	100	
	…	…	…	
	Participant n	0	0	
…	…	…	…	…
Event no. n:	…	…	…	5.5%

The above steps indicate that the main difficulty associated with the proposed ermergency demand response program is to solve the nonlinear optimization problem described by (A.1). The other tasks, such as the time-domain simulation, are quite straightforward and can easily be done by using any commerical power system analysis softwares. In the next sections, the multistage optimization method is proposed in order to solve (A.1).

A.3 The sensitivities of operation reserves with respect to demand relief amount

In order to minimize the cost while achieving the required operation reserves $\Delta\lambda^{req}$, equation (A.1) has to be solved. A common strategy is to reduce the demand from the most sensitive loads until the achieved margin increase $\Delta\lambda^{*}$ exceeds the required one $\Delta\lambda^{req}$. According to this strategy, $\Delta\lambda^{*}$ is calculated by (A.2).

$$\Delta\lambda^{*} = \sum_{i=1}^{l} Sen_i \times \Delta S_i \qquad l \le m \qquad \text{(A.2)}$$

Sen_i is the sensitivity of the operation reserves with respect to the demand reduction at a particular location and can normally be defined as (A.3), which is modified from the sensitivity formula in [4].

$$\lambda = \lambda(z, s)$$

$$Sen_{\lambda s} = \nabla_s \lambda - \varphi_s^T \left(\varphi_z^T\right)^{-1} \nabla_z \lambda$$

$$Sen_i = \frac{1}{c_i} Sen_{\lambda s,i} = \frac{\Delta\lambda}{c_i \Delta S_i} \qquad i = 1,2,\cdots,m \qquad \text{(A.3)}$$

where ΔS_i is the load reduction amount at load bus *i*, λ is the scaling factor ($\lambda = 1$ at the base operation case), $Sen_{\lambda s}$ is the sensitivity of the operating scaling factor with respect to the load demand *s*, $\Delta\lambda$ is the operation reserves increment after the load reduction, c_i is the unit-price which should be paid for demand reduction at bus *i*, and *m* is the total number of demand response participants.

The method using (A.2) to obtain the minimum cost depends on the assumption that the sensitivities remain constant no matter how much the load is reduced at the selected location. Although this relationship has been evaluated in Chapter 4, some extra evaluations are also conducted in this work to further explore the limitations of using this relationship to design the demand response program. This section uses the same IEEE 14 bus system as an example to investigate how well this assumption represents the real situation. Three different conditions with increasing orders of practicality will be considered in this study. For each condition, the sensitivities Sen_i, which change with the amount of demand reduction, are recorded.

Condition 1: the cost of demand reduction and nonlinear effects such as the adjustment of the switched shunts, the reactive power output limit of the generators, and the tap changer movement are not considered during the system is stressed. Figure A.3(a) shows the operation reserve increment $\Delta\lambda$ versus the load reduction amount ΔS_i at every load bus for this condition. As this figure reveals, the curves are almost linear. In other words, the sensitivity $\Delta\lambda / \Delta S_i$ for each load is almost constant. Therefore, the explained assumption is supported in this case.

Condition 2: the cost of demand reduction is considered. The cost of demand reduction is generally demand-related, as mentioned in [93]. For example, the cost information is considered as described by (A.4). Note that this cost function is an approximation of the function described in [93].

$$c_i = 50 + 5\left(\frac{\Delta S_i}{S_i}\right)^2, \; i = 1,2,\cdots,m \tag{A.4}$$

When the cost information is considered, the results presented in Figure A.3 (b) are obtained. This figure illustrates the operation reserve increment $\Delta\lambda$ versus the cost of the load reduction $c_i \Delta S_i$ at every load bus.

As Figure A.3(b) shows, the nonlinearities of the curves have been increased. In other words, the sensitivity $\Delta\lambda / (c_i \Delta S_i)$ for each load can no longer be considered constant.

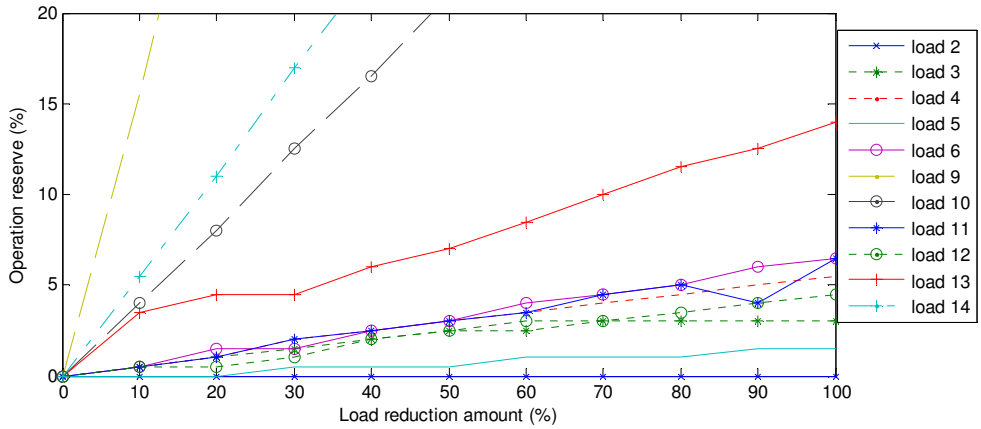

(a) The sensitivties of operation reserves with respect to demand reduction

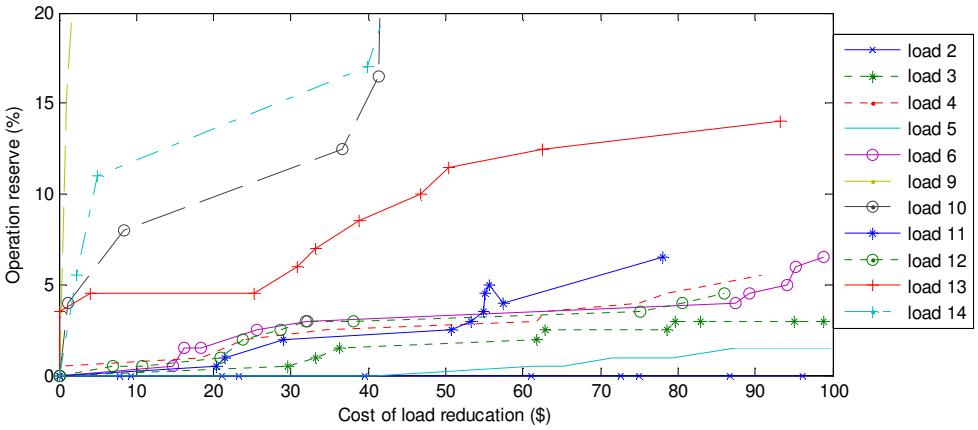

(b) The sensitivites of operation reserves with respect to cost

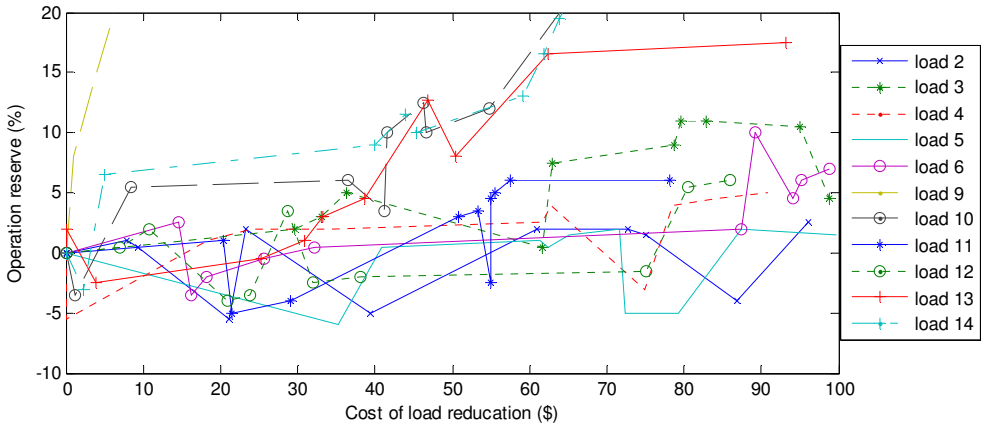

(c) The sensitivites of operation reserves with respect to cost and nonlinear effects

Figure A.3 The variation of the sensitivities of the operation reserve with respect to the cost of demand reduction

Condition 3: the nonlinear effects such as the adjustment of the switched shunts, the reactive power output limit of the generators, and the tap changer movement are considered. This condition produces the results shown in Figure A.3(c). This figure shows that the curves are not linear and do not follow any specific trend. Therefore, the sensitivities for this condition are very hard to predict. This problem indicates that the assumption of constant sensitivities is not valid in practice. The sensitivities could vary significantly during the process of demand relief. In addition, the results shown in Figure A.3 reveal another important phenomenon: letting more customers participate in the demand relief program does not necessarily lead to higher operation reserves if the power flow pattern does not change.

Because of the major variation of the sensitivities of the operation reserves with respect to the cost, it is hard to use the method described by (A.2) to get the optimal EDRP. Therefore, a new algorithm is needed to solve (A.1) while considering the variations of these sensitivities. For this purpose, the proposed multistage optimization method is used in this work.

A.4 Applying the proposed multistage optimization method

The sensitivity analysis conducted in Section A.3 indicates that the relationship between the operation reserves and the load reduction is inherently nonlinear and hard to predict. Furthermore, the relationship between the cost and the load

reduction is also a nonlinear function g, which is predefined based on the contract between the utility companies and the demand response providers [80]. These nonlinear features make the problem described by (A.1) difficult to solve. In this work, the proposed multistage optimization method is used to solve the problem (A.1) and to obtain the optimized demand response scheme for each critical contingency event.

In order to make the solutions of these linearized problems approximate the solution of the original nonlinear optimization problem as closely as possible, two conditions are considered when the original problem is linearized:

- The load reduction is applied at only one location at a time.

- The load reduction amount at one time is limited to a small value (let's say 10% of the available demand) so that the sensitivities and the unit-price can be considered constant.

The above conditions can be described by (A.5).

$$\begin{aligned} \Delta\lambda_i &= f\left(S_1, \cdots, S_{i-1}, \Delta S_i, S_{i+1}, \cdots S_m\right) = h \times \Delta S_i \\ c_i &= g\left(\Delta S_i\right) = k \end{aligned} \tag{A.5}$$

where ΔS_i is the load relief amount at load bus i, $\Delta\lambda_i$ is the operation reserves increment after the load reduction at bus i, and m is the total number of demand

response participants, c_i is the unit-price which should be paid for reduction at bus *i*, and *h* and *k* are constant values, which denote that the functions *f* and *g* have been approximated by using the piecewise linear method.

By using the condition described by (A.5), the original problem (A.1) can be solved stage by stage. At each stage, a linear optimization problem as shown by (A.6) is formulated. In order to solve (A.6), it suffices to calculate the sensitivities and select the load with the highest sensitivity.

$$\begin{aligned} Max \quad & \left\{ \frac{\Delta\lambda_i}{c_i \times \Delta S_i} \right\} \\ & \Delta\lambda_i = Sen_{\lambda s,i} \times \Delta S_i \\ & c_i = k \\ \text{st.} \quad & \text{power flow constraint} \\ & \text{power system components limits} \\ & i = 1, 2, ..., m \end{aligned} \tag{A.6}$$

At each stage, the operation reserve $\Delta\lambda$ will be slightly improved until, at the final stage, the desired $\Delta\lambda^*$ will be obtained. Therefore, the solution of the original problem (A.1) is the combination of the solutions at each stage. The solution to problem (A.1) can be written as (A.7). In (A.7), ΔS_{stagex} indicate the solution to the problem (A.6) at stage *x*.

$$EDRP = \left\{ \Delta S_{stage1}, \Delta S_{stage2}, \cdots, \Delta S_{stagej} \right\} \tag{A.7}$$

The above procedure is depicted in Figure A.4, which shows that the sensitivities are calculated at each stage and that the load with the highest sensitivity is

selected as the most effective demand response provider. The demand reduction is then applied at the selected provider. After this demand reduction, a new operation case is constructed and the next stage starts. This process will be repeated until the required operation reserve is obtained. The final emergency demand responses are the combination of the results from all stages. The term "multistage" is used only to describe the problem-solving procedure, not to reflect the stages of implementation. In the real operation, all the demand providers should operate at the same time to ensure that the desired operation reserve is obtained.

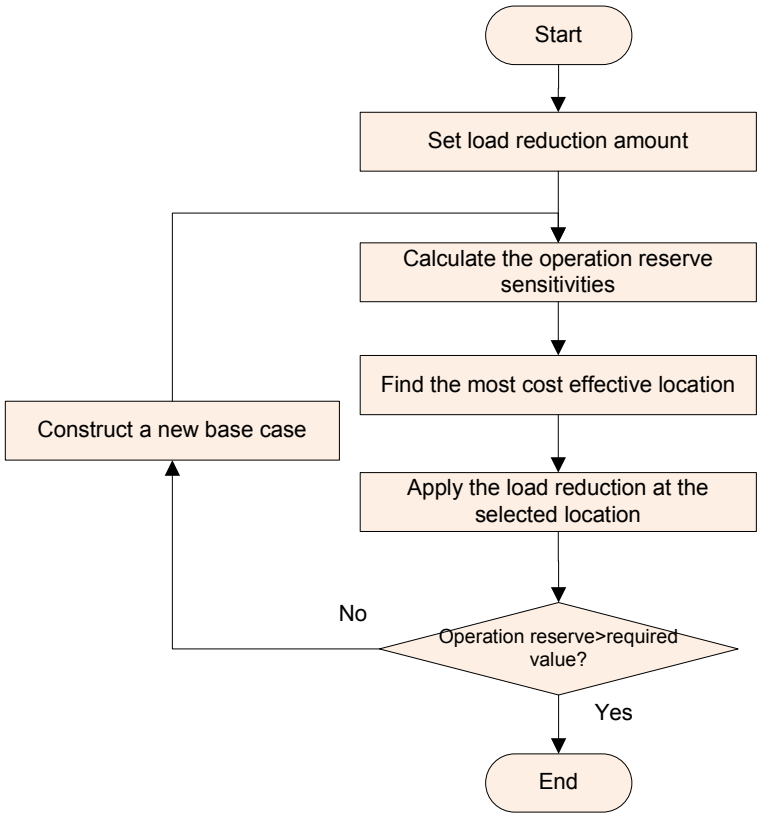

Figure A.4 The flowchart of the multistage optimization method for demand response

The sensitivities of the operation reserve with respect to the demand reduction need to be calculated at each stage. Many algorithms and indices can be used to perform this task, such as those presented in [46][73]. In this work, the industry standard PV curve method [46] is used to calculate the system operation margin $\Delta\lambda$. Then the sensitivities of each demand response participant at each stage are obtained by using (A.3).

In the next section, the multistage optimization method represented in Figure A.4 will be illustrated by using the IEEE 14 bus system, the IEEE 118 bus system, and a 2038 buses real power system.

A.5 Illustration studies of the selected power systems

In order to verify the effectiveness of the proposed event-driven emergency demand response strategy, it is used to design the EDRP for several test systems, and the results are investigated in this section. The operation reserves are calculated by using the power flow method in the commercial power system analysis software PSS/E and by assuming that the loads are scaling up with the same ratio. The method is the common practice used by WECC [46].

These test systems are pre-stressed close to their load limits before the critical contingency (or the event) is applied. The demand reduction amount for each stage is 10% of the selected load for both the conventional method described by

(A.2) and the proposed multistage optimization method. The unit-price for each load is assumed to be \$50/MWh at the base case and changes with a second-order polynomial function (see (A.8)) of the demand reduction amount (percentage), which is a piecewise linear function derived from the function in [95]. The unit-cost remains the same for any 10% load reduction interval. The unit-cost information is shown in Figure A.5.

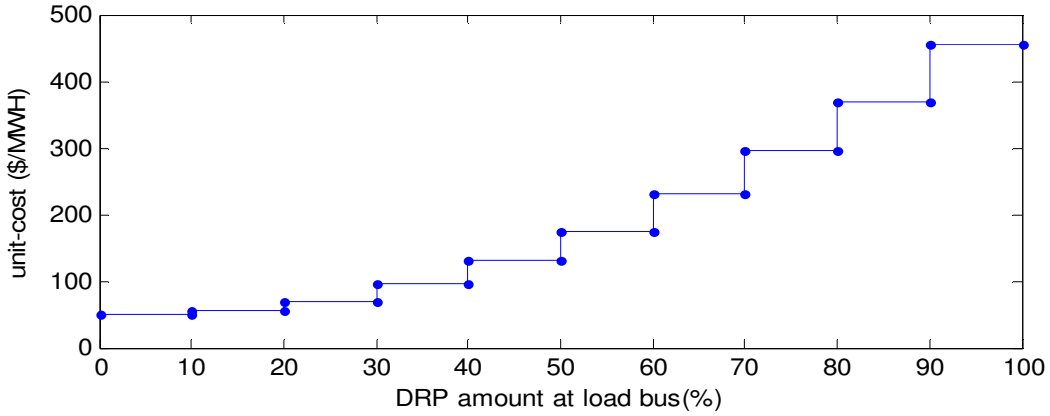

Figure A.5 The function of unit-cost

$$c_m = 50 + 0.05 x_m^{\,2}, \qquad m = \{0,10,20,...,100\} \tag{A.8}$$

where c_m is the unit-cost of the load at each 10% stage. x_m is the demand relief amount in percentage.

IEEE 14-bus system: This case study is a stressed system from the base IEEE 14 bus system [45]. The operation scenario has a load demand 0.85 times more than the base case. After a N-2 contingency or two transmission lines outages (bus 2 to

bus 4, and bus 2 to bus 5 lines), the system loses its power flow solvability. The event-driven EDRP should be applied to ensure that the operation reserve is no less than the required value, which is set to be 5%.

Based on the cost-effectiveness results from (A.3), load bus 14 is chosen at the first stage, and the load reduction amount is 10% for this stage. The sensitivities of the locations change with the demand reliefs. For the second stage, the load bus 10 becomes the most cost-effective load. Thereafter, bus 10 is chosen at the second stage. Then at the third stage, load bus 14 is again the most cost-effective load. This procedure is repeated until the required operation reserve is obtained.

Table A.2 Results of the EDRP for IEEE 14-bus system

<table>
<tr><th rowspan="2">Methods</th><th colspan="3">Emergency demand response</th><th rowspan="2">Total amount (cost)</th><th rowspan="2">Operation reserve</th></tr>
<tr><td>Stage</td><td>location</td><td>Amt (%)</td></tr>
<tr><td rowspan="7">The proposed strategy</td><td>1</td><td>14</td><td>10</td><td rowspan="7">14.22 MW,
7.06 MVar

$822.0 per hour</td><td rowspan="7">5%</td></tr>
<tr><td>2</td><td>10</td><td>10</td></tr>
<tr><td>3</td><td>14</td><td>10</td></tr>
<tr><td>4</td><td>9</td><td>10</td></tr>
<tr><td>5</td><td>9</td><td>10</td></tr>
<tr><td>6</td><td>14</td><td>10</td></tr>
<tr><td>7</td><td>9</td><td>10</td></tr>
<tr><td rowspan="2">The method in (A.2)</td><td colspan="2">Location</td><td>Amt (%)</td><td rowspan="2">29.79 MW,
14.12 MVar
$4910.5 per hour</td><td rowspan="2">6%</td></tr>
<tr><td colspan="2">14</td><td>100</td></tr>
</table>

Table A.2 shows the emergency demand response results obtained by using the proposed strategy and those obtained by using the conventional strategy, which is described by (A.2). As Table A.2 reveals, in order to maintain the required operation reserve, the proposed method costs much less than the one obtained from the conventional strategy.

IEEE 118-bus system: The studied base case is 1.4 times more stressed than the base IEEE 118 bus system [21]. After a N-1 contingency or the loss of the line between bus 75 and bus 77, the system reserve shrinks to 0.6%, so that the system is in an emergency condition. The multi-stage optimization method and the conventional method are applied to this operation scenario. The results are listed in Table A.3, which contains the final results of the EDRP. In order to save space, the results for each stage have not been listed.

Table A.3 Results of the EDRP for IEEE 118-bus system

Methods	Emergency demand response			
	Location	Amt (%)	Load reduction amount (cost)	Operation reserve
The proposed strategy	Bus 44	30	49.7 MW, 21.2 Mvar $4981.5 per hour	6%
	Bus 45	70		
	Bus 22	10		
	Bus 21	10		
	Bus 43	30		
The method in (A.2)	Bus 44	100	69 MW, 30 Mvar $13283.0 per hour	5%
	Bus 45	100		

The results clearly show the advantage of the proposed strategy over the conventional method. The proposed multi-stage optimization method uses nearly 20 MW less power reduction to obtain the desired system operation reserve. Furthermore, the cost of the proposed multistage optimization method is less than half of the cost of the conventional method.

A real 2038 bus power system: A real 2038-bus system is considered as the last case study. The operation reserve for this system is around 10% at the normal operation condition. After a N-1 contingency or the loss of the line between bus 74 and bus 814 (a 138 kV transmission line), the system operation reserve becomes negative, indicating that the system is in an emergency condition. As a result, an EDRP is needed to improve the system operation reserves.

Table A.4 Results of the EDRP for a real 2038-bus power system

Methods	Emergency demand response			
	Location	Amt (%)	Load reduction amount (cost)	Operation reserve
The proposed strategy	4220	100	34.89 MW, 15.49 MVar $5706.3 per hour	5.0%
	4219	30		
	99393	10		
The method in (A.2)	4220	100	36.56 MW, 16.54 MVar $5892.8 per hour	6.0%
	4219	40		

To save space, the results for each stage are not listed here. The final results for the EDRP are listed in Table A.4, which shows that the proposed method uses 1.67 MW less active power and 1.05 Mvar less reactive power than the method in (A.2). The proposed strategy can save $186.5 per hour, compared to the conventional method.

The above study shows the following advantages of the proposed strategy:

- In order to optimize the emergency demand response program, a nonlinear optimization problem needs to be solved. The proposed multistage optimization method can easily solve this nonlinear optimization problem.

- Unlike the conventional method, the proposed multistage optimization method can consider the cost-related sensitivities between the demand reduction and the operation reserve. Using the proposed method, to achieve a certain level of operation reserves is much less expensive than using the method in (A.2).

- The proposed event-driven EDRP strategy can be integrated into the power system EMS. Based on the status (obtained from SCADA and PMUs) of the power system, the critical event is recognized, and thus, the corresponding EDRP is applied to restore the system from the emergency operating condition.

A.6 Conclusions

The operation reserve is a key index in power system security operation. In this work, an event-driven based emergency demand response scheme was proposed, and its design/tuning technique was developed. It is aimed at choosing the proper demand response participants and minimizing the total cost while achieving a certain level of operation reserves. Under the paradigm of the smart grid, the implementation of the event-driven based scheme was also presented.

The sensitivities of operation reserve with respect to the cost of the demand reduction were investigated. The results showed the nonlinearity between the sensitivities and the demand reduction amount. Moreover, the cost of demand reduction generally varies with the amount of reduction. Therefore, the problem associated with the emergency demand response program became a nonlinear optimization problem.

In order to solve the above optimization problem, a multistage optimization method is used in this work. By dividing the nonlinear problem into a series of linear optimization problems, the original nonlinear problem was solved stage by stage. The performance of the proposed method was verified by the results from three test power systems. The proposed algorithm can be easily adopted by utility companies due to its simplicity and practicality.